2011-01-01

Free Radical Stress-Induced Parkinsonian Lewy-Like Aggregation Prevented Through Polyphenolic Phytochemical Analog Intervention: Implications For Subcellular Trafficking And Neurodegenerative Disorders

Rituraj Pal
University of Texas at El Paso, rpal@miners.utep.edu

FREE RADICAL STRESS-INDUCED PARKINSONIAN LEWY-LIKE AGGREGATION PREVENTED THROUGH POLYPHENOLIC PHYTOCHEMICAL ANALOG INTERVENTION: IMPLICATIONS FOR SUBCELLULAR TRAFFICKING AND NEURODEGENERATIVE DISORDERS

Rituraj Pal

DEPARTMENT OF CHEMISTRY

_____
Mahesh Narayan, Ph.D.

_____
Chuan Xiao, Ph.D.

_____
Siddhartha Das, Ph.D.

_____
Jose Nunez, Ph.D.

_____
Benjamin C. Flores, Ph.D.
Interim Dean of the Graduate School

FREE RADICAL STRESS-INDUCED PARKINSONIAN LEWY-LIKE AGGREGATION PREVENTED THROUGH POLYPHENOLIC PHYTOCHEMICAL ANALOG INTERVENTION: IMPLICATIONS FOR SUBCELLULAR TRAFFICKING AND NEURODEGENERATIVE DISORDERS

By

Rituraj Pal, M.S.

Dissertation

Presented to the faculty of the

The University of Texas at El Paso

in Partial Fulfillment

of the Requirements

for the Degree of

Doctor of Philosophy

DEPARTMENT OF CHEMISTRY

THE UNIVERSITY OF TEXAS at EL PASO

December 2011

Acknowledgements

I would like to express my sincere gratitude to my dissertation advisor, Dr Mahesh Narayan. Thank you for providing me the opportunity to work in your laboratory; it has been a great honor for the faith you have shown in me during my tenure in your group. Your vision, guidance and suggestions for my project are greatly appreciated. Finally it has been an immense pleasure to work with you. I would also like to express my sincere thanks to all of my committee members, Drs. Chuan Xiao (River), Siddhartha Das, and Jose Nunez for providing helpful comments whenever it was needed. Your valuable suggestions have been appreciated. I am also grateful to Dr.Armando Varela, Dr. Marc B. Cox, Dr. Manuel Miranda and Dr. Felicia Manciu for their generous help during my collaborative work with them. I would like to acknowledge Border Biomedical Research Center (BBRC) core facilities at Biological Sciences at University of Texas at El Paso (UTEP) for allowing me to access all the instruments.

I would also like to acknowledge all my laboratory members, past and present. Special thanks to Veronica Gonzalez for helping me through the experiments. Similarly I appreciate the thoughtful advice of Saemin Chang during the earlier days; Marisol Romero, Parijat Kabiraj Emmanuel Zubia, Laura Garcia and Rene Duran for being great friends and for helping me in different projects and to understand the local colloquialisms unique to local cultures. I also thank my many supportive friends Debarshi Roy, Sarit Pal and Berenice Munoz who have made my stay lovely and enjoyable in El Paso.

Last but by no means, my deepest gratitude goes towards my father Mr. Madan Pal, mother Mrs. Krishna Pal, my elder brother Dr. Angshuman Pal and my uncle Dr. Uttam Khamrai. Their enduring love and support have been the greatest gift I could ever receive.

Abstract

Protein disulfide isomerase (PDI), the chief endoplasmic reticulum (ER)-resident oxidoreductase chaperone, is known to catalyze the maturation of disulfide-bond-containing proteins primarily through oxidation-reduction and isomerization functions. The rate-determining step in the oxidative regeneration path of disulfide-bond-containing proteins generally couples chemical thiol-disulfide-exchange reactions to a physical conformational folding reaction. I have determined the impact of PDI and its subdomains on the rate-determining step in ribonuclease A folding and on the physical structure-forming step of select ER-processed proteins including RNase A. This was facilitated through application of a novel chemical tool to exclusively populate native-disulfide-containing intermediates in unstructured forms. The described biochemical inroad permits a deconvoluted study of the physical half-process in the rate-determining step from its chemical counterpart. Analysis of folding kinetics of RNase A and other proteins reveal that the highly evolved oxidoreductase activity of PDI masks its chaperone-like activity, impedes conformational folding of ER-processed proteins, and limits its potential to accelerate the rate-determining step in oxidative regeneration. Implications of the heretofore unknown and anomalous self-limiting behavior of PDI are discussed in the context of oxidative maturation and misfolding *in vivo*.

Nitrosative stress has recently been demonstrated as a causal in a select sporadic variant of Parkinson's (PD) and Alzheimer's (AD) diseases. Specifically, elevated levels of Nitric Oxide (NO) disrupt the redox activity of protein disulfide isomerase by S-nitroso modification of its redox-active cysteines. This leads to accumulation of misfolded AD- and PD-specific proteins. I have recently demonstrated *in vitro* that polyphenolic phytochemicals, curcumin and masoprocol, can prevent S-nitroso-PDI formation by scavenging NO*. In this study, using

dopaminergic SHSY-5Y cells, I have monitored the aggregation of green-fluorescent protein (GFP)-tagged synphilin-1 (a known constituent of PD Lewy neurites) as a function of rotenone-induced nitrosative stress. Importantly, I demonstrate a marked decrease in synphilin-1 aggregation when the cell line is previously incubated with 3, 5-bis (2-flurobenzylidene) piperidin-4-one (EF24), a curcumin analogue, prior to rotenone insult. Furthermore, my data also reveal that rotenone attenuates PDI expression in the same cell line, a phenomenon that can be mitigated through EF24 intervention. I was also interested to investigate the bioavailability of EF 24 through binding assay with a specific carrier protein, human serum albumin (HSA). With high affinity binding sites, HSA is a major transporter for delivering several endogenous compounds and drugs *in vivo*. In this dissertation, the binding parameters of EF 24 to HSA have been determined.

Together, these results suggest that polyphenolic phytochemical EF24 can exert neuroprotective effects by ameliorating nitrosative stress-linked damage to PDI and the associated onset of PD in tested models. Essentially, EF24 can serve as a scaffold for the design and development of PD and AD specific prophylactics.

Another aspect of this dissertation was to investigate the role of PDI in cancer. PDI can bind to estrogens as well as interact with its receptor protein (i.e., estrogen receptors (Er) α and β, respectively). It has previously been shown that PDI also acts as an intracellular 17β-estradiol (E2)-binding protein that transports and accumulates E2 in live cells. Intracellular PDI-bound E2 can be released from PDI upon a drop in E2 levels; the released E2 can augment estrogen receptor-mediated transcriptional activity and mitogenic action in cultured cells by modulating the Erβ/Erα ratio. In this dissertation, I observed a significant increase in Erβ/Erα ratio, upon rotenone-induced insult to PDI. Specifically, rotenone-induced insult to PDI leads to the down-

regulation of ERα and up-regulation of ERβ proteins, respectively. My data also shoId that the PDI-dependent disruption of the estrogenic status of cells can be restored through intervention by the polyphenolic curcumin analog, diphenyl difluoroketone (EF24), which acts by rescuing PDI from reactive oxygen species-induced damage. My study indicates that EF24 can play a vital role in maintaining estrogenic status in target cells suggesting future applications in select cancers.

Table of Contents

List of Tables

List of Figures

List of Schemes

Abbreviations:

α-lactalbumin (α-lac);
Alzheimer's disease (AD);
active site;
apoptosis;
α-synuclein;
binding;
bovine pancre atic ribonuclease A (RNaseA);
Calmodulin (CaM);
catalyzes;
curcumin;
cysteines;
Differential Interference Contrast (DIC);
dithiothreitol reducing agent (DTTred);
dithiothreitol oxidizing agent (DTTox);
disulfide;
dimythyl sulfoxide (DMSO);
docking;
Dulbecco's Modified Eagle Medium (DMEM);
3,5-bis (2-flurobenzylidene) piperidin-4-one (EF-24);
endoplasmic reticulum (ER);
estrogen receptor (Er);
estrogen;
estrogen receptor α (Erα);
estrogen receptor β (Erβ);
fetal bovine serum (FBS);
free radicals;
Glyceraldehyde 3-phosphate dehydrogenase (GAPDH);
green fluorescense protein (GFP);
fully-reduced protein/species (R);
humans;
human serum albumin (HSA);
hydrogen peroxide (H_2O_2);
hydroxyl species (*OH);
isomerization;
Lack (Des);
Lewy body;
masoprocol;
molecular Iight (MW);
N-methyl, D-aspartase (NMDA);
native protein/species (N);
Neuronal NO synthase (nNOS);
NO synthase (NOS);
neurodegenerative disorders;
nitrosative stress;
nitric oxide;
nitrosation;
nitrogen species (NO*);
oxidative folding;
oxidative stress;
Parkinson's disease (PD);
polymer;
protein transport; protein disulfide isomerase (PDI);
Propidium Iodide (PI);
Reactive nitrogen species (RNS);
rate-determining step (RDS);
reactive oxygen species (ROS);
Reaction (RXN);
synphilin-1;
S-nitrosylation;
secretory pathway;
thiols;

Chapter 1:

Introduction

1.1 Mechanism of protein synthesis and protein folding

Proteins are macromolecules composed of amino acids and are responsible for carrying out many cellular functions within an organism (1). Proteins are gene products encoded by DNA (1). Each protein has a specific structure that is determined mostly by its primary amino acid sequence (1). Some biological processes that proteins are involved in include signaling and trafficking of substrates, catalysis of biochemical reactions, defense against pathogens and folding of other proteins (1). Protein synthesis involves the transcription of a DNA template into messenger RNA folloId by the translation of mRNA to a primary amino acid sequence. Translation is the last step of gene expression but can be considered the first step in the formation of a fully functional protein (scheme 1.1). Synthesis of peptide chains determined by mRNA occurs on ribosome located outside of the endoplasmic reticulum (ER) (1).

There are four levels of organization of a protein through which the eventual structure and function are acquired. The primary structure of a protein is the linear sequence of amino acids (1). In 1953, Frederick Sanger determined the first full-length amino acid sequence of insulin. The secondary structure of a protein is regular arrangements of amino acids within localized regions of the polypeptide chain (2). α-helices and β-sheets stabilized by hydrogen bonds are examples of a protein's secondary structure (2). The tertiary structure of a soluble protein is acquired through the interactions between side-chain amino acids that lie in different regions of one single peptide chain (2). In general hydrophobic amino acids reside within the interior of the protein whereas hydrophilic amino acids tend to be solvent-exposed (1).

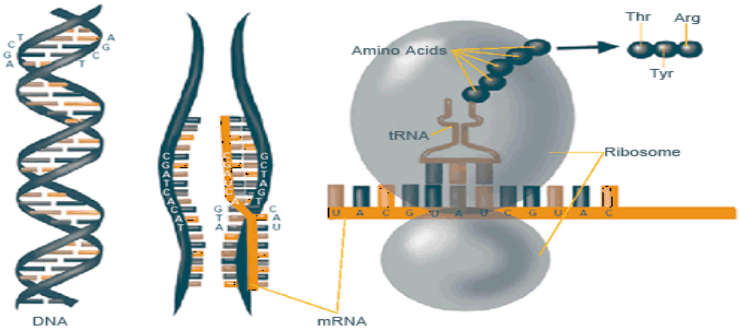

DNA is transcribed to RNA and RNA is translated to an amino acid sequence

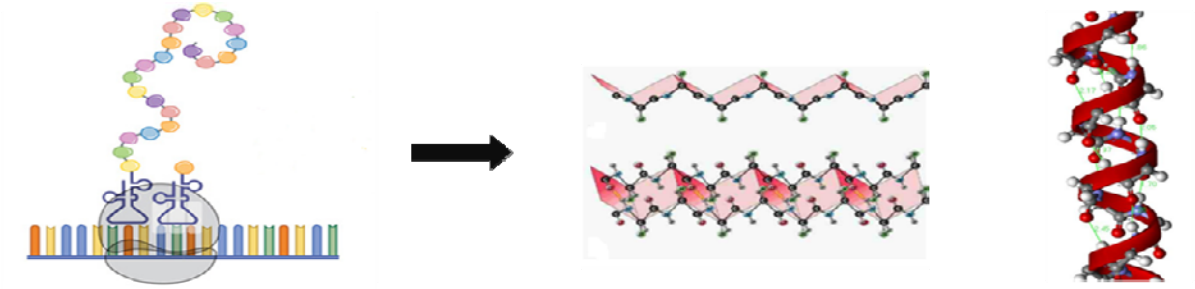

Primary amino acid sequences fold to secondary, tertiary, and quaternary structures (β-sheets and α- helices shown)

SMyce: National Institute of General Medical Sciences (NIGMS)

Post translational modification and formation of a functional protein

Scheme 1.1. Summary of protein synthesis: transcription, translation, and folding

Often, contributing to tertiary structure is the formation of disulfide bonds between thiol-containing amino acid residues. Disulfide-bond is a covalent bond that is formed by the coupling of two thiols (-SH) (1). In chemistry, it is recognized by S-S bond. The chemistry of disulfide

bond is very well-known. The formation of disulfide bond from two thiols is a two electron reaction, which involves an oxidant or electro acceptor (2). *In vitro*, disulfide bond can be formed by loss of electrons from two cysteine thiols coupled with the gain of electrons by an available acceptor, such as molecular oxygen (2).

Finally, the fourth level of protein organization is the quaternary structure in which two or more peptide chains may assemble together as subunits to form one functional entity (1). Scheme 1.1 summarizes the different steps in protein synthesis and the formation of a functional protein.

Nobel Prize recipient Christian B. Anfinsen, known for the "Anfinsen Dogma", demonstrated that denatured proteins can spontaneously fold back to their native three-dimensional conformation and regain activity. This indicates that the native structure of the protein is determined by the information given in the primary amino acid sequence (3). Under physiological conditions the primary amino acid sequence will give rise to the most thermodynamically stable conformation (4). It has been determined that chaperones facilitate the protein in its acquisition of native structure. During and after synthesis, proteins may undergo modifications before becoming fully-functional. Secreted, plasma membrane and lysosomal proteins contain a signal sequence that will translocate them into the ER lumen for post-translational modification such as disulfide-bond formation. Disulfide bond formation occurs when thiol groups from a cysteine are oxidized and forms a covalent bond with thiol group of another thiol-containing moiety.

The ER retains an oxidizing environment wherein disulfide-bond formation occurs (5). Aside from disulfide bond formation, other functions of the ER include further fold maturation, multi-subunit formation, initiation of glycosylation, and addition of glycolipid anchors (5). ER proteins

such as Protein Disulfide Isomerase (PDI) catalyze the assembly and formation of secreted proteins (5). When the correct three-dimensional structure is acquired, the protein is ready for transport to its intended location. Secretory proteins are transported from the ER to the Golgi and finally secreted out of the cell (6). Proteins that are to reside in the ER, such as PDI, are retained via a KDEL signal sequence (7).

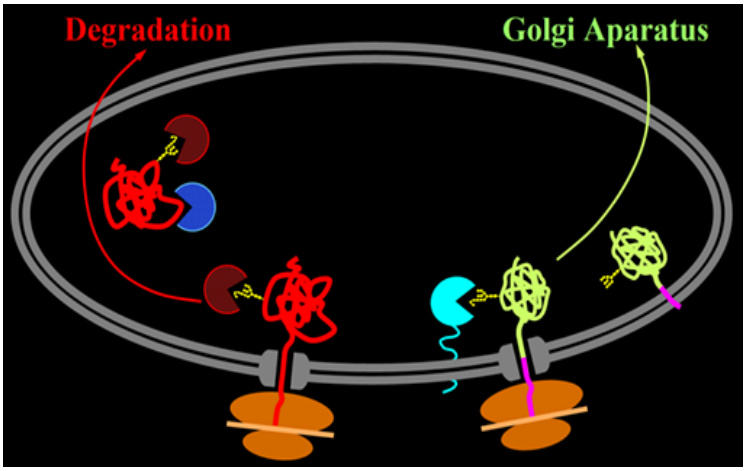

Scheme 1.2. Organization of the cell. Secretory proteins are synthesized in ribosome, translocated into the ER lumen, oxidized and transported to the Golgi, then to their final destination and misfolded proteins go to degradation process (Sitia and Braakman, 2003).

Scheme 1.2 represents a simplified organization of the cell and pathway that secreted proteins undertake prior to reaching their destination. Correct disulfide bond formation is significant to the structure and function of a protein (6). When unfolded proteins cannot acquire their conformation, they will form aggregates with exposed hydrophobic regions of other unfolded proteins (6). Without proper disulfide bond formation, the peptide is degraded or may form aggregates that will disrupt the overall function of the cell (6).

Endoplasmic Reticulum Associated Degradation (ERAD), a process where misfolded proteins are labeled and sent to proteosomes for degradation, helps reduced accumulation of protein aggregates within ER (8). Many diseases such as Alzheimer's and Parkinson's involve the formation of large insoluble aggregates. Enzymes and chaperones located in the ER can facilitate the correct folding of proteins, thereby reducing the formation of aggregates. If accumulation of misfolded proteins occurs, the cell will experience stress and may become apoptotic (9).

1.2 Protein disulfide isomerase (PDI)

Protein Disulfide Isomerase (Molecular weight of approximately 57 kDa) is an oxidoreductase enzyme found in the ER lumen of eukaryotic cells (10). PDI has the ability to oxidize, reduce, and isomerize disulfide bonds. Disulfide bonding is highly error prone and PDI has the ability to reshuffle disulfides until acquisition of substrates' native structure that prevents access to PDI (11). The abundance of PDI in the cell indicates the importance of its role in fold maturation of newly synthesized proteins that are destined to transit via the secretory pathway. Such disulfide-bond-containing proteins constitute 1/3 of the known proteome (5). PDI is part of the thioredoxin super family (11) and the PDI family of proteins (5). PDI also demonstrates limited chaperone function through hydrophobic interactions with unfolded proteins (12). PDI-related studies are important to the understanding of its function and medical advances in neurodegenerative disorders (11).

PDI is a multi-domain thioredoxin-like (TRX) protein with its active site composed of two –CGHC- sequences (scheme 1.3). Numbers and positions of the TRX-like catalytic domains vary among members within the family and it is believed that these variations result from duplication

and deletions of an ancestral enzyme over time (13). The two "a" type domains in PDI contain the oxidoreductase catalytic motif whereas the "b" type domains are implicated in its chaperone-like activity (13).

Scheme 1.3. Schematic diagram of Protein disulfide isomerase (PDI)

1.3 Structure of PDI

The full amino acid sequence of PDI was first determined by Edman and co-workers in 1985. The complimentary DNA from rat liver was analyzed by amino terminal sequence analysis using microsequentator (13). The cloned sequence encoded a 508 amino acid protein with a molecular weight of about 57 kDa and correlated well with the *in vitro* translated protein (13). It was presumed that PDI contained two regions homologous to E. coli thioredoxin protein. A sequence of 19 hydrophobic amino acids at the N terminal was characteristic of a signal sequence extension possibly localizing the protein in the ER (13).

The two active site-containing regions denoted a and a' showed 40% homology to each other (13). The b and b' are 28% homologous to each other but have no homology to thioredoxin or other proteins (13). The final domain, c contains a high density of negatively charged amino acids (13, 14, 15, 16).

There are several PDI paralogs in humans (7) and to a lesser extent also in yeast (15), but their detailed roles and specificities have not been described. Furthermore, though the exact boundaries for the domains differ from species to species, there are significant similarity between

PDI domains. Individual domains of human PDI as well as constructs of combinations of domains have been characterized by NMR (17, 18).

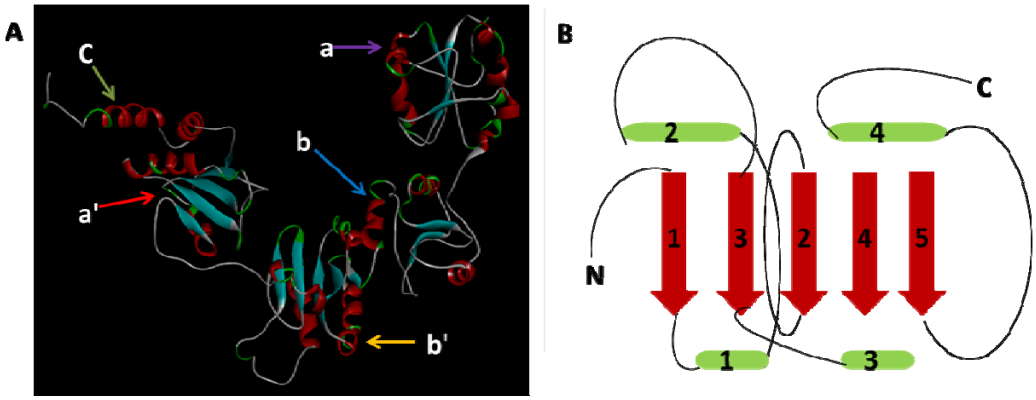

Figure 1.1. Overall Structure of PDI, (A) Ribbon diagram of PDI with the a, b, b′, and a′ domains in magenta, cyan, yellow, and red arrows, respectively, and the C-terminal extension in green arrow. The two orientations roughly differ by a 90º rotation around the horizontal axis. The side chains of the active site cysteines in the a and a′ domains are shown in spacefilling representation with the sulfur atoms in yellow. (B) Secondary structure diagram of the canonical thioredoxin fold with α-helices in green and β strands in red. The location of the active site is indicated by a red oval (Tian et. al., cell, 2005)

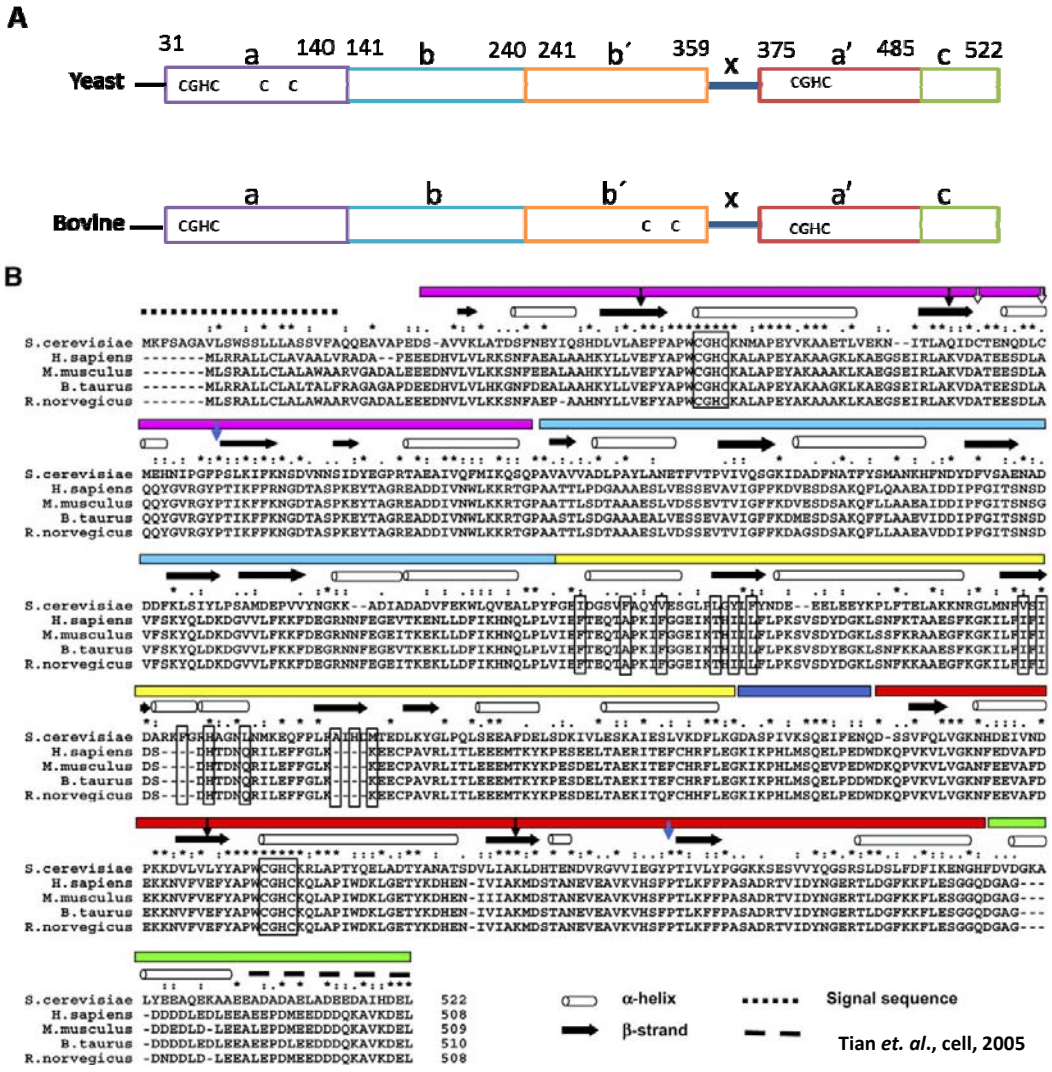

Figure 1.2 Primary Structure of Mammalian and Yeast PDI.(A) Domain organization of bovine PDI as deduced from biochemical studies and that of yeast PDI based on the crystal structure (c represents the C-terminal tail). The C-G-H-C motifs indicate the location of the active sites, the Cs the nonactive site cysteines, and x the loop connecting the b´ and a´ domains. (B) Multiple sequence alignment of yeast and mammalian PDIs. Helices and strands are represented by cylinders and arrows, respectively. Active-site residues in the a and a´ domain are boxed. Black arrows highlight the two buried polar residues in the vicinity of the active site; white arrows the nonactive site cysteines; and blue arrows the cis-prolines near each active site. Boxed residues in

the b′ domain form a hydrophobic pocket are presumably involved in substrate binding. The symbol above the sequence represents the secondary structure with arrow standing for β-sheet and rod standing for α-helix.

1.4 Function of PDI

PDI is one of the highly expressed in mammalian cells because there is a vast number of proteins that must undergo processing before secretion to their final destinations (5). PDI has several functions: oxidation and reduction of nascent proteins and isomerization of existing disulfide bonds. It also possesses chaperone activity and participates in protein degradation. Because of its structure, PDI can exist in a reduced or oxidized form (5).

Oxidation

Correct folding of proteins is essential for the function of cells and the overall well-being of organisms. Cytosolic proteins lack disulfide bonds due to the reducing environment of the cystosol. Proteins destined for secretion must be translocated into the ER and oxidized to obtain disulfides and become fully functional. The cysteine containing catalytic domains allow PDI to introduce disulfide bonds to newly-synthesized substrates (19). For disulfide bond formation, oxidized PDI must transfer its disulfide equivalents to nascent proteins (19). As a result, PDI becomes reduced. Another ER-resident protein, Ero1 transfers oxidation equivalents to PDI, thereby recycling the enzyme for oxidation of other substrates (19). The substrate thiol group, partially deprotonated as a result of ambient pH, attacks PDI disulfide bond and a mixed disulfide between the substrate and PDI is created (19). Another substrate thiolate can then attack the mixed disulfide bond resulting in an intramolecular substrate disulfide bond (19). Scheme 3.1A is an illustration of how PDI functions as an oxidation.

Isomerization

PDI can also isomerize substrate disulfides by shuffling existing disulfide bonds thereby allowing the substrate to eventually acquire its native component of diusulfide bond. Early disulfide bond formation in nascent proteins is error prone. Incorrect disulfide bonds must be broken and correct disulfide bonds must be made (11). It is PDI's role to accelerate shuffling so that the substrate can find its thermodynamically favorable native structure in a timely manner (11).

Isomerization can be viewed as repeated cycles of reduction and reoxidation of disulfide bonds via PDI. Cycles will be repeated until a stable structure is formed and the substrate disulfides are no longer accesible to PDI (11). Both reduction and oxidation reactions are essential to this pathway (11). The first step in isomerization is breaking an existing intramolecular substrate disulfide bond by forming a mixed disulfide with (formerly reduced) PDI. The second step is reoxidation of disulfide bonds between two different cysteine residues. A brief description follows: the N-terminal cysteine of PDI is deprotonated at physiological pH due its low pKa (4.5-5) (11). Deprotonation of the cysteine creates a highly reactive thiolate that attacks an existing disulfide within the substrate. As a result, a mixed disulfide betIen the substrate and the catalyst will form and several scenarios can follow (11). First, the thiol participating in the original disulfide bond can attack the mixed disulfide and the substrate will return to its original state; PDI will be released, and no isomerization occurs (11). Another scenario is that a third substrate thiolate attacks the mixed disulfide resulting in a disulfide between two different thiols (isomerization). This mechanism is depicted in scheme 3.1B. Reduced PDI can attack and reshuffle any exposed disulfide bond and the unfolded substrate is

thus subject to continual reshuffling of its disulfides (19). A conformational folding event resulting in the burial of its (native) disulfides is the only means to escape PDI.

1.5 Free-radical stress

Glutamate is the major excitatory neurotransmitter in the brain and is important for normal functioning of the nervous system; however, excessive activation of glutamate receptors is implicated in neuronal damage in many neurological disorders ranging from acute hypoxic-ischemic brain injury to chronic neurodegenerative diseases. John Olney coined the term "excitotoxicity" to describe this phenomenon (20). This form of toxicity is mediated at least in part by excessive activation of N-methyl, D-aspartase-type receptors (NMDA-type receptors), resulting in excessive Ca^{2+} influx through a receptor's associated ion channel (20). Excessive Ca^{2+} leads to the production of damaging free radicals [e.g., NO* and reactive oxygen species (ROS)] and other enzymatic processes, contributing to cell death. Intracellular Ca^{2+} triggers the generation of NO* by activating neuronal NO-synthase (nNOS) in a Ca^{2+}calmodulin (CaM)-dependent manner (20).

It is currently thought that overstimulation of extrasynaptic NMDA receptors mediates this neuronal damage; in contrast, synaptic activity may activate survival pathways (20). Intense hyperstimulation of excitatory receptors leads to necrotic cell death, but more mild or chronic overstimulation can result in apoptotic or other forms of cell death (20). Increased levels of neuronal Ca^{2+}, in conjunction with the Ca^{2+} binding protein CaM, trigger the activation of nNOS and subsequent generation of NO* from the amino acid L-arginine (20). NO* is a gaseous free radical (thus highly diffusible) and a key molecule that plays a vital role in normal signal transduction; However, in excess it can lead to neuronal cell damage and death. Mitochondrial

respiratory chain complex 1 inhibitors can produce ROS such as, NO* and *OH. Like NO*, hydroxyl (*OH) radicals also produces stress in cell and leads to apoptotic cell death (20, 21).

1.6 Free-radical stress mediated chemical modification of PDI

Inhibition of mitochondrial respiratory chain can generate excess production of nitrogen species (NO*) and in the presence of oxygen, ferrous ions frequently result in oxidative stress through the generation of hydroxyl radicals via the Fenton reaction ($Fe^{2+} + H_2O_2 \rightarrow Fe^{3+} + *OH + {}^{-}OH$) (8). The discovery that the free radical reactive oxygen species (ROS) are synthesized and used as a major transducer molecule by cell promoted dramatic changes in the field of free radical research; it lead to the current view that free radicals and oxidants play an important role in cellular homeostasis and stress (11).

This free radical-induced stress can result in posttranslational modification of PDI (22). It has recently been established that cysteine residues (Cys) in PDI are prominent targets for protein oxidation, as they easily react with NO* and *OH free radicals (22). Deprotonation of the Cys thiol group of PDI to generate the thiolate anion increases its nucleophilicity, and hence reactivity towards free radicals (22). When a thiolate group of PDI is attacked by the NO* and *OH free radicals, inactive S-nitrosylated-PDI and S-hydroxylated-PDI are formed (22). This chemical modification of PDI by free radicals destroys PDI's catalytic activity in oxidative protein folding.

1.7 Neurodegenerative disease

A shared histological feature of many neurodegenerative diseases is the accumulation of misfolded proteins that adversely affect neuronal connectivity and plasticity, triggering cell death

signaling pathways (16). For example, regions of the brain often contain aberrant accumulations of misfolded, aggregated proteins, such as α-synuclein and synphilin-1 in PD, and amyloid-β (Aβ) and tau in AD. The inclusions observed in PD are called Lewy bodies and are mostly found in the cytoplasm of neuronal cells. AD brains show intracellular neurofibrillary tangles, which contain tau, and extracellular plaques, which contain Aβ. Other diseases with inclusions include Huntington's (polyQ), ALS, and prion disease (20). The above-mentioned aggregates consist of oligomeric complexes of nonnative secondary structures, and demonstrate poor solubility in aqueous or detergent solvents. It has been suggested that either genetic mutations, or an increase in nitrosative/ oxidative stress, can facilitate protein aggregation (24). In general, protein aggregates do not accumulate in unstressed, healthy neurons due in part to the existence of cellular 'quality control machineries'. For example, molecular chaperones are believed to provide a defense mechanism against the toxicity of misfolded proteins because chaperones can prevent inappropriate interactions within, and between, polypeptides, and can promote refolding of proteins that have been misfolded because of cellular stress (24).

In addition to the quality control of proteins provided by molecular chaperones, the ubiquitin-proteasome system (UPS) is involved in the clearance of abnormal or aberrant proteins (20). When chaperones cannot repair misfolded proteins, they may be tagged via addition of polyubiquitin chains for degradation by the proteasome. In neurodegenerative conditions, intra- or extracellular protein aggregates are thought to accumulate in the brain as a result of a decrease in molecular chaperone or proteasome activities. In fact, several mutations that disturb the activity of molecular chaperones or UPS-associated enzymes can cause neurodegeneration (24).

1.8 Ubiquitin protease system (UPS)

The UPS represents an important mechanism for proteolysis in mammalian cells (24). Formation of polyubiquitin chains constitutes the signal for proteasomal attack and degradation. An isopeptide bond covalently attaches the C-terminus of the first ubiquitin in a polyubiqutin chain to a lysine residue in the target protein (8). The cascade of activating (E1), conjugating (E2), and ubiquitin-ligating (E3) type enzymes catalyzes the conjugation of the ubiquitin chain to proteins (20). In addition, individual E3 ubiquitin ligases play a key role in the recognition of specific substrates (8).

1.9 Role of free-radical stress-induced modification of PDI in UPS

Chemically, NO* and *OH are often a good "leaving group," facilitating further oxidation of critical thiol to disulfide bonds among neighboring (vicinal) cysteine residues or, via reaction with ROS, to sulfenic ($^{-}$SOH), sulfinic ($^{-}$SO$_2$H) or sulfonic ($^{-}$SO$_3$H) acid derivatization of the protein (16). Alternatively, S-nitrosylation and S-hydroxylation may possibly produce a nitroxyl disulfide or hydroxyl disulfide, in which the NO* or *OH group is shared by close cysteine thiols (20). In addition, free radicals ameliorates the progression of disease pathology in animal models of PD, AD, and ALS, suggesting that excess generation of NO* and *OH play a pivotal role in the pathogenesis of several neurodegenerative diseases by disrupting the UPS (8). Although the involvement of NO* and *OH in neurodegeneration has been widely accepted, the chemical relationship between nitrosative stress and accumulation of misfolded proteins needs further investigation. Recent findings, however, have shed light on molecular events underlying this relationship (24).

1.10 Free-radical scavengers-polyphenolic phytochemicals

It has been previously demonstrated that polyphenolic phytochemicals, masoprocol (from Larrea Tridentata) curcumin [a turmeric (Curcuma Longa) spice] protect PDI catalytic function under conditions of nitrosative and oxidative stress. Curcumin has a wide spectrum of biological and pharmacological functions including anti-inflammatory, antimicrobial, and anticarcinogenic (23). It has already been used clinically and is approved by the FDA as a safe food additive (23). Masoprocol (nordihydroguaiaretic acid (NDGA)) is a potent antioxidant whose derivatives and analogues are potentially useful in treating diseases related to cancers, diabetes, viral, bacterial infections, and inflammation (23). Recent efforts to improve its bioavailability (co-administration with other agents and structural modifications) have met with success by synthesizing curcumin analog, 3, 5-bis (2-flurobenzylidene) piperidin-4-one (EF24) (23). Bioavailable EF24 can mitigate nitrosative and oxidative stress by scavenging excess NO* and *OH by forming stable adducts.

1.11 Prophylactic effect of EF24 against free-radical stress mediated misfolded protein aggregation

Mitochondrial complex-I inhibitors assist production of excess NO* and *OH. Elevated level of NO* and *OH induces nitrosative and oxidative stress, which is linked to activate certain caspases and initiates one of the apoptotic pathways in cells (24). Free radical stress has also been linked to PDI dysfunction and downstream aggregation of misfolding-prone- proteins such as synphilin-1 and α-synuclein. Formation of Lewy bodies and aggresomes leads to apoptotic cell death (24). It is hypothesized that scavenging of free radicals by EF24 can prevent covalent

modification of PDI; EF24 can thereby potentially protect against loss of oxidoreductase function of PDI and against Lewy neurite deposits, the pathogenesis of PD and AD (23).

1.12 Role of PDI in the estrogenic status of cells

PDI can interact directly with Erα (25) and demonstrates estrogen (Er)-interacting behavior very similar to Hsp90 and Hsp70 [two well-known chaperone proteins that can alter Er functions (25)]. PDI, with its possible Erα chaperoning activity, acts as a modulator of estrogen's hormonal activity in different target cells. The intracellular PDI-bound estrogens can be released from PDI to instigate the Er-mediated transcriptional activity as well as mitogenic actions (25). Studies suggest that PDI plays a critical role in estrogen responsiveness by functioning as a molecular chaperone and PDI alone is capable of interacting with Erα and influencing its activity (26). I have observed that PDI can alter Erβ to Erα ratio significantly by altering the levels of two proteins in opposite directions, down-regulation of Erα and up-regulation of Erβ.

1.13 Role of Nitrosative stress-induced modification of PDI on estrogenic status

It is well-known that nitrosative stress, originating from elevated levels of nitric oxide (NO*), results in the S-nitrosylation of PDI cysteines (i.e. the covalent modification of PDI active site cysteines by NO) (23). Initially, I have showed that PDI gets S-nitrosylated (SNO-P) under nitrosative stress, and NO-induced chemical modification of PDI abolishes its ability to maintain the normal level of ERβ/ERα ratio by altering the levels of ERβ and ERα. Using biochemical and molecular techniques, I have studied co-lecolaization of PDI with ERα in cancer cells (MCF-7) under normal and nitrosative stress condition. Under nitrosative stress, PDI loses its activity which in turn, may impact estrogenic status.

1.14 Effect of EF24 in the nitrosative-stress-mediated modification of PDIs' role in estrogenic status

Polyphenol, EF24 can scavenge free radicals by forming stable adducts and prevent PDI from getting S-nitrosylated. PDI can alter Erβ to Erα ratio significantly by altering the levels of two proteins in opposite directions, down-regulation of Erα and up-regulation of Erβ. PDI plays an active role in maintaining estrogenic status by controlling the levels of Erβ and Erα. It is of interest to investigate the role of a ROS-scavenger (EF24) on any alteration of estrogenic status upon ROS-insult to PDI

1.15 Serum protein human serum albumin (HSA)

Human serum albumin (Scheme 1.4) is the most abundant serum protein, which carries several endogenous compounds including fatty acids (27). Due to its ability to bind various drug molecules and alters their pharmacokinetic properties, HSA has long been the center of attention of pharmaceutical industry (27). HSA is a globular protein composed of three structurally similar domains (I, II and III), each containing two sub-domains (A and B) and stabilized by 17 disulfide bridges (28). Aromatic and heterocyclic ligands were found to bind within two hydrophobic pockets in sub-domains IIA and IIIA, namely site I and site II (28). Seven binding sites for fatty acids are localized in subdomains IB, IIIA, IIIB and on the subdomain interfaces (28). HSA has also a high affinity metal binding site at the N-terminus (29). These multiple binding sites underline the exceptional ability of HSA to interact with many organic and inorganic molecules and make this protein an important regulator of intercellular fluxes, as Ill as the pharmacokinetic behavior of many drugs (28).

Therefore, it was of interest to study the binding of EF24 on protein. The spectroscopic analysis of HSA complexation with EF24 was carried out in aqueous solution at physiological conditions, using constant protein concentration to understand the binding affinity of HSA with EF24.

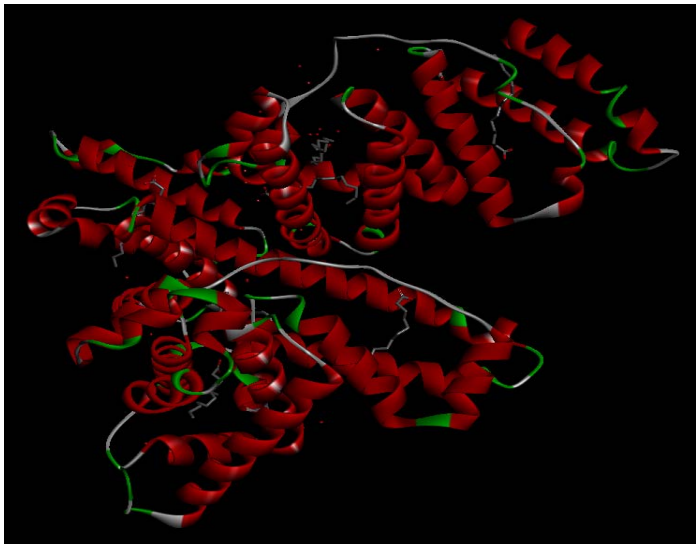

Scheme 1.4 Diagram of human serum albumin (HSA), PDB: 1E7H

1.16 Dissertation goals

Considering that the ER-resident oxidoreductase and neuroprotectant is involved in protein misfolding linked to Alzheimer's in a NO-sensitive manner, PDI is a valuable target for therapeutic intervention in AD and perhaps other age- and neurodegeneration-related disorders. Overexpression of PDI may not be a practical solution to neurodegenerative diseases prevention. Instead, small-molecules that combat the effects of nitrosative stress by scavenging NO*, rescuing PDI function, and restoring ER homeostasis represent the desired modes of PD and AD intervention.

I also hypothesize that under homeostasis, even "healthy" PDI can contribute to debris accumulation within the cytosol, albeit due to a different reason, will also be tested, making this study significant from a basic science viewpoint. The aims of this dissertation include determining mechanisms by which to advance methods to rescue PDI damage and thereby prevent neurodegenerative diseases and cancer onset; to illuminate a fundamental and heretofore unknown reason as to how and why protein processing and trafficking within a particular compartment may have consequences leading to misfolded debris accumulation in a distant site, eventually contributing to neurodegenerative diseases onset. Eventually I plan to translate my data to animal models to find therapeutics that target neurodegenerative diseases and cancer.

Specific aim 1:

Rotenone induced nitrosative stress causes apoptotic cell death through caspase activation. S-nitrosylation of PDI- cysteines due to nitrosative stress is associated with cytosolic aggresomes and Lewy bodies. I want to determine if these aggresomes will also lead apoptotic to cell death in PD and AD brains.

Specific aim 2:

To investigate whether EF24 can act as prophylactic for nitrosative-stress associated AD, PD and other neurodegeneration-related disorders.

Specific aim 3:

To determine if HSA can bind EF24 and act as a transporter for EF24.

Specific aim 4:

Rotenone induced nitrosative stress mediated chemical-modification of PDI leads alteration of estrogen receptor proteins levels. I want to determine the preventive effect of EF24 against nitrosative stress and ability to maintain homeostasis of the estrogen level.

Chapter 2:

The Impact of Oxidoreductase Behavior of Protein Disulfide Isomerase on Protein Maturation

2.1 Introduction

Oxidative protein folding is characteristic of many proteins that are secreted outside the cell or, are membrane-bound, and possess disulfide bonds (1-4). It is a composite process because it involves the chemical formation of the native set of disulfide bonds from the fully-reduced polypeptide, an event that is coupled to a physical conformational folding reaction to obtain the native, biologically active structure (1-3). Proteins required to oxidatively fold are processed (mature) within the endoplasmic reticulum (ER), which facilitates disulfide bond formation because of a favorable redox potential (4).

A typical oxidative folding reaction comprising the regeneration of bovine pancreatic ribonuclease A (RNase A) has been done (Fig. 2.1). During its regeneration from the fully-reduced state (R), 28 one-disulfide (1S), 210 two-disulfide (2S), 420 three-disulfide (3S) and 104 scrambled (i.e. nonnative) four-disulfide (4S) containing intermediates are formed (Fig. 2.1) (5-8). Additionally, two native-like species accumulate in the rate-determining step (RDS) of the reaction. These are Des [40-95] and Des [65-72] (Des stands for lack) which possess native-like structure and lack the (40-95) and (65-72) disulfide bond, respectively (9, 10). These structured intermediates (also referred to as 3S*) are then oxidized to form N (Figure 2.1) (1). The formation of 3S* from 3S is rate-determining because it involves the formation of two native-disulfide-bond-containing structured intermediates from an isomer ensemble of 420 unstructured

intermediates which mostly contain nonnative disulfide bonds, making the search for those two (3S*) species statistical and hence time-consuming; in RNase A this search is compounded by a slow conformational folding process. These two processes are elaborated below.

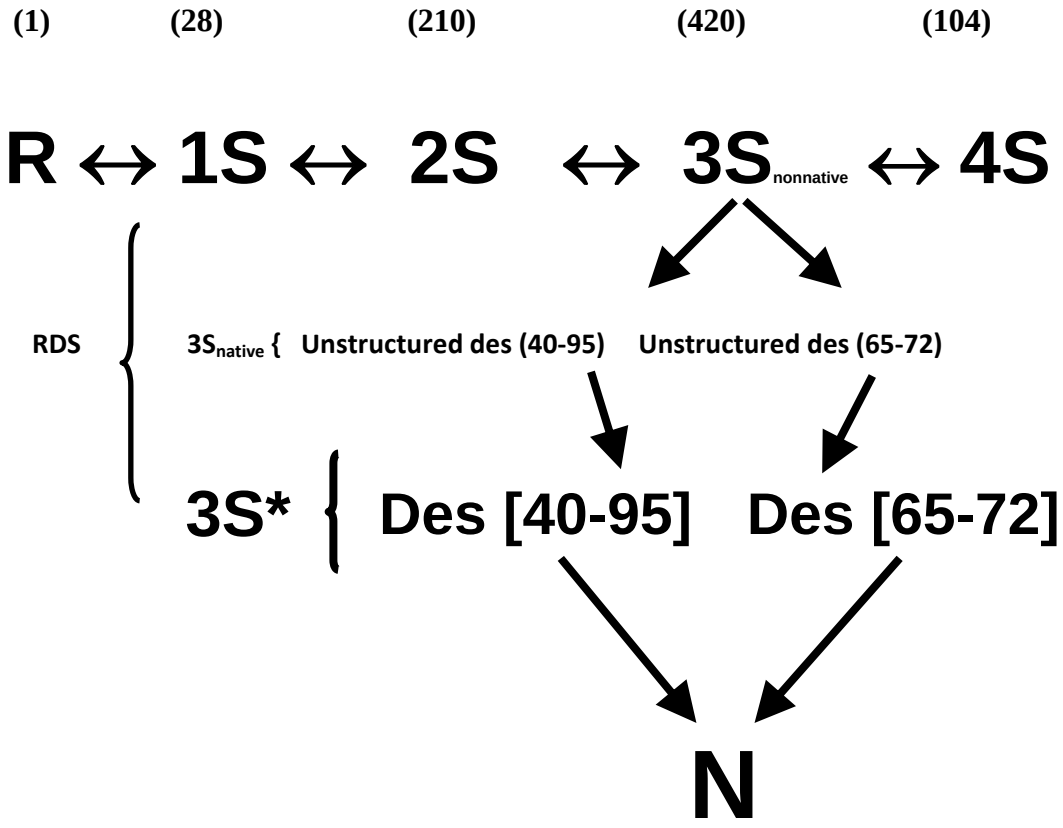

Figure 2.1. Regeneration scheme of RNase A (pH 8, 25 ^{o}C). R, 1S, 2S, 3S and 4S are unstructured intermediates (the numbers above each species refers to the number of existing isomers when no mixed disulfide containing intermediates are present; such as when using glutathione as the redox reagent). Des [40-95] and Des [65-72] are native-like three-disulfide-bond-containing intermediates and are also referred to as the 3S* species. They are formed from their unstructured native-disulfide-bond-containing precursors (collectively known as 3Snative)

by a conformational folding reaction in the rate-determining step (RDS; 3S→3S*). N is the native protein and is eventually formed by oxidation of native-like 3S* species.

The RDS in most oxidative folding pathways, including that of RNase A, is composed of chemical and physical half-processes (5-7). The chemical half of the RDS in RNase A involves thiol-disulfide exchange reactions to populate an unstructured intermediate with native disulfide bonds ($3S_{native}$) from its nonnative-disulfide-bond-containing isomers ($3S_{nonnative}$) [($3S_{nonnative} \rightarrow 3S_{native}$) (Fig. 2.2). For example, consider the formation of unstructured Des (40-95) from its 419 unstructured 3S isomers (Panel B). These isomers must chemically reshuffle to produce an unstructured intermediate ($3S_{nonnative}$) that is one step away from a chemical reshuffling reaction to produce unstructured Des (40-95). Such a $3S_{nonnative}$ species will contain two native disulfide bonds (solid lines) and one nonnative disulfide bond (dotted line). Similar scenarios are depicted for unstructured Des (65-72) in Panel C. In both cases, the statistical dependence of the formation of unstructured Des (40-95) and Des (65-72) from 419 isomers prolongs the process and contributes to the step becoming rate-determining.

The physical half of the RDS involves a conformational folding event; viz., the native-disulfide-bond-containing intermediate ($3S_{native}$) conformationally folds to generate a native or native-like structure (3S*) that preserves newly acquired native disulfide bonds by preventing access to chemical exchange (5-7).

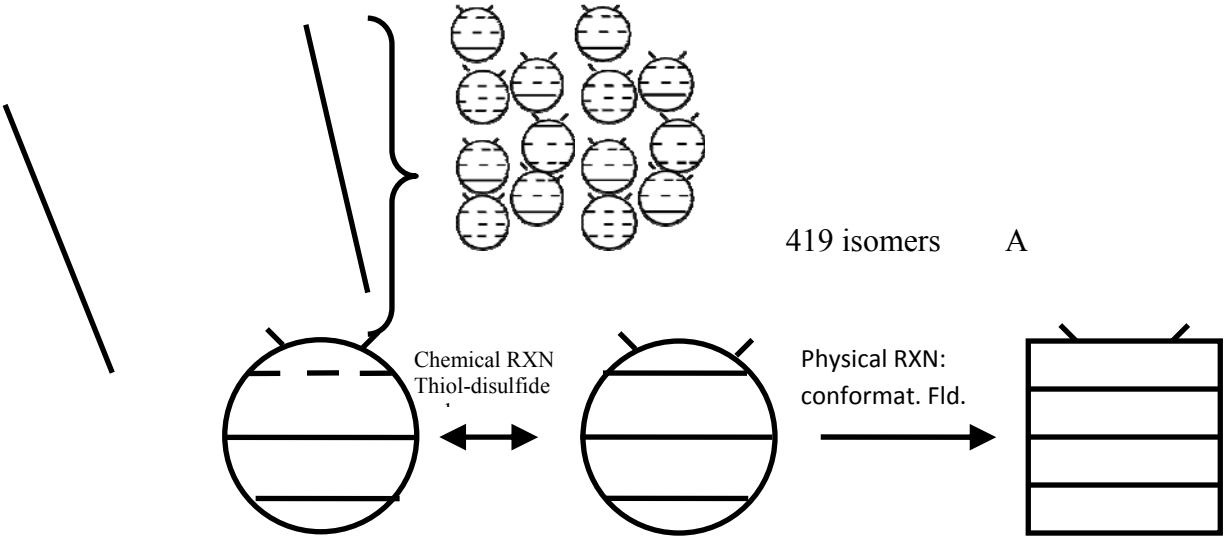

$3S_{nonnative}$ $3S_{native}$ 3S*

B

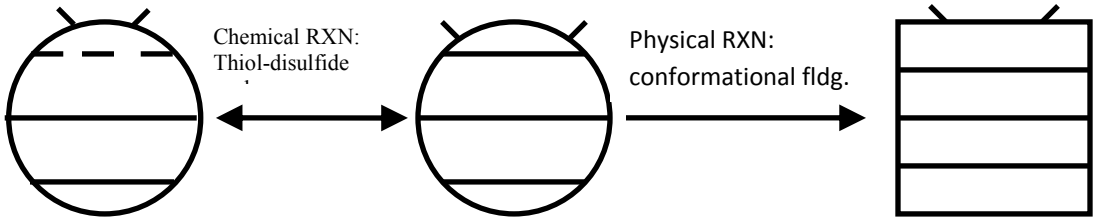

$3S_{nonnative}$ Unstructured des (65-72) Des [65-72]

C

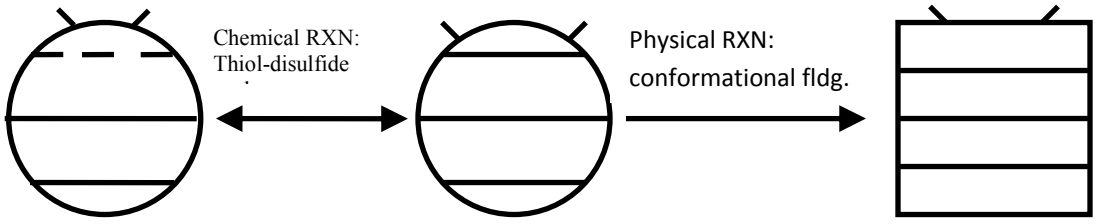

$3S_{nonnative}$ Unstructured des (40-95) Des [40-95]

Figure 2.2. Representation of the rate-determining step (RDS) involving the formation of a structured species from its unstructured precursors via thiol disulfide exchange (chemical reaction) and confornmational folding (physical reaction) during oxidative folding. Dashed horizontal lines are nonnative disulfide bonds in an unstructured intermediate, viz. $3S_{nonnative}$; Solid horizontal lines are native disulfide bonds in unstructured ($3S_{native}$) and structured intermediates (3S*). Vertical lines are thiols. A competition exists between reshuffling (isomerization) reactions [$3S_{native} \leftrightarrow 3S_{nonnative}$] and the structure-forming step [$3S_{native} \rightarrow 3S^*$]. A) Generic pathway of a RDS involving the formation of 3S* via thiol disulfide chemical reactions and a physical conformational folding reaction from its unstructured isomers. B) Pathway showing the formation of des [65-72] from unstructured des (65-72) in RNase A RDS C) Pathway showing the formation of des [40-95] from unstructured des (40-95) in RNase A RDS. (RXN in figure stands for reaction).

The physical conformational folding reaction is pivotal to the oxidative folding process because it removes the newly-structured intermediate from the quasi-equilibrium pool of unstructured intermediates that are prone to unfruitful oxidation, reduction and reshuffling reactions (Fig 2.1) (8, 9).

Importantly, the physical conformational folding half of the RDS competes with its chemical counterpart (thiol-disulfide exchange reactions) (Fig. 2.2) (5-7, 11, 12). The forward conformational folding reaction ($3S_{native} \rightarrow 3S^*$) must outcompete back-reshuffling reactions ($3S_{native} \rightarrow 3S_{nonnative}$) if a structured (native-like or native) species is to be formed (10, 13).

In RNase A, proline isomerization slows conformational folding of both unstructured des (40-95) and unstructured des (65-72) to des [40-95] and des [65-72], respectively. Therefore, a

major fraction of $3S_{native}$ species formed in each case reshuffles to its precursor nonnative disulfide-bond containing isomer ($3S_{nonnative}$) which can then reshuffle to any of the other 419 nonnative disulfide-bond-containing unstructured isomers (13). Thus, unless a $3S_{native}$ species can fold rapidly, it becomes susceptible to thiol-disulfide exchange. Another search through a series of time-consuming chemical exchange steps is then required to repopulate $3S_{native}$.

In other protein folding scenarios, the dependence of tertiary structure on a cofactor may impact conformational folding rates. The competition betIen the "chemical" thiol-disulfide exchange reaction and the "physical" conformational folding reaction are unique to disulfide-bond-containing proteins (7). *In vivo*, oxidative protein folding is catalyzed by protein disulfide isomerase (PDI) which possesses oxidase and "shufflase" activity using surface-exposed cysteines residues (Scheme 1.3) (12, 14-17). Although *in vitro* studies have demonstrated that PDI is able to accelerate oxidative folding reactions and catalyze the regeneration of multi-disulfide-bond-containing proteins including RNase A (18), the impact of PDI and its domains on the pivotal structure-coupled step that immediately precedes maturation is yet unknown. Furthermore, even under surveillance by PDI, a large fraction of ER-processed proteins misfold, and are trafficked to the proteosome (4).

Given this scenario, and that PDI is the principal machinery charged with oxidative maturation of ER-processed proteins, it is of interest to examine its catalytic impact on both the structure-coupled step and the overall rate-determining step in oxidative folding, which is the subject of this study.

Heretofore, a study of the impact of PDI on the physical half of the RDS has not been reported; this is now made possible by deconvoluting the chemical half of the RDS from its

physical half and is essential to obtain a fundamental understanding of the impact of PDI on the microscopic steps of the RDS. Note that the RDS generally precedes maturation and export from the ER of disulfide-bond-containing proteins. In this study, I report a tool to exclusively populate native-disulfide-containing intermediates in unstructured forms that are poised-to-fold or backreshuffle to "futile" unfolded precursors. The described biochemical inroad permits a deconvoluted study of the physical half-process in the rate-determining step from its chemical counterpart and facilitates assessment of PDI's impact on this step and on ER trafficking in general. My results reveal that though the chief ER-resident oxidoreductase successfully catalyzes the overall rate-determining step in RNase A regeneration, it hampers the piviotal structure-forming step in the maturation of RNase A and other ER-processed proteins. Furthermore, the chaperone and isomerase catalytic activities of PDI contrast in their ability to accelerate the formation of the native fold. The implications of these results on trafficking in the ER, protein misfolding and the onset of neurodegenerative disorders are discussed.

2.2 Materials and Methods

Materials.

RNase A was purchased from Sigma and purified as previously described (8). Protein disulfide isomerase, null PDI and ab, b'a' and bb' constructs were gifts from the laboratory of Prof. Arne Holmgren (Karolinska Institute, SIden) and were expressed and purified as previously described (19). Oxidized and reduced dithiothreitol (DTT^{ox} and DTT^{red}, respectively) were purchased from Sigma and used without further purification. All other chemicals were of the highest grade commercially available.

Preparation of fully-reduced RNase A.

Fully-reduced RNase A (R) was prepared by incubating native protein (10 mg/ml) in 6 M Gdn HCl and 100 mM DTT^{red} (pH 8, 100 mM Tris-HCl, 1 mM EDTA) for a period of 2 hours (8). The mixture was then repeatedly dialyzed against 50 mM acetic acid at 4 ^{o}C prior to lyophilisation. The fully-reduced protein was dissolved into 10 mM acetic acid to obtain a stock solution (5 mg/ml protein) that was kept frozen (-20^{o}C) until further use.

HPLC isolated Des [40-95] and Des [65-72] were pooled and introduced into 6 M GdnHCl (pH 8, 100 mM Tris-HCl) as previously described (13). After 5 minutes, the pH of the solution was quenched by the addition of 20 μL glacial acetic acid. The sample was then desalted using a G-25 column and lyophilized.

Reductive unfolding of native RNase A (5 mg/mL) was initiated by incubation of the protein in a buffer containing 100 mM DTT^{red} (pH 8, 100 mM Tris-HCl, 1 mM EDTA, 15 ^{o}C). 20 hrs after initiation of reduction, glacial acetic acid was added to reduce the pH to 3. The sample was desalted using a G-25 column and native-like Des [40-95] and Des [65-72] Ire separated using strong cation-exchange chromatography as previously described (9).

Des [40-95] and Des [65-72] were pooled and introduced into a pH 2 buffer (containing 50 mM acetic acid) as previously described (13). After 30 minutes of incubation, the solution was freeze-dried and the lyophilized protein was introduced into a buffer containing 20 mM acetic acid (pH 3).

Oxidative folding of RNase A.

Aliquots of fully-reduced RNase A (30 μM final conc.) were incubated into solutions (pH 8, 50 mM DTT^{ox}, 20 mM Tris-HCl, 1 mM EDTA, 25 ^{o}C) containing either 4 μM of WT PDI, ab, bb' or b'a' domains. [Note: The use of DTT^{ox}, a weak oxidizing agent permits good kinetic control over regeneration rates and does not lead to the formation of mixed disulfide bonds. DTT^{red} is not initially added to the regeneration mixture because it is naturally formed upon oxidation of protein thiols to disulfide bond] A control experiment that did not contain PDI or any of its domains was run in parallel (8). Aliquots from the regeneration mixture were withdrawn at several time points after the initiation of oxidative folding and subjected to a reduction-pulse [(application of 2 mM DTT^{red} for a period of 2 minutes) (9)], before addition of glacial acetic acid (which reduced the pH to 3). Samples were desalted on a G-25 column prior to application on a C-18 column for reversed-phase chromatographic analysis.

The rate of regeneration of the native protein (N) was determined by integrating the areas of the peaks corresponding to the native protein (N), any structured intermediates (3S*) and the fully-reduced protein (R) at each time point. The fractional increase in N was plotted as a function of time; the data were fitted to a single-exponential function to obtain the rate constant for the formation of N from R (20).

Impact of PDI on the rate-determining step (3S→3S) of RNase A regeneration.*

Lyophilized 3S was introduced into a folding buffer (30 μM protein, pH 8, 100 mM Tris-HCl). Aliquots were withdrawn and subjected to the reduction-pulse at various time intervals (13). The reaction was quenched and then analyzed by HPLC as described above (section 2.4). In other experiments, the folding buffer contained either 4 μM WT-PDI or its constructs. The rate

of formation of 3S* was determined from analysis of the peak areas corresponding to 3S* and $3S_{nonnative}$ (R) as a function of time, as described previously (20).

Preparation of $3S_{native}$ (an intermediate "poised-to-fold").

Des [65-92]and Des [40-95] Ire obtained by strong cation-exchange fractional separation of native RNase A that had been exposed to strongly reducing conditions as previously described (I.e through reductive unfolding of the native protein) (6, 13). Des [65-72] and Des [40-95] were separately collected and desalted on a reversed phase HPLC.

They were then lyophilized before being separately introduced into solutions of dilute acetic acid (50 mM) as previously described to obtain unstructured Des (65-72) and unstructured Des (40-95), respectively (13).

Impact of PDI and its domains on the structure-forming step of RNase A.

$3S_{native}$ species (i.e., unstructured Des (65-72) and unstructured Des (40-95)) incubated at pH 2 in 50 mM acetic acid (and added HCl to bring the pH to 2) was introduced into a pH 8.2 solution (100 mM Tris-HCl, 1 mM EDTA) such that the final pH was 8 (30 μM protein). One minute later, the sample was subjected to a reduction pulse, as described above (section 2.4). All samples were then desalted and analyzed by reversed-phase HPLC (C18 column; 1%/min acetonitrile gradient).

The reduction pulse facilitates reduction of any unstructured intermediate such as unreacted $3S_{native}$ and its chemical isomerisation product ($3S_{nonnative}$) to the fully-reduced protein (R) (6). These can be easily separated on a reversed phase column as described above. The peak areas

corresponding to 3S* and the fully-reduced protein (R) are integrated to obtain the fraction of 3Snative that was able to fold physically and form 3S*.

Percentage of $3S_{nonnative}$ was calculated using the formula (12):

Percentage of $3S_{nonnative}$ = 100 x [peak area (R)]/[peak area (R) + peak area 3S*].

Percentage of 3S* was determined by subtraction of percentage of $3S_{nonnative}$ from 100.

In other experiments reduced wild-type PDI, null PDI or each domain (at 4 μM, respectively) was introduced into the pH 8.2 buffer, prior to introduction of the 3S species.

Measurement of the impact of PDI, null PDI and domains on the structure-forming step was assessed by measuring the areas under the HPLC peaks corresponding to fully-reduced protein (R) and the structured 3S* species as previously described (20, 21).

2.3 Results

Regeneration of RNase A.

The kinetic data pertaining to the regeneration of RNase A Ire fitted to a first-order rate equation, ln (1-N) = -kt, where 1 - N is the fractional concentration of all nonnative species, k represents the rate constant for the formation of the native protein, and t is the reaction time (20). Figure 2.3 is a plot of the regeneration data of RNase A catalyzed by PDI and its sub-domains. The data indicate that the regeneration rate is highest in the presence of WT PDI. For comparison, an uncatalyzed regeneration profile (control) is also included (O) and is in good agreement with previous reports (18).

Figure 2.3. Plot of Ln (1-N) as a function of time. N is the fractional concentration of native RNase A regenerated. The regeneration conditions were (a) pH 8, 50 mM DTT^{ox}, 20 mM Tris-HCl, 1 mM EDTA, 25 ^{o}C for the control, O; b) control + 4 μM PDI, □; c) control + 4 μM null PDI, ▲; d) control + 4 μM ab, x; e) control + 4 μM b'a', ◊; and f) control + 4 μM bb' Δ

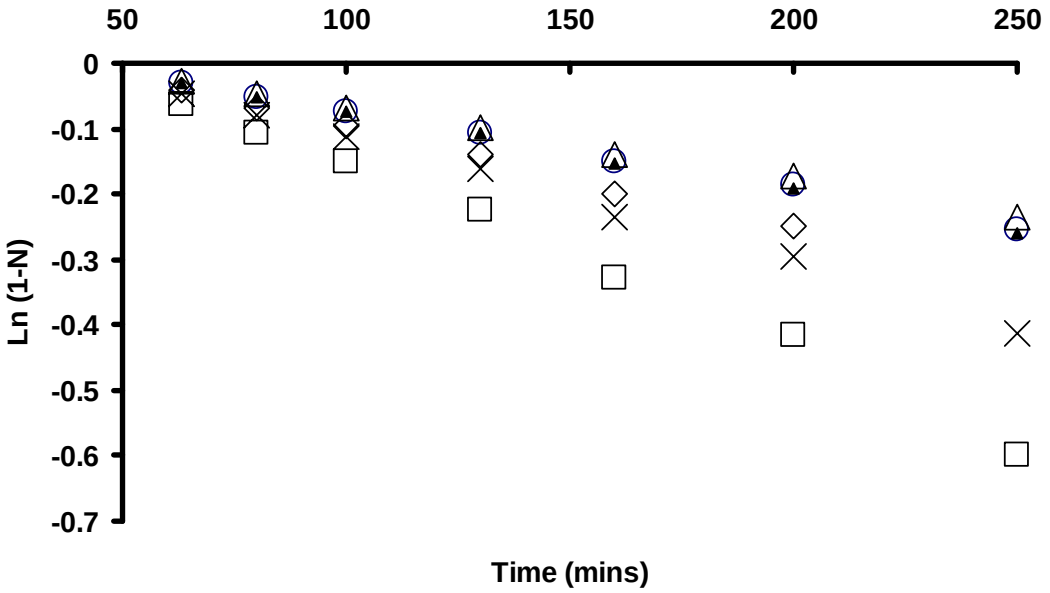

Table 2.1 summarizes the rate-constants for the formation of the native protein as a function of PDI or any added domain. The oxidative folding rate of RNase A (50 mM DTTox, pH 8) is enhanced by the presence of composite ab and b'a'. At pH 8, a ~ 2.1-fold increase in the rate of formation of the native protein is observed in the presence of ab (4 μM) whereas a 1.5-fold enhancement is induced by b'a', compared to the control. These values are relatively low compared to catalysis by WT PDI (7.4-fold increase over the control). The addition of the hydrophobic bb' did not impact, within error, the oxidative regeneration of RNase A (Table 2.1).

Table 2.1. Regeneration of RNase A (50 mM DTT^{ox}, 100 mM Tris-HCl, 1 mM EDTA, 25 ^{o}C)

Folding condition pH 8	Rate constant (pH 8) for R→N ($x10^4$ min^{-1})	Catalytic impact (Adjuvant/control)
R	11 ± 0.5	-
R + 4μM WT PDI	81.3 ± .4	7.4
R + 4μM null PDI	11.2 ± 0.1	1.02
R + 4 μM ab	23 ± 0.3	2.1
R + 4 μM b'a'	16 ± 0.25	1.45
R + 4 μM bb'	10.3 ± 0.7	0.93

Measurement of the impact of PDI on the rate-determining step (3S→3S) of RNase A regeneration.*

Table 2.2 lists the rate constants for the formation of 3S* species at pH 8 as a function of added domain. WT PDI catalyzed the formation of 3S* from its 3S ensemble by a factor of ~11, over the control (without PDI). The individual domains had lesser catalytic efficiencies; the ab and b'a redox-active domains contributed approximately two-fold over the rate observed in the uncatalyzed reaction. The bb' domain does not appear to impact the reaction of the control experiment.

Table 2.2. Rate-constants (min^{-1}) for the formation of 3S* species of RNase A from their unstructured 3S isomers as a function of added PDI or PDI domain (4μM, pH 8, 100 mM Tris-HCl)

Adjuvant	akf [3S→3S*] (-PDI) (×103)	kf(Adjuvant)/kf(control)
Control	1.6 ± 0.2	-
WT PDI	18 ± 0.7	11.25
Null PDI	2.1 ± 0.4	1.3
ab	4 ± 1.3	2.5
b'a'	3.2 ± 0.3	2
bb'	1.75 ± 0.4	1.1

Measurement of PDI and mutant variant impact on structure-forming step of disulfide-bond-containing proteins.

Figure 2.4 depicts a typical HPLC chromatogram showing the formation of 3S* species and $3S_{nonnative}$ from $3S_{native}$ (at a particular time along the reaction pathway; using Des (65-72)). The peak labeled R corresponds to $3S_{nonnative}$. This is because the applied reduction pulse converts unstructured intermediates to R (21).

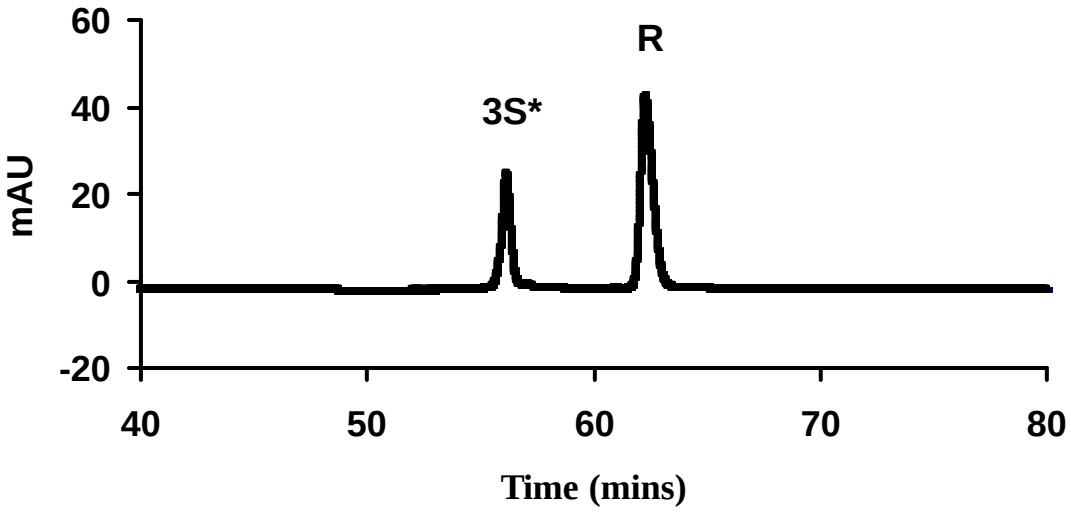

Figure 2.4. Typical reversed-phase HPLC chromatogram (C18 column) showing results of the competition between the structure forming step ($3S_{native} \rightarrow 3S^*$) and thiol-disulfide exchange reactions ($3S_{native} \rightarrow 3S_{nonnative}$). Any 3S* formed by the physical conformational folding reaction of $3S_{native}$ can easily be separated from the remainder of $3S_{native}$ that chemically reshuffles and isomerizes to forms $3S_{nonnative}$ and eventually populates all 419 unstructured isomers. This is possible by the application of a reduction pulse that reduces any unstructured intermediate (such as $3S_{nonnative}$ and 419 isomers) to the fully-reduced protein (R). Reversed-phase HPLC is then used to separate 3S* from R (formerly $3S_{nonnative}$ and 419 unstructured isomers). The fraction of 3S* formed can then be quantified as described in Materials and Methods.

Table 2.3 summarizes the quantity of $3S_{native}$ species that conformationally folds to a stable intermediate (3S* species). Note: the results Ire identical whether Des (65-72) or Des (40-95) was used as the starting material. Hence, Des (65-72) was used because quantity in hand was larger than the quantity of des (40-95) that was available. In the absence of any added PDI or PDI subdomain, ~ 32% of the $3S_{native}$ species is able to conformationally fold to the stable 3S*

intermediate, in agreement with previously reported literature (13). The addition of WT PDI results in a large decrease in the amount of 3S* formed (eight-fold over the control). Similarly, the rate of formation of 3S* by conformational folding of $3S_{native}$ is reduced addition of either ab or b'a' composite domains, although their ability to reshuffle $3S_{native}$ to $3S_{nonnative}$ is diminished relative to WT PDI. In contrast to these results, the addition of null PDI or the hydrophobic bb' domain results in an enhanced conformational folding rate of the $3S_{native}$ species to 3S* relative to the control that lacks PDI (40% and 38% respectively, relative to 32%).

Table 2.3. Measurement of oxidoreductase impact on structure-forming step of RNase A (pH 8, 100 mM Tris-HCl, 25 ^{o}C)

Species	$3S_{nonnative}$ (%)	3S* (%)
-	68 ± 1.7	32 ± 1.4
WT PDI	96 ± 2.2	4 ± 1.2
Null PDI	60 ± 0.7	40 ± 0.34
ab	81 ± 0.8	19 ± 1.9
b'a'	79 ± 0.67	21 ± 0.89
bb'	62 ± 2.3	38 ± 1.22

2.4 Discussion

In vivo, oxidative protein folding takes place within the oxidizing environment of the ER lumen (4). Within the ER environment, nature has invested in an oxidoreductase chaperone, protein disulfide isomerase (PDI), which facilitates rapid exchange betIen thiols and disulfides and catalyzes oxidative folding of "substrate" proteins (15, 23, 24).

However, during maturation of disulfide-containing proteins, the rate-determining step is often a composite process comprised of chemical and physical half-processes (5-7). Furthermore, the physical conformational folding reaction that is required for the generation of native (native-like) structure competes with thiol-disulfide exchange reactions (such as reduction and/or isomerization reactions) (Figure 2.2). The role of PDI in the pivotal conformational folding step, which inherently competes with thiol-disulfide exchange, has heretofore not been explored.

In this study, I have examined the impact of PDI and its domains on the rate-determining step in the regeneration of RNase A, with emphasis on dissecting its role in conformational folding of RNase A and other disulfide-bond-containing proteins. Furthermore, I have also studied the role of null and domains ab, b'a' and bb' in the RDS of RNase A oxidative regeneration. The ab and b'a' are composite in that they contain both redox-active and hydrophobic components and permit "overall" assessment of mixed domain contribution to the structure-coupled step; bb' is a largely hydrophobic domain previously implicated in chaperone activity (17). This domain permits assessment of the contribution of the hydrophobic domain of PDI to the rate-determining and conformational folding steps.

The viability of each expressed domain was examined by evaluating its ability to regenerate fully-reduced RNase A. Regeneration data of fully-reduced RNase A (Table 2.1) indicates that

both composite domains are catalytically active in agreement with previous studies (19). Null PDI and the hydrophobic bb' domain does not significantly impact the overall oxidative folding rate at both pH's tested (Table 2.1). Taken together, the results obtained suggest that catalysis of redox reactions play a greater role in facilitating oxidative folding than any "chaperone-like" activity.

The roles of WT PDI and sub-domains in catalyzing the rate-determining step of RNase A regeneration Ire next examined. Since the formation of $3S_{native}$ is mandatory to conformational folding (species with nonnative disulfides do not acquire stable tertiary structure (5)), a catalyst that can increase the frequency with which $3S_{native}$ forms from its unstructured isomers ($3S_{nonnative}$) would catalyze the overall formation of 3S* from $3S_{nonnative}$ (the RDS). The hydrophobic domains, along with null PDI, barely impact the RDS, suggesting that hydrophobic interactions do not play a significant role in the RDS.

To investigate the role played by PDI and its domains in the pivotal structure-forming step of the oxidative folding process I first populated a RNase A transient three-disulfide intermediate containing only native disulfide bonds ($3S_{native}$) by pH denaturation of (native-like) structured RNase A intermediates, Des [40-95] and Des [65-72] (13). This technique results in the preservation of native disulfide bonds (by protonating cysteine sulfurs) while resulting in the denaturation of the native-like des species. i.e. 3S* is converted to $3S_{native}$ at low pH and native disulfide bonds are prevented from becoming reshuffled through intramolecular thiol-disulfide exchange. Through this tool, the previously transient intermediate ($3S_{native}$) is now "frozen" and amenable to further experimentation. Similarly, through analogous chemical tools I was able to manipulate and trap ALAC and C65AC72A RNase A into states that are "poised-to-fold" (not

shown). This biochemical inroad is critical to deconvoluting the physical folding step from the chemical thiol-disulfide-exchange step in the RDS of oxidative protein folding.

In the absence of any added PDI/sub-domain, my data indicate that 30% of the $3S_{native}$ species conformationally folds to form structured (native-like) 3S* species (Table 2.3). The remainder back-reshuffles to $3S_{nonnative}$ due to intramolecular attack by free cysteines on the native disulfide bonds before the conformational folding reaction can lock in the native disulfide bonds within stable tertiary structure. In the conformational folding of RNase A, proline isomerization is rate-limiting and hence back-reshuffling predominates (~70% of $3S_{native}$ is backreshuffled to $3S_{nonnative}$) (10, 13). The addition of WT PDI results in a drastic decrease in the percentage of 3Snative that can undergo successful conformational folding to form 3S* (Table 2.3). This is because PDI cysteine's accelerate the thiol-disulfide exchange betIen free cysteines of $3S_{native}$ and its native disulfide bonds and convert native bonds to nonnative bonds. The PDI-facilitated thiol-disulfide exchange outcompetes the conformational folding of 3Snative to 3S*. Hence, a larger fraction of $3S_{native}$ is converted to $3S_{nonnative}$ in the presence of PDI. The addition of null PDI or the hydrophobic bb' domain results in a slightly improved conformational folding rate as evident from the percentage of 3S* formed (Table 2.3).

This may be due to binding of the hydrophobic bb' domain to the unstructured 3Snative species and stabilization of the unstructured intermediate in agreement with previous peptide binding data which suggest that the bb' domains are able to bind to unstructured peptides (17). In conjunction with results obtained upon the addition of WT and null PDI, the addition of composite ab and b'a' domains confirmed that the redox-active domains have a higher impact on back-reshuffling than the hydrophobic domain has on the forward rate resulting in a net loss in formation of structured-intermediates in the presence of PDI.

Importantly, my data demonstrate remarkable conflicting catalytic actions of PDI and its domains on the pivotal structure-forming step which precedes maturation of disulfide-bond-containing proteins. Although WT PDI facilitates oxidative folding and catalyzes the RDS, by virtue of its redox-active domains it is highly detrimental to the forward folding reaction of those species that are poised to conformationally fold (viz., RNase A $3S_{native}$ species). On the other hand, null PDI and the hydrophobic bb' domains bestow chaperone-like conformational folding assistance during the structure-forming step (as seen in RNase A $3S_{native}$ species) even though they do not have a significant effect on the overall regeneration rate and the RDS.

Notably, the highly evolved redox-activity of PDI, finely tuned to catalyze the highly redox dependent oxidative folding process becomes self-limiting in the pivotal and mandatory conformational folding event in oxidative regeneration. It overwhelms the promotion of the forward reaction by the limited chaperone-activity demonstrated by the hydrophobic domains. The impact of PDI on the various stages of oxidative folding is discussed, using the RNase A regeneration pathway as a model.

Previous data have shown that PDI accelerates oxidation and isomerization reactions along the regeneration pathway of ER-processed proteins (15, 16, 18). In this study, I demonstrate that the oxidoreductase activity of PDI is instrumental in accelerating the RDS of RNase A regeneration. However, I also observed that PDI hampers the conformational folding step, which forms the latter half of the RDS. I.e. the ~11-fold acceleration in the RDS includes an observed 8-fold inhibition in the formation of 3S* due to back-reshuffling of species that are poised to fold. The highly evolved oxidoreductase activity of PDI thus limits its full potential in catalyzing the RDS and the overall oxidative folding rate. In other model folding scenarios involving disulfide-bond-containing proteins, the presence of PDI was again detrimental.

Chapter 3:

EF24 Intervention in Free-Radical Stress-Mediated Dysfunction of Protein Disulfide Isomerase

3.1 Introduction

Oxidative folding of disulfide-containing proteins is a well-established method for understanding protein folding mechanisms of disulfide-bond-containing proteins (1). Oxidative protein folding comprises chemical and physical conformational changes which allow construction of so-called disulfide folding pathway of a fully-reduced and denatured disulfide bond-containing protein (2). Oxidative folding permits tracking and identification of partially oxidized intermediates. This technique, first used in the study of bovine pancreatic trypsin inhibitor (BPTI) and bovine pancreatic ribonuclease A, has been applied in elucidating the folding pathway of numerous disulfide bond-containing proteins (2). It has long been studied as a means to understand how the disulfide-bond reactions in proteins may be used to investigate protein structure and stability, as well as the mechanism of protein folding (3).

Thiol/disulfide exchange is the prime chemical reaction involved in disulfide-bond studies in which the thiolate anion R_1S^- displaces one sulfur of the disulfide bond R_2SSR_3 (4, 5); $R_1S^- + R_2SSR_3 \rightarrow R_2S^- + R_1SSR_3$ (Scheme 3.1). The formation and reduction of disulfide bonds consisted by two such thiol/disulfide exchange reactions with a redox reagent, the first of which involves the formation of a mixed disulfide bond between the protein and the redox reagent (3). Thiol/disulfide exchange reactions can also occur intramolecularly; e.g., a protein thiolate group may attack a disulfide bond of the same protein, leading to disulfide reshuffling (3).

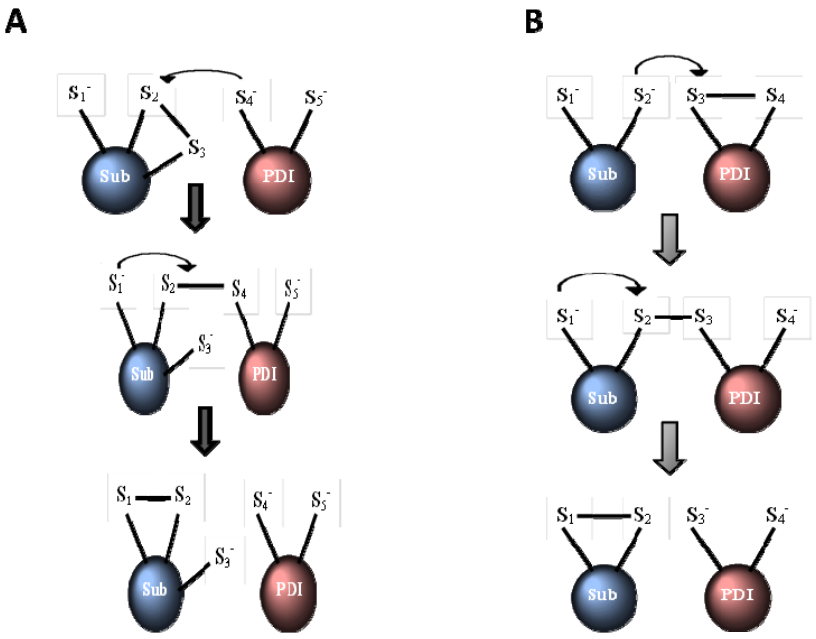

Scheme 3.1. Schematic diagram shows the activity of PDI on disulfide bond containing model protein folding; (A) Isomerization activity of PDI; (B) Oxidation activity of PDI.

Since the chemical reaction of formation of disulfide bond mainly goes through the oxidation of thiols, disulfide bonds can be formed spontaneously by molecular oxygen. For instance, under aerobic conditions, a thin layer of cystine is generated at the air–liquid interface when a cysteine solution is left exposed to air (6). However, this type of spontaneous, random air-oxidation reaction is slow and insufficienct to meet protein throughput within a cell (6). This discrepancy resulted in studies leading to the discovery of the catalyst for disulfide bond formation (6). The search for enzymatic catalysts of oxidative refolding led to the finding of chief ER-resident oxidoreductase chaperone, protein disulfide isomerase (PDI) (Scheme 1.3) (7). Intensive

investigation of the activities of PDI *in vitro* has shown that the enzyme can catalyze the oxidation or isomerization of disulfide bonds depending upon the redox conditions of the assay and the nature of the substrate protein (8). PDI function is thus important role in regulating traffic along the secretory pathway, for prevention of terminally misfolded proteins that would otherwise constitute traffic along the retrotranslocatory pathway and mitigation of several neurodegenerative diseases onset (9).

The activity of PDI mostly depends on two pairs of cysteines located within a domain homologous (a and a' domains) to thioredoxin and each of which are found in the motif Cys-X-X-Cys (10). The disulfide (oxidized) form of cysteines of PDI can transfer disulfide bonds directly to substrate proteins, suggesting a physiological role for PDI as a protein dithiol oxidase. However, when the active-site cysteines of PDI are present in dithiol (reduced) form, the enzyme is suited for catalysis of disulfide reshuffling. The thiol/disulfide exchange ability of PDI also leads the correction of incorrect disulfide bond formation (11).

Applications of disulfide-bond chemistry in studies of protein folding, structure, and stability are highlighted and illustrated with α-Lactalbumin (α-LA) (Fig. 3.2). The general properties and advantages of disulfide-bond studies have great impact on oxidative folding of α-Lactalbumin in the structure formation during the regeneration of the native disulfide bonds. The structure of α-LA consists of an α-helical and a β-sheet domain which are stabilized by by binding to calcium ions (12-14). During the fold-maturation of α-LA, a partially folded intermediate α-LA-IIA is generated which is capable of folding to form native α-LA (15). Reduced α-LA-IIA comprises a structured β-sheet (calcium-binding) domain linked by two native disulfide bonds (Cys61-Cys77 and Cys73-Cys91) and an unfolded reduced-helical domain with four reduced free cysteines (Cys6, Cys28, Cys111, and Cys120) (2).

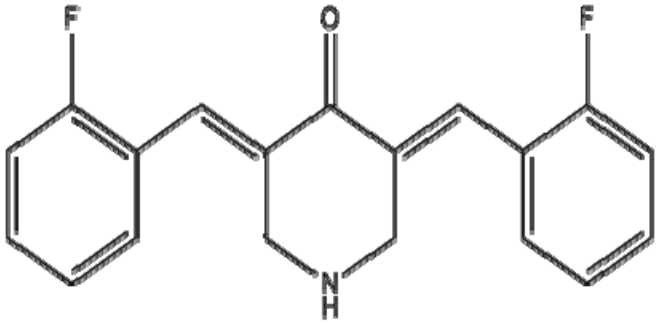

Figure 3.1. Diagram of EF24

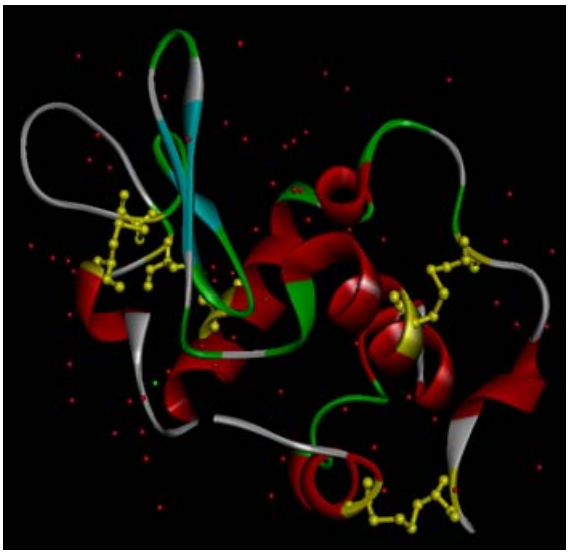

Figure 3.2. Diagrams of α-lactalbumin, PDB: 1HFX, the yellow color representing the disulfide bridges of the protein.

As the impact of ROS has been discussed on page 14, free radicals, such as peroxynitrite, nitrogen dioxide, hydroxyl radicals have become immensely significant in recent (16). Free radical NO* and *OH undergo variety of reactions including hydrogen atom abstraction from

thiols (17). This free radical-based stress can induce posttranslational modifications, resulting in overall conformational and structural changes in disulfide-bond containing proteins (18). It is well-known that cysteine residues (Cys) in proteins are prominent targets for protein oxidation, as they easily react with NO* and *OH free radicals. Oxidation of Cys by free radicals involves nucleophilic attack of the cysteine thiol group on the electrophilic center of free radicals. Deprotonation of the Cys thiol group to generate the thiolate anion increases its nucleophilicity, and hence reactivity towards free radicals (Scheme 3.2) (18).

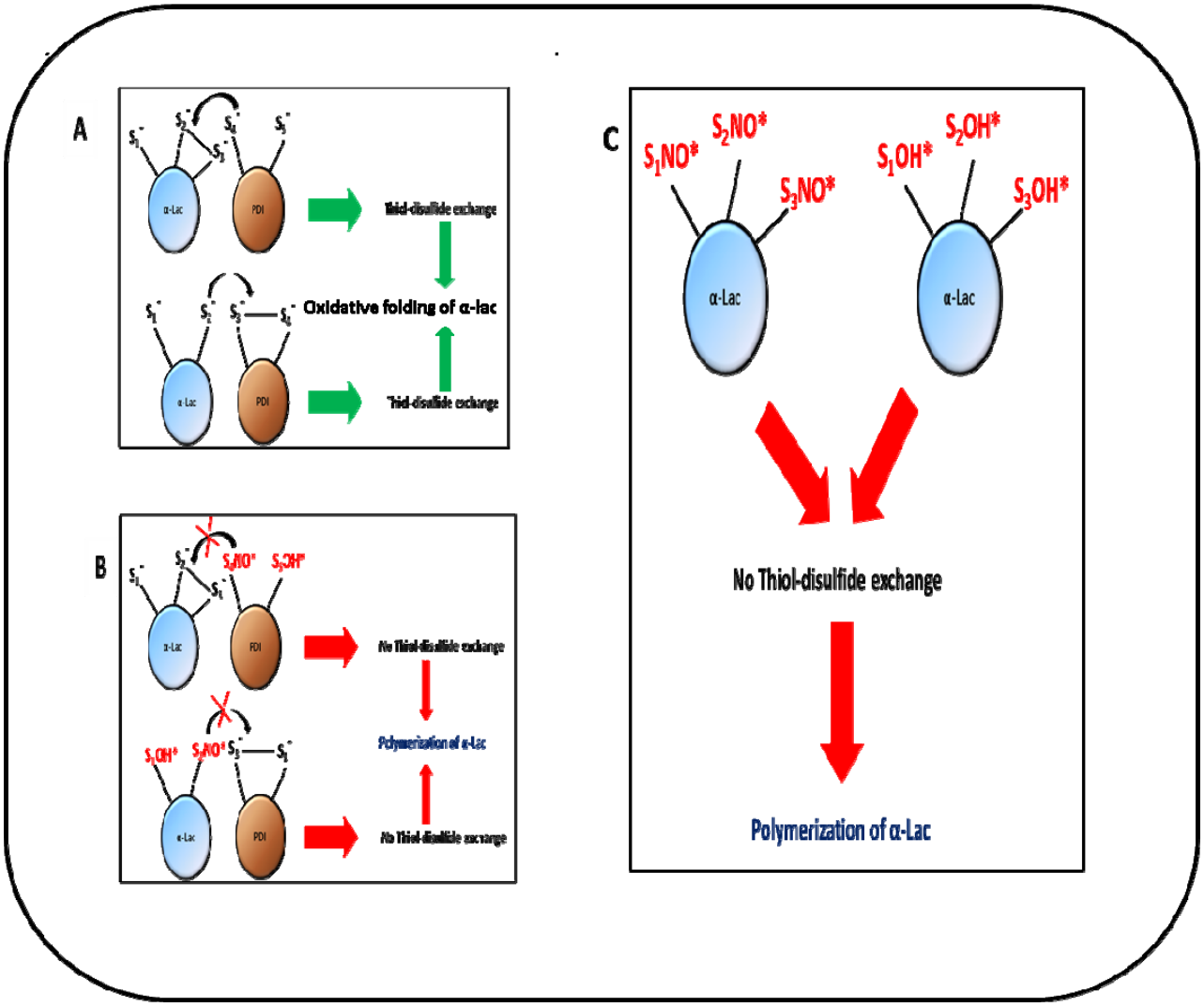

Scheme 3.2. Schematic diagram shows thiol-disulfide exchange between α-Lac and PDI, α-Lac itself; (A) Free thiols of α-Lac and PDI are capable of thiol-disulfide exchange leads oxidative folding of α-Lac, (B)Free radical stress on thiols causes hindrance in thio-disulfide exchange between α-Lac and PDI leads polymerization of misfolded α-Lac and (C) Free radical stress on thiols causes hindrance in thiol-disulfide exchange within α-Lac leads polymerization of misfolded α-Lac.

In this dissertation I have exposed α-LA to NO* and *OH radicals during its oxidative folding. I have found the formation of high molecular weight of polymeric α-LA. My data confirms the hypothesis that free radicals cause hindrance in disulfide-bond mediated oxidative protein folding by reacting with thiols (17). This ultimately results in aggregation of misfolded proteins and polymer formation. Since PDI increases the rate of oxidative folding of disulfide-bond containing proteins, I have also examined the catalytic activity of PDI under nitrosative stress during the oxidative folding of completely reduced α-LA.

The present investigation also was designed to determine the ability of the polyphenol, Diphenyl difluoroketone, (EF24, Fig. 3.1) to scavenge the free-radicals. Curcumin and masoprocol have already been used clinically and approved by the FDA to scavenge excess ROS and protects cysteinyl thiols from free radical stress (9) (Table 3.4). Currently, EF24 is being used as an anticancer drug and found that EF24 is more efficacious and considerably less toxic commonly used chemotherapeutic agent (19). My lab is investigating the reactive oxygen species scavenging properties of EF24. In this study, I chose to assay the free radical scavenging property of EF24 to prevent the chemical modification of thiols. My data show that EF24 can scavenge the NO* and *OH by forming stable abducts. Thus EF24 can intervene in the ROS-

induced misfolding of disulfide-bond containing proteins resulting in mitigation of misfolded aggregates.

Human serum albumin (HSA) (Scheme 1.6) is a principal extracellular protein with a high concentration in blood plasma and a carrier of many drugs and endogenous compounds to different molecular targets (20, 21). The physical properties and possible binding domains are discussed in introduction section (Reference 27, 28, 29 in introduction). In this study, the spectroscopic analysis of HSA complexation with EF24 was carried out in aqueous solution at physiological conditions, using constant protein concentration.

3.2 Materials and Methods

Reagents and cell line.

α-Lactalbumin (ALAC; >99.5% purity) was purchased from Sigma Chemical Co. (St. Louis, MO, USA) and used without further purification. PDI was expressed and purified as previously described (22). Reduced and oxidized dithiothreitol (DTT^{red} and DTT^{ox}, respectively) Ire purchased from Sigma Chemical Co and used without further purification. Protein ladder was purchased from Fisher Scientific (PA, USA). EF24 was synthesized in collaboration with Dr. Katja Michael (Dept. of Chemistry, UTEP) using a previously reported procedure (23). It was further purified by HPLC and characterized by mass spectrometry. HPLC analysis of re-purified EF24 showed purity ≥99%. Tetra-nitromethane (TNM) was obtained from Sigma-Aldrich (St. Louis, MO., USA).

Characterization of NO and *OH adducts of EF24*.

A stock soln. of EF24 (prepared by weight in acetonitrile) was diluted to obtain concentrations ranging from 10-200 μM (in acetonitrile). Tetranitromethane was added from a

stock solution (freshly prepared by weight in acetonitrile) to EF24 so as to obtain different ratios of NOx/EF24. EF24 was also exposed to Fenton reaction with 100 μM H_2O_2. The samples were desalted and separated using reversed-phase HPLC (Supelco C18 column; 1% acetonitrile/min) and collected peaks were lyophilized. The lyophilized peaks were analyzed on a Q-TOF mass spectrometer.

Preparation of fully-reduced α-Lactalbumin (αLA).

Fully-reduced α-LA was prepared by incubating native protein (10 mg/ml) in 6 M Gdn- HCl and 100 mM DTT^{red} (pH 8, 100 mM Tris-HCl, 1 mM EDTA) for a period of 2 hours. The mixture was then dialyzed three times against 50 mM acetic acid at 4° C prior to lyophilization. The fully-reduced protein was dissolved into 10 mM acetic acid to obtain a stock solution (5 mg/ml) that was kept frozen (-20°C) until further use.

Native gel electrophoresis.

Native gel 15% was prepared to run protein samples. Fully-reduced α-LA (36 μM final concentration) was incubated with oxidizing buffer (pH 8, 100 mM DTT^{ox}, 100 mM Tris-HCl, 25°C). Regeneration mixture was separately stressed by the addition of 100 μM TNM and 100 μM H_2O_2 via the Fenton reaction. Separate regeneration mixtures were seperately stressed under the same conditions as above after preincubation with 300 μM EF24 to determine the effect of EF24. All samples were collected after 5 hrs and run in 15% native gel.

Densitometric analysis.

Densitometric analysis of all the bands formed in native-gel electrophoresis was done by using Epi Chemi Darkroom, UVP imaging system in the Bio-core facility of Department of Biological Sciences at UTEP.

PDI-catalyzed oxidative folding of α-LA under nitrosative stress and EF24.

Fully-reduced α-LA (36 μM final concentration) was incubated into a solution (pH 8, 100 mM DTT^{ox}, 100 mM Tris-HCl, 25°C) containing 4 μM of PDI and oxidative regeneration was followed as previously described (24). A control experiment was separately performed without the presence of PDI. Aliquots from the regeneration mixture were periodically withdrawn after initiation of oxidative folding and subjected to a reduction pulse (application of 2 mM DTT^{red} for a period of 2 minutes), before addition of glacial acetic acid (which reduced the pH to 3). Samples Ire desalted on a G-25 column prior to application on a C-18 column (Supelco Discovery® BIO Wide Pore C18, 5 μM, 15cm x 100.0mm) for reversed-phase chromatographic analysis using an acetonitrile gradient (1%/min) (9).

In other experiments, EF24 (8 μM final concentration from stock acetonitrile solutions prepared by Iight) was incubated with the regeneration mixture prior to the addition of tetranitromethane (6 μM obtained by dilution of the stock compound). The regeneration and sample analysis was carried out as above. The rate of regeneration of the native protein (N) was determined by integrating the areas of the peaks corresponding to the native protein (N), structured intermediates and the fully-reduced protein (R) at each time point. The fractional

increase in N was plotted as a function of time; the data Ire fitted to a single exponential function to obtain the rate constant for the formation of N from R (9).

Preparation of stock solutions of HSA.

Human serum albumin, obtained from Sigma-Aldrich, was dissolved in aqueous solution (30 mg/40 ml or 13.4 uM) containing 200 mM Tris-HCl, 1 mM EDTA buffer (pH 8). The protein concentration was determined spectrophotometrically using the extinction coefficient 39,900 M^{-1} cm^{-1} at 280 nm (25). Removal of any bound fatty acids to human serum albumin was carried out using a charcoal treatment for 30 minutes followed by 10 minutes of centrifugation at max speed (4000 rpm). EF24 [3,5-bis(2-flurobenzylidene)piperidin-4-one] 3 mM was first prepared in water/ethanol 50% and then diluted to stock of 0.500 μM, 1 mM, and 2 mM in water/ethanol 50%.

Fluorescence spectroscopy.

Fluorimetry-based binding experiments were carried out on a DM-45 Spectrofluorimeter (Olis). Titrations Ire conducted using 100 μL of ligand (500 μM, 1 mM, 2 mM, and 3mM) in 5 μL aliquot addition to 2.0 mL of HSA (Tris-HCL, pH8). The fluorescence spectra were recorded at λexc = 280 nm and λem from 300 to 500 nm. For the fluorescence titrations, the observed emission intensities were converted to a response factor, which is defined as the fractional quenching (enhancement) between the free protein and the saturated 1igand: protein complex. The data Ire fit to a simple hyperbolic binding model by nonlinearegression analysis using DeltaGraph (Deltapoint, Inc, Monterey, California).

3.3 Results

Ability of EF-24 to scavenge NO and *OH radicals.*

Mass-spectrometric analysis was performed to examine the ability of EF24 to form adducts with NO* and *OH. Fig. 3A is a mass spectrum of EF24 prior to treatment with tetranitromethane (MW 312 Da corresponds to protonated EF24). A mass addition of 45 Da to EF24 post TNM treatment is indicative of nitration (Table 3.1). Note: addition of a nitro group adds 46 Da. However, the nitro group replaces a hydrogen atom, resulting in the net addition of 45 Da. Further loss of a proton results in a MW of 356 Da. Fig. 3B is a mass spectrum of EF24 after it is exposed to Fenton chemistry with 100 μM H_2O_2. Mass addition of EF24 due to OH* addition was characterized and reported (Table 3.1).

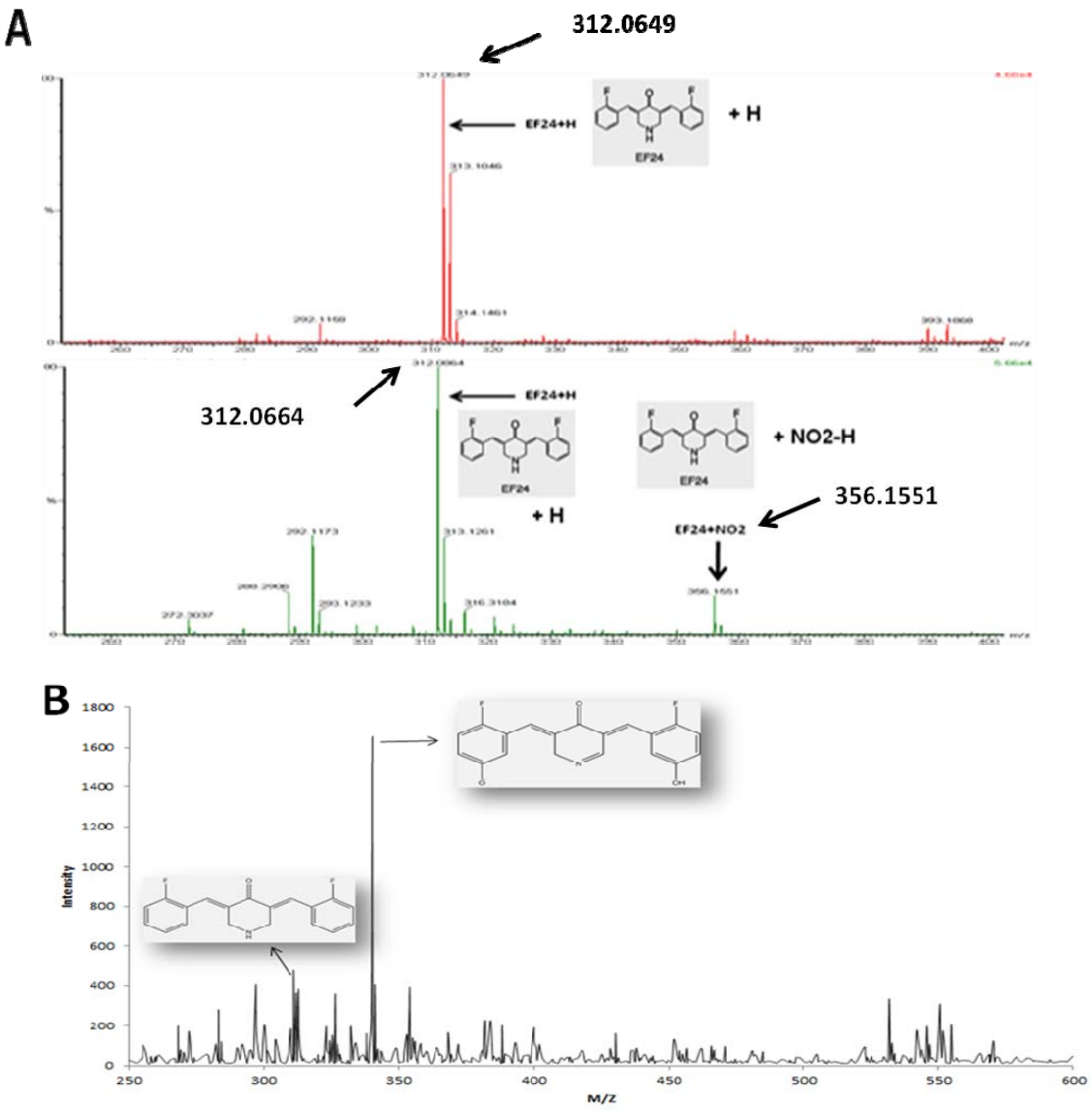

Figure 3.3. (A) MS-QTOF of EF24 exposed to tetranitromethane. Mass addition (~45) indicates the adduction of NO_2 group to EF24; (B) MS-TOF of EF24 exposed to Fenton reaction. Mass addition (~16) indicates the adduction of OH group to EF24

Table 3.1. Adduct formation between polyphenol EF-24 with NO* and OH* (pH 8, 100 mM Tris–HCl, 25°C).

Experimental conditions	Mass (Da)+Identity	Mass (Da)+Identity
EF24 (Control)	312.0649	----------
NO_2+EF24	312.0664	356.1551
OH+O_2^-+ EF24	312.0664	340.080

Analysis of polymerization of α-LA

Reduced α-LA was exposed to different conditions of ROS-stress (100 μM NO* or 100 μM *OH). The sample was then analyzed by native gel electrophoresis. Densitometric analysis of all the bands formed in native gel was done to quantify the polymer formation of α-LA under different conditions (Fig. 3.5). My data demonstrate that high molecular weight of polymeric α-LA was detected under NO* and *OH stress. Dimer, trimer and tetramer of reduced α-LA protein were detected via gel seperation (Fig. 3.4).

In the absence of externally introduced free radicals, reduced and native proteins mostly remain in monomeric form and ~11% of protein is found to be polymeric. Upon addition of *OH and NO* radicals with reduced protein, polymer formation increases to a significant level (to 40% and 60%, respectively). In contrast, the addition of EF24 under ROS stress results in increased levels of monomeric protein by mitigating the polymeric form. My data shows EF24 abrogates the *OH and NO*-induced polymerization by ~ 14% and ~57%, respectively.

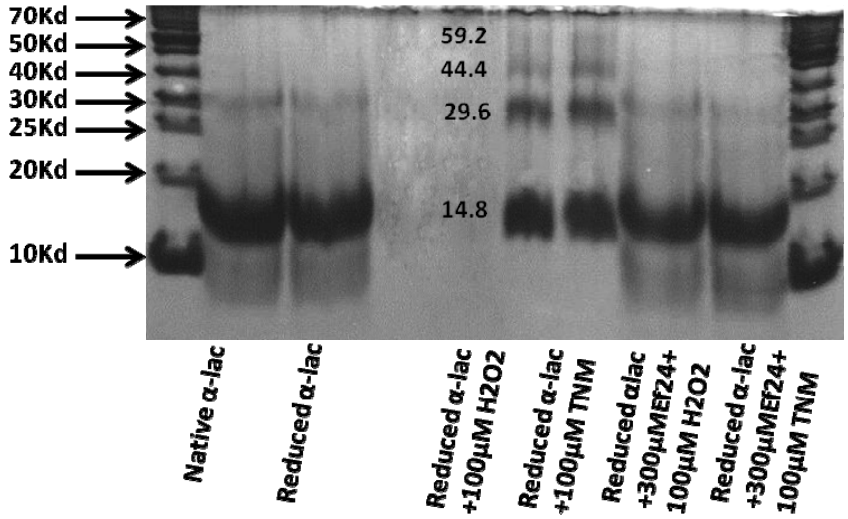

Figure 3.4. Native gel electrophoresis of α-lactalbumin protein shows polymer formation under NO* and OH* stress. From left to right: lane 1-native α-LA; lane 2-reduced α-LA; lane 3- reduced α-LA exposed to Fenton reaction (produce *OH); lane 4- reduced α-LA exposed to TNM (NO* donor); lane 5- reduced α-LA was exposed to Fenton after EF24-preincubation; lane 6- reduced α-LA was exposed to TNM after EF24-preincubation. My data reveals that preincubation with EF24 can rescue the polymerization of protein by scavenging NO* and OH*. The diagram is a representative triplicate experiment and experimental conditions are as decribed in the Methods section.

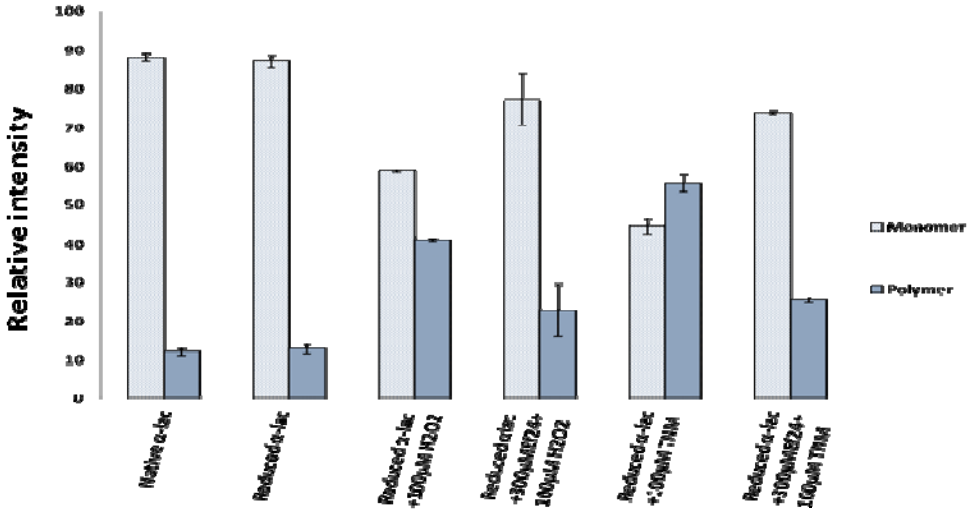

Figure 3.5. Densitometric analysis of native gel electrophoresis of α-lactalbumin protein shows high amount of polymer formation under NO* and OH* stress; preincubation with EF24 can mitigate the amount of polymerization of protein by scavenging NO* and OH*. Each bar represents average of triplicate values, and error bars their corresponding standard deviation.

Regeneration of studies of α-LA by PDI.

The data pertaining to the regeneration of α-LA under select conditions of nitrosative stress were fitted to a first-order rate equation, ln (1 -N) = -kt, where 1 – N is the fractional concentration of all nonnative species, k represents the rate constant for the formation of the native protein, and t is the reaction time (26). Table 3.2 summarizes the rate-constants obtained for the formation of the native protein under the applied conditions. The relative fraction of native protein formed as a function of time was plotted as a semi-log plot [ln (1-n) vs t]. The rate-constant was calculated from the slope of each regeneration assay (not shown).

Table 3.2. Regeneration of α-lactalbumin under control and NO* stress conditions (pH 8, 100 mM Tris-HCl, 25°C).

Reaction	Rate constant (min^{-1})	Ratio
α-lactalbumin (30μM ALAC)	52.0±0.04×10-4	1
α-lactalbumin+ (4μM)PDI	183±0.25×10-4	3.51
With (4μM)PDI + (6μM) TNM	54.0±0.06×10-4	1.04
With (4μM)PDI + (8μM) EF24)+(6μM) TNM	170.0±0.03×10-4	3.14

Figure 3.6 shows relative regeneration rates pertaining to the formation of native α-LA from the fully-reduced protein. The addition of PDI (4 μM) to the regeneration mixture enhanced the folding rate of the protein by ~3.5-fold over the control. However, the addition of NO* (6 μM) resulted in reduced regeneration levels. The data also reveal that EF24 was able to rescue PDI catalytic function to a significant level (~46%) under conditions of nitrosative stress. The oxidative folding rate of α-LA (100 mM DTT^{ox}, pH 8) is enhanced by the presence of PDI (~183 $\times 10^{-4}$ min^{-1} compared to ~52 $\times 10^{-4}$ min^{-1} for the control), but is diminished upon introduction of 6 μM TNM (~54× 10^{-4} min^{-1}). The addition of the model NO* donor in the presence of 8 μM EF24 resulted in a regeneration rate (~170 $\times 10^{-4}$ min^{-1}) that was comparable to unmodified PDI.

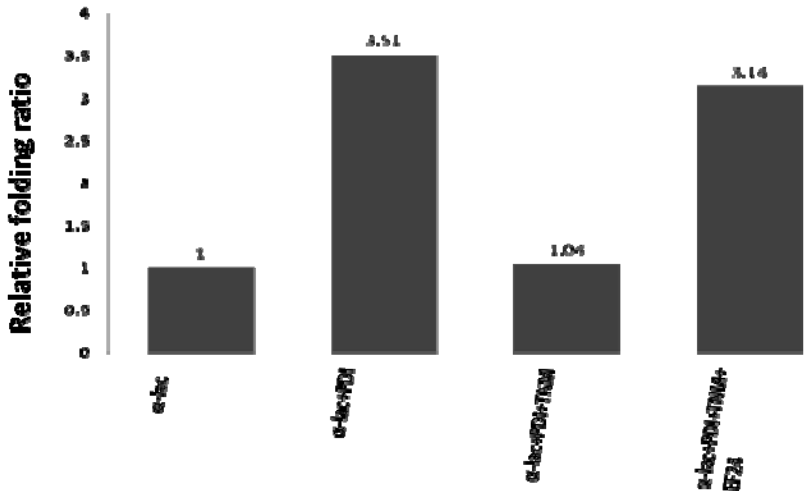

Figure 3.6. The protective effect of EF24 against NO* induced S-nitrosylation of PDI was measured by using oxidative folding assay. From left to right, bar1, fully reduced α-lactalbumin (R), control; bar2, (R), + 4 μMPDI; bar3, (R) + 4 μMPDI + 6 μM tetranitromethane; bar4, (R) + 4 μMPDI + 8 μM EF24+6 μM tetranitromethane. The regeneration conditions Ire 30 μM fully-reduced α-lactalbumin, 100 mMDTT_{ox}, pH 8, 20mMTris–HCl, 25°C.

Binding of EF24 to human serum albumin (HSA).

Figure 3.7 shows a typical intrinsic fluorescence emission intensity titration profile (λexc = 280 nm and λem = 326 and 340 nm) for the binding of EF24 to HSA at pH 8. Based on my spectroscopic results EF24 has very strong binding affinity toward HSA. EF24 shows high affinity to HSA with consistent dissociation constants (Kd) of ~1.27 μM and ~1.37 μM when repeated using independent and varying stock ligand concentrations (Table. 3.3).

Table 3.3. Dissociation constant and summary of binding stoichiometries for the interaction of EF24 and Human Serum Albumin (HSA) (200mM Tris-HCl, pH 8, 25°C)

Concentrations of EF24 (interacting with HAS)	Kd (μM)	Stoichiometry
500μM	1.27±0.63	1.6±0.21
1mM	1.37±0.45	1.4±0.14

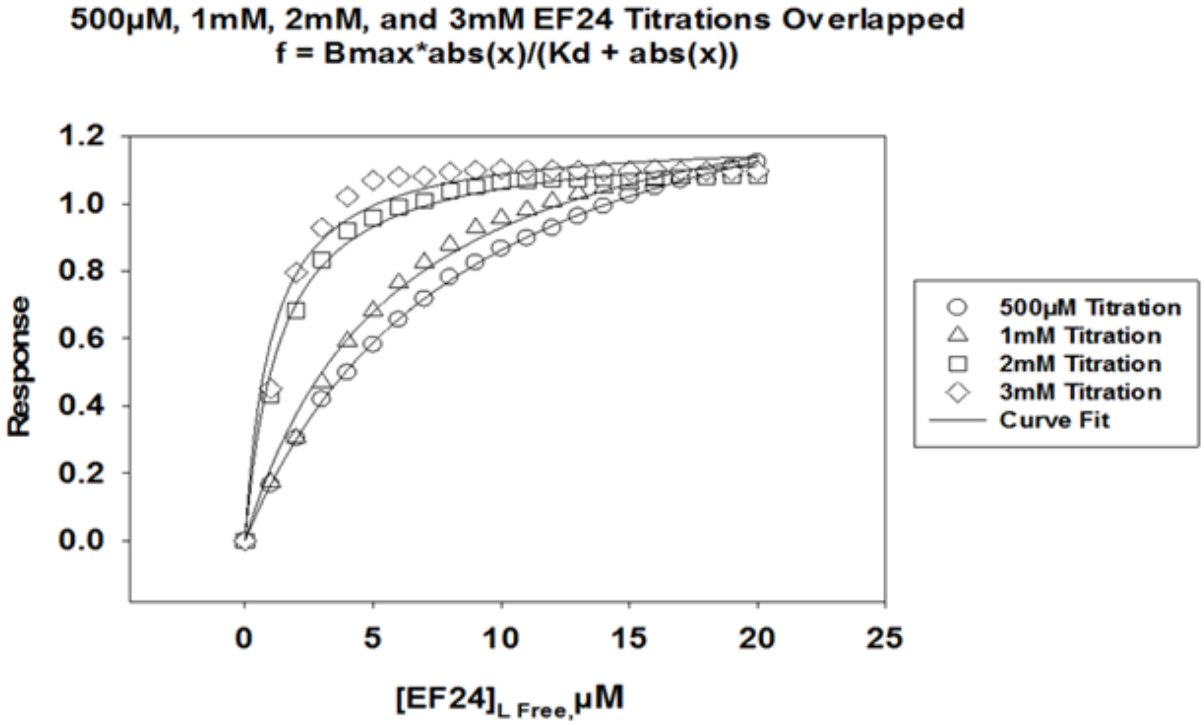

Figure 3.7. Fluorescence emission profiles for the binding of EF24 (500μM-3mM) to native human serum albumin (13.4μM) (A) Solid line represents a theoretical one-site binding profile.

Fluorescence parameters Ire: λexc = 280 nm and λem = 326 and 340 nm from a scan over 300-500 nm. All solutions Ire at 200 mM Tris-HCl, 1 mM EDTA, pH 8 and Ire prepared at room temperature 24 ± 1 °C. Spectrometer conditions are noted in Materials and methods.

3.4 Discussion

Proteins that are destined for secretion typically required disulfide bonds formed through oxidation of cysteines and rectified through thiol-disulfide exchange for their maturation and biological function (28, 29). This takes place in ER. Proteins that do not fold or assemble correctly are destined for degradation through retrotranslocatory pathway and subsequently get aggregated in the cytosol.

The ER is a specialized compartment with a redox potential designed to facilitate the (oxidative) formation of disulfide bonds in secretory or membrane-bound proteins (30). This is an essential process preceding their export from the ER and is catalyzed by protein-disulfide isomerase, the chief ER-resident oxidoreductase chaperone. The catalytic function of PDI, executed through two redox-active cysteine-containing active sites is essential to balance the flux betIen incoming nascent polypeptides and outgoing biologically viable folded proteins (30). Compromise or failure in the catalytic efficiency of PDI can reduce the maturation of nascent substrates and lead to terminal misfolding and retrotranslocation (30).

Previous studies have demonstrated that as a nucleophile, cysteines can be modified by various electrophiles, thus participating in the regulation of protein function (31). Therefore, protein post-translational modification involving cysteins have long been characterized as important regulatory mechanisms for signal transduction. There are different types of redox-

related cysteine modifications including S-nitrosothiol ($^{-}$SNO), sulfenic acid ($^{-}$SOH), sulfinic acid ($^{-}SO_2H$), and sulfonic acid ($^{-}SO_3H$) (31).

Here, I hypothesized addition of external NO* and *OH can react with cysteinyl thiolate (S^{-}) of reduced α-LA protein and leads to polymeric protein formation (via thiyl radical formation). I have also hypothesized that EF24 can abrogate the aggregation of polymeric protein forms through scavenging NO* and *OH radicals by forming stable adducts. Our previous study demonstrated that polyphenol curcumin and masoprocol are capable of scavenging free radicals and helps in oxidative protein folding (Table 3.4).

Table 3.4. Regeneration of RNaseA under control and NO* stress conditions (pH 8, 100 mM Tris-HCl, 25°C).

Reaction	Rate constant for R→N ($\times 10^4$ min^{-1})
RNaseA (R) (30μM)	10.4±0.2
R+ (4μM)PDI=A	86.1±1.3
A+1μM TNM	35.5±2.6
A+2 μM TNM	19.7±0.4
A+4 μM TNM	11.3±2.1
A+4 μM TNM+ 30 μM curcumin	84.2±0.9
A+4 μM TNM+ 30 μM masoprocol	79.1±0.5

To test my hypothesis, I first exposed EF24 to model NO* and *OH donor under *in vitro* conditions. My data indicated the formation of nitrated and hydroxyl products suggesting that EF24 was capable of scavenging NO* and *OH.

Next, I investigated the exposure of reduced α-LA to NO* and *OH. I found high molecular weight of polymers when fully reduced α-LA was exposed to NO* and OH* donors. On the other hand, protein pre-incubated with EF24 shows mitigated levels of polymerization. These data support my hypothesis that EF24 can mitigate the aggregation of misfolded protein by forming stable adducts with free radicals.

Since, PDI plays a crucial role in oxidative folding of disulfide-bond containing proteins by assisting thiol-disulfide-exchange, I was interested in determining whether EF24 was capable of rescuing PDI from nitrosative attack. In agreement with previous studies (9), my data reveal that nitrosative stress results in the loss of PDI catalytic function; i.e., PDI-facilitated regeneration rate of the well-known PDI substrate protein α-LA, in the presence of a model NO* donor, reverts to values obtained in the absence of PDI, suggesting the loss of catalytic activity due to modification of PDI active-site thiols by NO*. However, the observed rate of regeneration of α-LA in the presence of PDI, NO* and EF24 equals levels observed with unmodified PDI (i.e., rate observed in the absence of NO*). This indicates EF24 is able to scavenge elevated levels of NO* and form stable adducts. Although the mechanism of action is not investigated here, my study demonstrates that PDI function can remain unaffected under conditions of nitrosative stress as long as scavenging EF24 is present. Altogether, my data suggest that EF24 can mitigate the misfolded protein aggregation by preventing free radical mediated modification of PDI.

Finally, I examined the binding affinity of human serum albumin (HSA) with EF24. My results suggest that EF24 binds strongly to HSA suggesting that the protein could be a potent carrier for EF24 from the site of absorption to tissues within the body.

Chapter 4:

Prophylactic Effect of EF24 against Nitrosative Stress Induced Apoptotic Cell Death in PD Model

4.1 Introduction

Among factors known to be associated with the etiology of apoptotic cell death, nitrosative stress induced cell death by the excessive generation of NO* species has been demonstrated with high importance in recent studies (1). However, the mechanism underlying this fact is still unclear. Inhibition of the mitochondrial respiratory chain by rotenone has been widely used to study the role of the mitochondrial respiratory chain in apoptosis (1). Recent evidence has demonstrated that rotenone, a mitochondrial respiratory chain complex I inhibitor, could induce cell-death in a variety of cells (2-6). Since it has been well-established that ROS play an important role in apoptosis, the molecules that stimulate formation of ROS can cause apoptosis (7, 8); a process likely to be inhibited by antioxidants (9-13). Mitochondrion-derived ROS are vital not only because mitochondrial respiratory chain components are present in almost all eukaryotic cells, but also because the ROS produced in mitochondria can readily influence mitochondrial function without having to cope with long diffusion times from the cytosol.

Apoptotic stimuli instigate the release of cytochrome *c* from the mitochondrial inner membrane space into the cytosol, where it triggers autocatalytic processing caspase-9 (21). Caspase-3 gets activated along with other effector caspases by caspase-9, resulting in the proteolytic cleavage of substrate nuclear poly (ADP-ribose) polymerase (PARP) (33). Importantly, PARP cleavage is directly related to nitrosative stress-mediated cell-death along with a variety of apoptotic responses (21).

A hallmark event characteristic of neurogenerative disorders such as Lewy body dementia, Alzheimer's (AD) and Parkinson's diseases (PD) is the accumulation of aggregated proteins to form Lewy-bodies in the cytosol of human neuronal cells, which results in apoptotic cell death of neuronal cells (14). This commonality exists in spite of the fact that causals for AD and PD are different, depend upon whether familial or sporadic, and differ in the proteins constituting the aggregates and Lewy neurites. There is also debate whether specific protein aggregates representative of these diseases are truly the cause of the disease or only a mechanism to rescue the cell upon onset of the neuronal pathology (14). Recent studies have demonstrated that in a particular sporadic form of AD and PD, a key endoplasmic reticulum-resident oxidoreductase chaperone protein disulfide isomerase (PDI) (Fig.3.1A) becomes chemically modified because of high levels of nitrosative stress (14). A common feature observed in the neuronal cells of AD and PD victims in this sporadic variant was the attachment of nitric oxide (NO) to the redox-active cysteines of protein-disulfide isomerase (PDI) to form S-nitroso-PDI (Fig. 4.1). The formation of S-nitroso-PDI coupled with the pathogenesis of AD and PD makes the oxidoreductase a chief target for the prevention of these two neurodegenerative disorders in the nitrosative-stress-linked variant of the diseases.

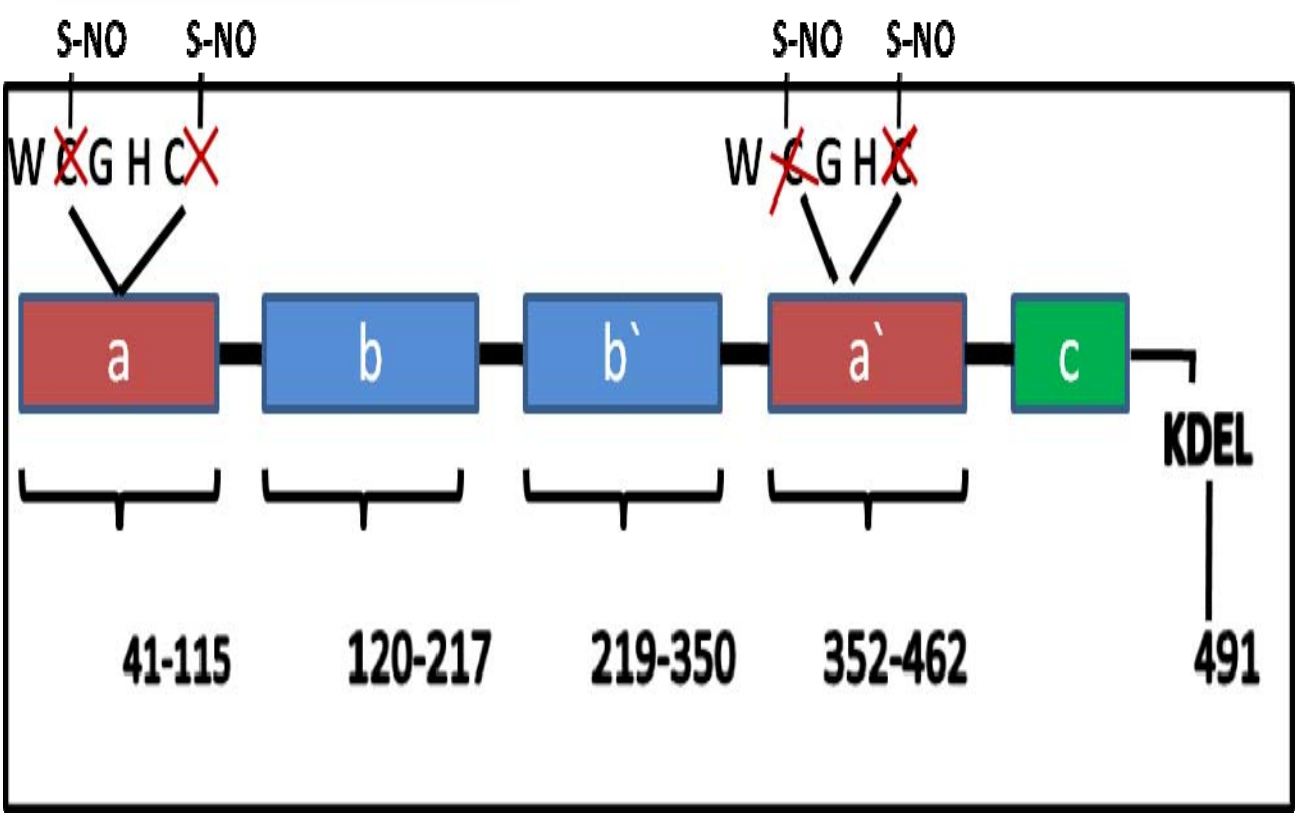

Figure 4.1. Schematic representation of S-nitroso-PDI

The main objective of the present investigation was to determine the prophylactic ability of the polyphenol, Diphenyl difluoroketone, (EF24, Fig.3.1B) in preventing ROS-associated PDI dysfunction in cell lines using the aggregation of PD-specific biomarkers as evidence of ROS-impact on neuronal cells. My data reveal that EF24 can scavenge the excess NO* species and prevent cells from rotenone induced apoptotic cell death.

Furthermore, it is known that during the nitrosative stress mediated apoptosis, Poly ADP ribose polymerase (PARP) cleavage is associated with the rotenone induced ROS stimuli. PARP, a 116 kDa protein, appears to be involved in DNA repair in response to environmental stress

(15). Many ICE-like caspases are responsible to cleave this protein *in* vitro (16, 17) and PARP is one of the main cleavage targets of caspase-3 *in* vivo (18, 19). In human PARP, the cleavage occurs between Asp214 and Gly215, which separates the PARP amino-terminal DNA binding domain (24kDa) from the carboxy-terminal catalytic domain (89kDa) (16, 18). PARP plays a very crucial role to maintain cell's viability; cleavage of PARP facilitates cellular disassembly and serves as a marker of cells undergoing apoptosis (20, 21, 22). I have found that EF24 can prevent the PARP cleavage significantly (Fig 4.7), mitigating rotenone-induced apoptotic stimuli by scavenging excess reactive nitrogen species.

In this study I have overexpressed green-fluorescent protein tagged synphilin-1 in both human neuronal (SH-SY5Y) and Porcine Aortic Endothelial (PAE) cell lines and monitored its aggregation as a biomarker for PD. My results reveal that exposure of this cell line to rotenone, a mitochondrial reactive oxygen species elevator, leads to the aggregation of synphilin-1 as observed by fluorescence microscopy and consistent with previous reports that NO* influences Lewy body formation via PDI modification (23). Importantly, cells that Ire preincubated with EF24 prior to rotenone insult demonstrated a marked resilience to synphilin-1 aggregation. These results suggest that it may be possible to mitigate nitrosative-stress induced aggregates in cell-lines using bioavailable polyphenolic phyto-analogs. Furthermore, it opens avenues for the design and development of more effective and less toxic analogs prophylactics against nitrosative-stress linked AD and PD.

4.2 Materials and Methods

Reagents and cell line

EF24 was synthesized as mentioned in materials and methods section of chapter 3 (3.2). It was further purified by HPLC and characterized by mass spectrometry. HPLC analysis of re-purified EF24 showed purity ≥99%. Tetra-nitromethane (TNM) and rotenone (Obtained from Sigma-Aldrich, St. Louis, MO., USA). Propidium iodide and annexin were bought from MP Biomedicals, Solon, OH. Human PDI plasmid was generously provided by Dr. Lloyd Ruddock (Department of Biochemistry, University of OULU, Finland), SHSY5Y and PAE cell line was obtained from ATCC, Manassas, VA.

Preparation of fully-reduced RNase

Fully-reduced RNase A (R) was prepared by incubating native protein (10 mg/ml) in 6 M Gdn HCl and 100 mM DTTred (pH 8, 100 mM Tris–HCl, 1 mM EDTA) for a period of 2 h (24). The mixture was then repeatedly dialyzed against 50 mM acetic acid at 4°C prior to Lyophilization. The "fully reduced" protein was dissolved into 10 mM acetic acid to obtain a stock solution (5 mg/ml) that was kept frozen (-20°C) until further use.

PDI-catalyzed oxidative folding of RNase A under nitrosative stress

Fully-reduced RNase A (30 μM final concentration) was incubated into a solution (pH 8, 100 mM DTTox, 100 mM Tris–HCl, 25°C) containing 4 μM of WT PDI and oxidative regeneration folloId as previously described (25, 26). A control experiment was run in parallel and did not contain any PDI. Aliquots from the regeneration mixture were periodically withdrawn after initiation of oxidative folding and subjected to a reduction pulse (application of 2 mM DTTred

for a period of 2 min) (27), before addition of glacial acetic acid (which reduced the pH to 3). Samples were desalted on a G- 25 column prior to application on a C-18 column (Supelco Discovery®BIO Wide Pore C18, 5 lm, 15 cm ×100.0 mm) for reversed phase chromatographic analysis using an acetonitrile gradient (1%/min) (25).

In other experiments, EF24 (8μM final concentration from stock acetonitrile solutions prepared by weight) were incubated with the regeneration mixture prior to the addition of tetranitromethane (4μM obtained by dilution of the neat compound). The regeneration and sample analysis was carried out as above. The rate of regeneration of the native protein (N) was determined by integrating the areas of the peaks corresponding to the native protein (N structured intermediates and the fully-reduced protein (R) at each time point. The fractional increase in N was plotted as a function of time; the data were fitted to a single exponential function to obtain the rate constant for the formation of N from R (28).

Cell Culture

Porcine aorta endothelial (PAE) cells were cultured using Ham's F12 medium and supplemented with 10% fetal bovine serum (FBS), 100U/ml of penicillin and 100 μg/ml of streptomycin. SH-SY5Y cells were cultured with DMEM/F12 (1:1) medium and along with the same supplements as was used for PAE cells. Cell lines Ire cultured around 70% of confluence using tissue culture flasks (Falcon, Franklin Lakes, NJ). The incubation conditions of the cells Ire at 37ºC in humidified 5% carbon dioxide (CO2) atmosphere.

Cytotoxicity assay of EF24 in PAE cell

PAE cells were grown in 96-well plate and left to attach for 12 hrs. After 12 hrs, cells were extensively washed with fresh media (formula of media mentioned in cell culture section, pg 69) , to eliminate cell debris and floating cells which correspond mainly to dead cells; such wells can introduce significant noise when used to perform cytotoxicity assays. Attached cells were treated with 100 nM to 2 μM EF24 for 42 hrs and cytotoxicity of EF24 was monitored by using live-cell imaging instrument.

Cytotoxicity assay and cellular protective effect of EF24 against rotenone aggression monitored by using live-cell imaging instrument

Cell preparation

To prepare an experimental multiwell plate, cells were extensively washed with fresh media. Adherent/live cell population were harvested by adding to the cells to 2 ml of 0.25% trypsin solution (Invitrogen, Carlsbad, CA), diluted in serum free media, and incubated for approximately 3 min at 37°C. After cell counting using Neubauer chamber (hemocytometer), cells were seeded at density of 10,000 cells per well in 200 μl complete media utilizing 96 well-plate format.

Differential nuclear staining cytotoxicity assay

The protective effect of EF24 against rotenone-induced ROS insult was tested using PAE cell lines. Cells in a multiwell plate prepared as described above were incubated for 12 h to allow for attachment. Next, cells were previously pretreated with 1 μM of EF24 for 6 hrs prior to rotenone exposed (100, 300, 500 nM and 1μM). Subsequently, cells were incubated for an extra 24 hrs and

images were captured in live mode. Several controls were included in each experiment. As a control for non-specific effects, the diluents of rotenone, EF24 and DMSO, as contained in the experimental samples, was included at final concentration of 2.5 v/v.

Cells treated just with rotenone, without previous exposure to EF24, were tested at the same concentration used in cells pretreated with EF24, to determine the cytotoxic effect of rotenone itself. Also, cells were treated with 1 μM of EF24 alone, to determine its possible toxic effect. Finally, untreated cells were prepared to determine the background levels of cell death, provoked by cell manipulations and inherent features within the cell culture system.

In this study, automated microscopic imaging was used to ascertain cell death via the use of a Differential Nuclear Staining (DNS). This mechanism has recently been validated as a high throughput screening (HTS) assay (29). To each experimental and control well, a mixture of two fluorescent dyes, Propidium iodide (PI) (MP Biomedicals, Solon, OH) and Hoechst 33342 (Invitrogen, Eugene, OR) at a final concentration of 1 μg/ml, were added 1h prior to image recording. Both dyes are nucleic acids intercalators (29). Hoechst easily crosses cell membranes of healthy and dead cells and stains nucleic DNA; However, PI is only capable of staining dead cells with compromised plasma membranes. The fluorescence signal from each individual fluorophore emitted by stained cells was captured in two separate channels, in fulfillment with the dye emission requirements. Images were acquired directly from a tissue culture mulitiwell plate utilizing a BD Pathway 855 Bioimager system (BD Biosciences Rockville, MD). To acquire adequate numbers of cells for statistical analysis purpose, montages (3X3) from nine adjacent image fields were captured per well, utilizing a 20X objective. Captured images and data analysis determining the percentage of dead cells from each individual well was performed by using BD AttoVision™ v1.6.2 software (BD Biosciences Rockville, MD), designed to assist

the Bioimager system. Every experimental point, as well as all controls, was assessed in quintuplicate.

Apoptosis/Necrosis Assay

PAE cells were seeded on 24-well microplate at density of 20,000 cell/well in 1ml of media and cultured at 37°C under 5% CO_2 humidified atmosphere. Cells were incubated overnight to promote adherence, followed by 6 hrs preincubation in presence of 1μM EF24 and then added with 500 nM rotenone and incubated for additional 48h. Cells from each individual well were collected, washed and processed essentially as previously described (30). Briefly, cell were concurrently stained by resuspending them in a solution containing Annexin V-FITC and PI dissolved in 100 μl of binding buffer (Beckman Coulter, Miami, FL). After incubation for 15 min on ice in the dark, ice-cold binding buffer (400 μl) was added to the cell suspensions, gently homogenized, and immediately analyzed by flow cytometry. For each sample, approximately 10,000 individual events were acquired using flow cytometer (Cytomic FC 500; Beckman Coulter, Miami, FL) and data analyzed with CXP software (Beckman Coulter, Miami, FL). Every experimental point, as well as all controls, was assessed in quintuplicate.

Western blotting

Total cell lysates were prepared by washing the cells with cold Tris-buffered saline, collected by centrifugation (3003g, 5 min at 48°C, and extracted by sonicating in buffer containing 10 mM Tris–HCl (pH 7.4), 10 mM EDTA, 2% (w/v) SDS and protease inhibitors (Sigma). Total protein concentrations were measured using a bicinchoninic acid kit (Pierce) and BSA as standard. Equal amounts of protein (approximately 10 μg per lane) were separated using SDS-polyacrylamide

gel electrophoresis and then transferred to polyvinyldifluoride (PVDF) membranes. Blots were incubated in blocking buffer (5%, w/v, dried skimmed milk in Tris-buffered saline, pH 7.4, and 0.1% TIen 20) folloId by incubation anti-PARP rabbit polyclonal antibody (1:1000, Cell Signaling Technology®) or anti-GAPDH (Glyceraldehyde 3-phosphate dehydrogenase, 1:1000 dilution) diluted in blocking buffer for 1 h then with horseradish peroxidase (HRP)-conjugated goat anti-rabbit (KPL Biomedical) in 1% BSA/TBST for 30 min. Chemiluminescence (ECL-plus or SuperSignal west Pico Chemiluminescent Substrate) was used according to the manufacturer's instructions (Amersham or Pierce Biotechnology Inc.).

Cloning of synphilin-1 and expression of EGFP- synphilin -1 fusion proteins

The full-length cDNA of the human synphilin-1 (Genbank accession code; NP 005451) was amplified *via* PCR, using as template pENTR 221 (Invitrogen). The primer set was designed to contain EcoRI in forward and BamHI in reverse restriction enzyme cleavage sites, providing directionality for cloning purposes into pEGFPC2 expression vector (Clontech. Palo Alto, CA); forward, 5'-aaatttgaattcatggaagcccctgaataccttgatttg-3' and reverse, 5'-aaatttggatcctacaagaagagttcttttgactc-3'; (underlined segments represent EcoRI and BamHI sites, respectively). PCR-amplified products were separated using 1% agarose gel stained with ethidium bromide, gel purified (QIAEX II, Qiagen, Valencia, CA) and verified by DNA sequencing reaction. After double digestion of purified amplicons with EcoRI and BamHI, the digested fragments were separated and purified as mentioned above and cloned into pEGFP-C2 expression vector (Clontech. Palo Alto, CA), previously digested with the same set of restriction enzymes used for the insert. After ligation and transformation reaction, a colony was selected,

its plasmid isolated and its insert sequenced, corroborating to correspond to the synphilin-1 gene. This pEGFP-C2; synphilin-1 construct was utilized to transiently transfect PAE mammalian cell.

Transfection and cell treatment

SH-SY5Y and PAE cells (1×10^6 cells/well) were seeded onto glass coverslips in 6-well plates and incubated at 37 °C in 5% CO_2 for 12-16 h. Cell transfections were performed next day as (recommended by manufacturer) using effectene reagent (Qiagen, Valencia, CA). Cells were then incubated with transfection complexes under normal growth condition for expression of pEGFP-C2 control or the fusion protein GFP-*synphilin*-1 gene. Transiently transfected SH-SY5Y and PAE cells were incubated overnight to allow expression of proteins. Cells were treated with DMSO vehicle or with 1 μM EF24 for 6 hrs followed by exposure to 300 nM of the toxicant rotenone for 12 hrs. After attachment, cells were prepared for microscopy as described below.

Confocal microscopy and immunocytochemistry

Cells transfected with EGFP-synphilin-1 fusion proteins were washed after treatments, fixed with 4% paraformaldehyde in PBS, stained with DAPI and mounted under ProLong antifade medium (Molecular Probes). To stain for PDI, cells were fixed as above, then permeabilized with 0.1% (w/v) saponin in PBS, blocked with PBS plus 5% goat serum, 5% FBS and 0.1% Tween 20, and incubated with primary antibody (overnight at 4ºC) folloId by incubation with rhodamine-conjugated goat anti-mouse (1:10000, KPL Biomedical), and DAPI staining. Fluorescence confocal images were captured utilizing LSM 700 confocal microscope (Zeiss. New York. NY) with 63X objective and assisted with ZEN 2009 software (Zeiss. New York, NY).

4.3 Results

*Ability of EF-24 to scavenge NO**

The ability of EF-24 to scavenge NOx from TNM was re-established and results obtained were similar to that described in Chapter 3.

Regeneration of studies of RNase A by human PDI

Fig. 4.2A shows the regeneration profile of fully-reduced RNase A. The kinetic data (Fig. 4.2A) pertaining to the regeneration of RNase A under select conditions of nitrosative stress were fitted to a first-order rate equation, $ln\ (1-N) = -kt$, where $1-N$ is the fractional concentration of all nonnative species, k represents the rate constant for the formation of the native protein, and t is the reaction time (30). The addition of human PDI (4 μM) to the regeneration mixture enhanced the folding rate of the protein by ~4-fold over the control (Fig 4.2B). However, the addition of NO* (4 μM data shown) resulted in reduced regeneration levels. The data also reveal that EF24 was able to rescue PDI catalytic function to a significant level (86%) under conditions of nitrosative stress. Table 4.1 summarizes the rate-constants obtained for the formation of the native protein under the applied conditions. The oxidative folding rate of RNase A (100 mM DTT^{ox}, pH 8) is enhanced by the presence of PDI (~112 $\times 10^{-4}$ min^{-1} compared to ~27 $\times 10^{-4}$ $min^{-1}$for the control), but is diminished upon introduction of 4 μM TNM (~39× 10^{-4} min^{-1}). The addition of the model NOx donor in the presence of EF24 resulted in a regeneration rate (~85 $\times 10^{-4}$ min^{-1}) that was comparable to unpoisoned PDI.

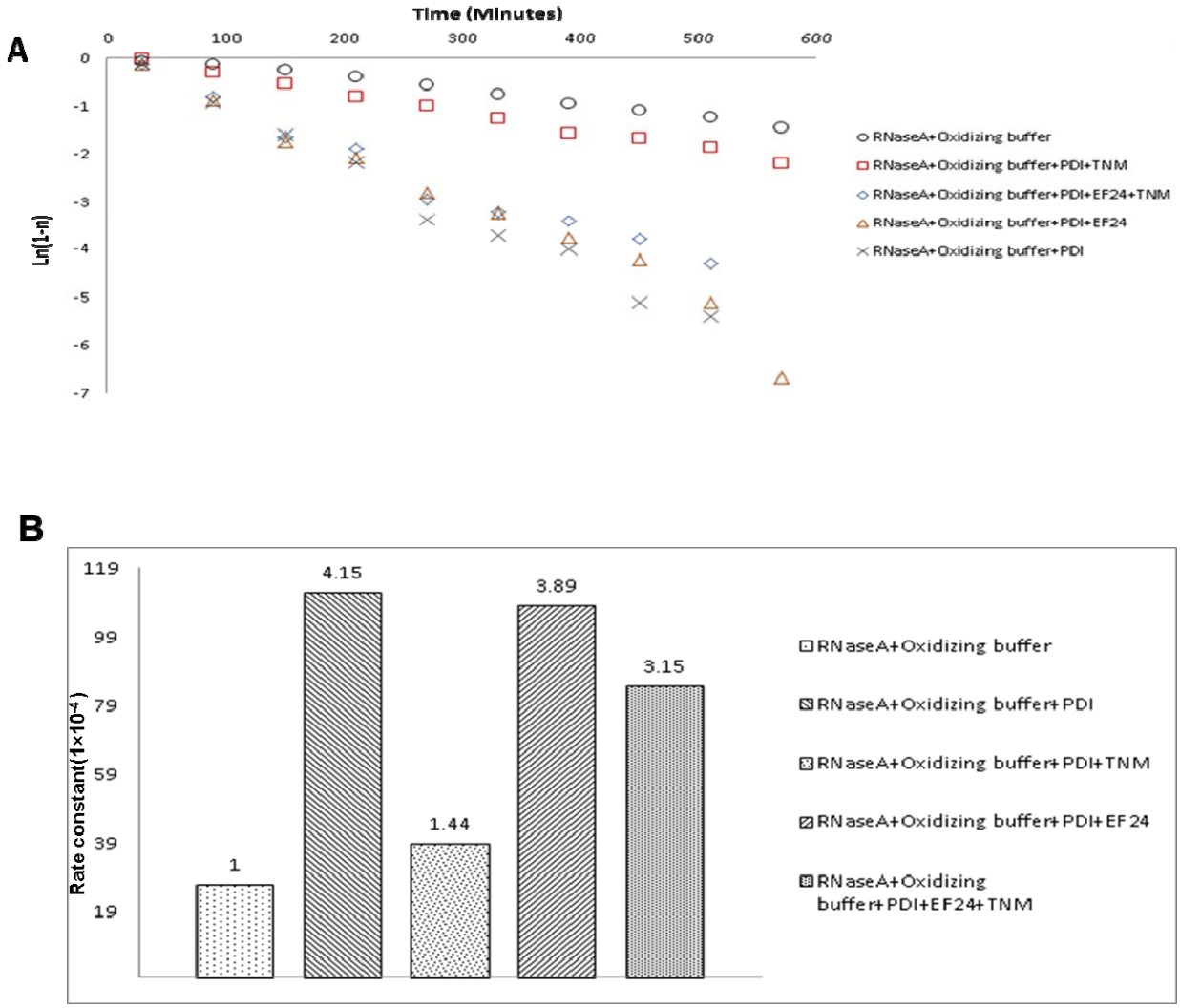

Figure 4.2. The protective effect of EF24 against rotenone induced S-nitrosylation of PDI was measured by using oxidative folding assay. (A) Regeneration of native RNase A formed from the fully-reduced protein (R). ○, control; ×, + 4 μM PDI; □, + 4 μMPDI + 4 μM tetranitromethane; Δ, + 4 μMPDI + 8 μM EF24; ◊, + 4 μMPDI + 8 μM EF24+4 μM tetranitromethane; The regeneration conditions were 30 μM fully-reduced RNase A, 100 mMDTTox, pH 8, 20mMTris–HCl, 25°C. (B)The rate constant and ratio of regeneration of RNaseA under same conditions are shown in bar diagram.

Table 4.1. Regeneration of RNase A under control and nitrosative stress conditions (pH 8, 100 mM Tris-HCl, 25 °C).

Folding condition	Rate constant for R→N ($\times 10^{-4}$ min^{-1})
R	27±0.2
R+4μM PDI	112±0.9
R+4μM PDI+4μM TNM	39±2.1
R+4μM PDI+8μM EF24	108±2.6
R+4μM PDI+8μM EF24+4μM TNM	85±1.2

R- Reduced RNaseA with oxidizing buffer (Control)

Differential nuclear staining assay to quantify cytotoxicity

The Differential nuclear staining assay revealed that rotenone increased cytotoxicity level in the presence of rotenone. The increase of cytotoxicity by rotenone insult was measured in a dose-dependent manner. Survival and death of PAE cells were simultaneously visualized by using a live/dead assay (Fig. 4.3). Treatment with 1μM EF24 lowered the level of cytotoxicity (Fig. 4.4). Dead cells, which were detected as red in fluorescence, apparently increased in number after rotenone exposure. A low concentration (100nM) of rotenone does not significantly increase cytotoxicity, but gradual increase in the concentration of rotenone (100nM→300nM→500nM→100nM) results in increased cytotoxicity. My data indicate 80% toxicity at 1000nM rotenone after 24 hrs incubation. Pre-treatment with 1μM EF24 for 6 hMys reduces the amount of cytotoxicity to a significant level (≥50%).

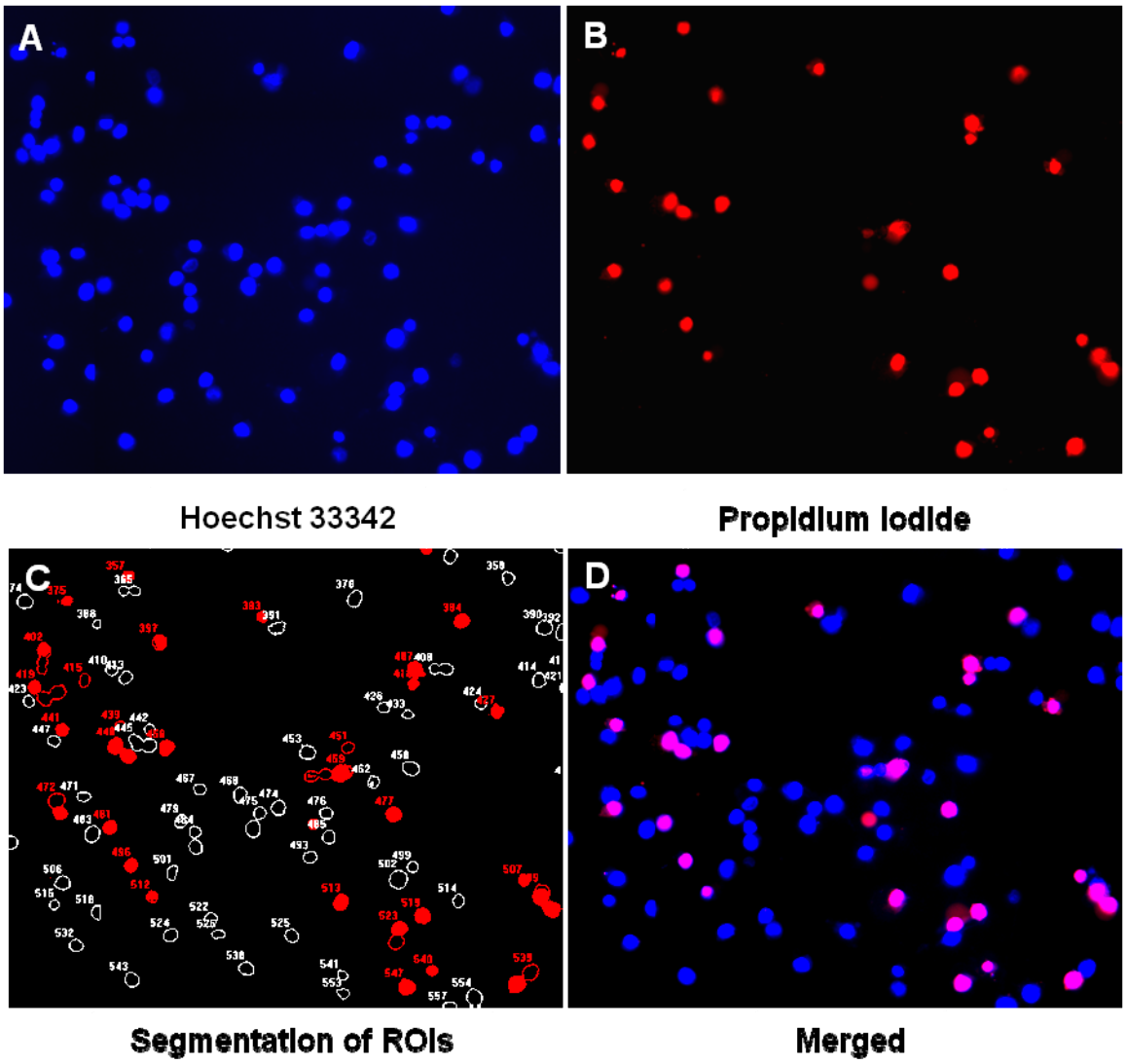

Figure 4.3. Cytotoxicity was monitored by using differential nuclear staining assay on PAE cells. Representative images of cells treated with 300 nM of rotenone. The four images correspond to the same portion of the 3X3 montage, captured with 20X objective utilizing BD Pathway Bioimager system and AttoVison software. Due that the BD Pathway system is equipped with monochrome Hamamatsu camera (black and white) and it was necessary to apply computerized (AttoVision sofware) pseudocolor to each fluorescence channel to achieve colored image. (A) Hoechst emission signal (excitation/emission maxima: 460/490 nm) from stained cells indicates the total number of nuclei (cells) present in the image, shown in blue. (B)

Propidium iodide emission signal (excitation/emission maxima: 535/617 nm) from labeled cell nucleus indicates the number of death cell in the image, shown in red. (C) Segmented image, showing regions of interest (ROI) utilized in the image analysis procedure, where nucleus of propidium iodide positive cells (death) appears in red, whereas nucleus of live cells are delimited by a white line. (D) Merged Hoechst and PI image, from signals of the two fluorescence channel; the magenta color is an outcome of colocalization of red and blue colors, indicating the number of death cells in the image. AttoVision software assigns a number to each ROI, which is annotated in the image (D).

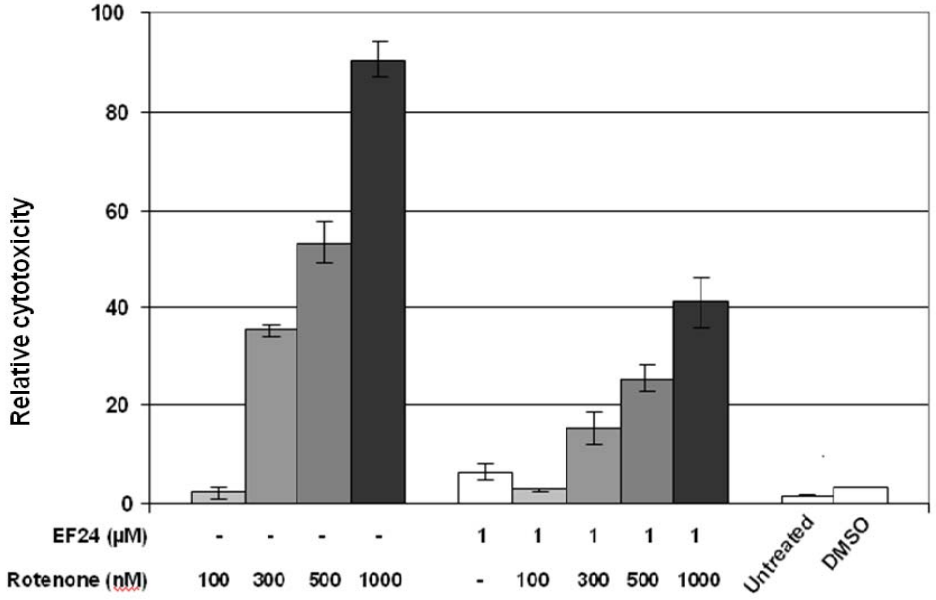

Figure 4.4. The prophylactic effect of EF24 against rotenone aggression was tested utilizing PAE cell line, measured by using differential nuclear staining cytotoxicity assay. Cells were pretreated with 1 μM of EF24 for 6 hrs and exposed to several concentrations (100, 300 500 and 1000 nM) of the toxicant rotenone for another 24 hrs. Three controls were included: cells treated with several concentration of just rotenone, 100, 300 500 and 1000 nM; cells treated with 2.5% v/v DMSO, as contained in the experimental samples: and untreated cells, as a control for non-specific effects. Each bar represents average of triplicate values, and error bars their corresponding standard deviation.

Apoptosis/Necrosis Assay

Fig. 4.5 shows the representative dual parameter flow cytometric histograms of the apoptosis/necrosis effects caused by EF24 (panel A), rotenone (panel B) and pretreated PAE cells with EF24/rotenone (panel C) treatments. Representative histograms of controls are also included; panel D, untreated cells; panel E, cells treated with DMSO; and panel F, cells treated

with H_2O_2 as positive control for apoptosis. The concentrations utilized are annotated on the top of each histogram. Each histogram is fragmented in four quadrants. Left top quadrant – necrosis, cells permeable to propidium iodide that lost their membrane integrity, without Annexin V-FITC signal, one color (red); right top quadrant - late apoptosis, cells with compromised plasma membrane, permeable to propidium iodide, but also with Annexin V-FITC signal, two colors (green and red); lower left quadrant - alive unstained cells, without propidium iodide or Annexin V-FITC fluorescent signal; lower right quadrant-early apoptosis, cells with only Annexin V-FITC signal, one color (green). Approximately 10,000 events were acquired per each individual sample and analyzed using CXP software (Beckman Coulter).

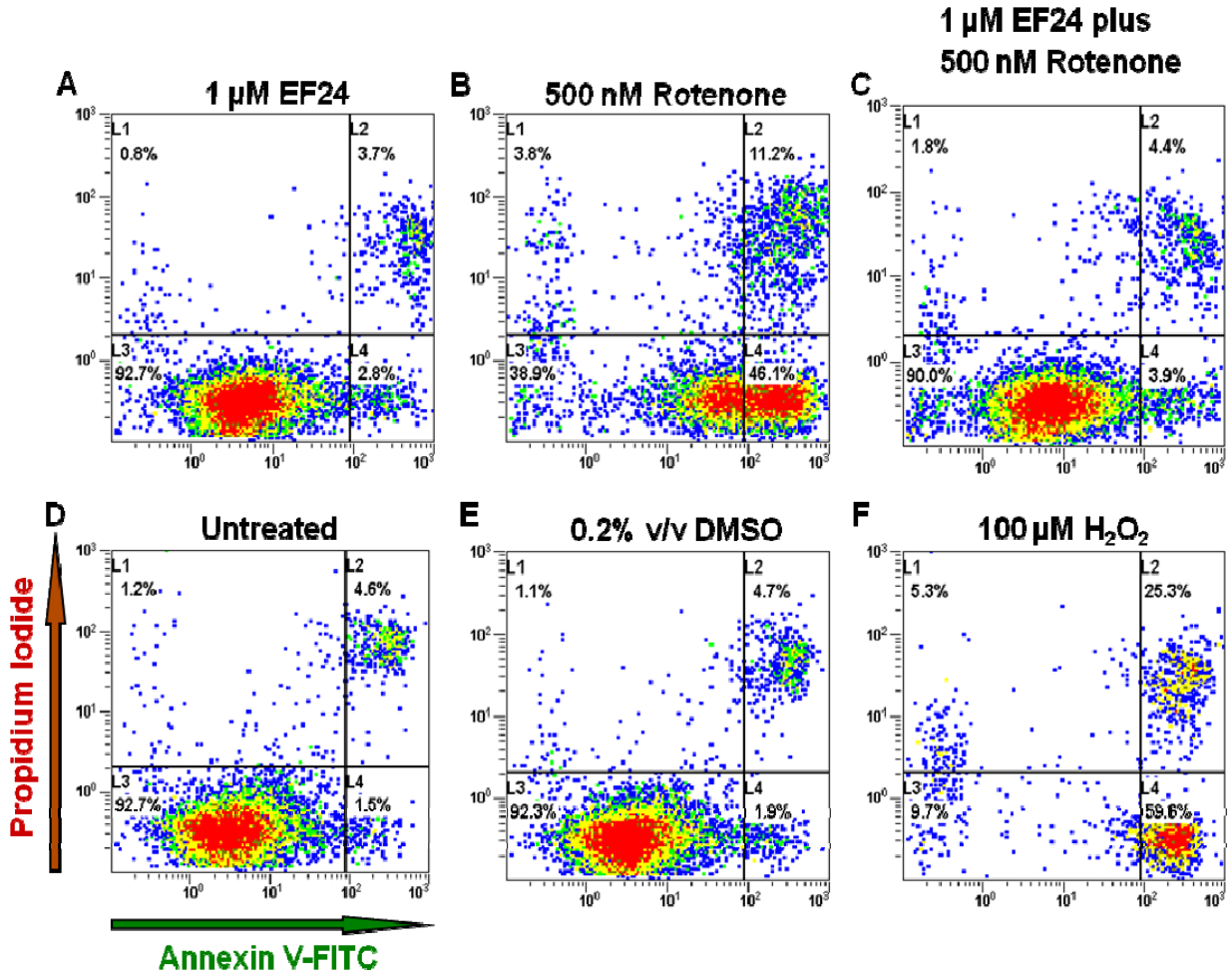

Figure 4.5. Representative two parameters flow cytometric histograms of the apoptosis/necrosis effects caused by EF24 (panel A), rotenone (panel B) and pretreated cells with EF24 /rotenone combinatorial (panel C) treatment on PAE cell line.

The prophylactic effect of EF24 against rotenone-induced toxicity in PAE cells was evaluated using flow cytometry. Cells were simultaneously stained with Annexin V-FITC and PI, after 48 hours of incubation, and the total percentage of apoptotic cells were expressed as the sum of both early and late stages of apoptosis (white bars) (Fig. 4.6). Cells permeable to

propidium iodide without Annexin V-FITC signal were considered as necrotic cells (black bars). Cells treated with H_2O_2 were utilized as positive control for apoptosis. The diluent of EF24 and rotenone, DMSO, was evaluated at the same concentration as included in the experimental samples, as a control for nonspecific diluent activities. Untreated cells were used as an indicator of overall cell viability. Results show that rotenone induced excessive generation of NO* leads cell death primarily *via* the apoptotic pathway. Necrotic cell death due to rotenone aggression was very low compared to control. My data also reveal that EF24 can mitigate the effect of nitrosative stress and prevent the apoptotic cell death.

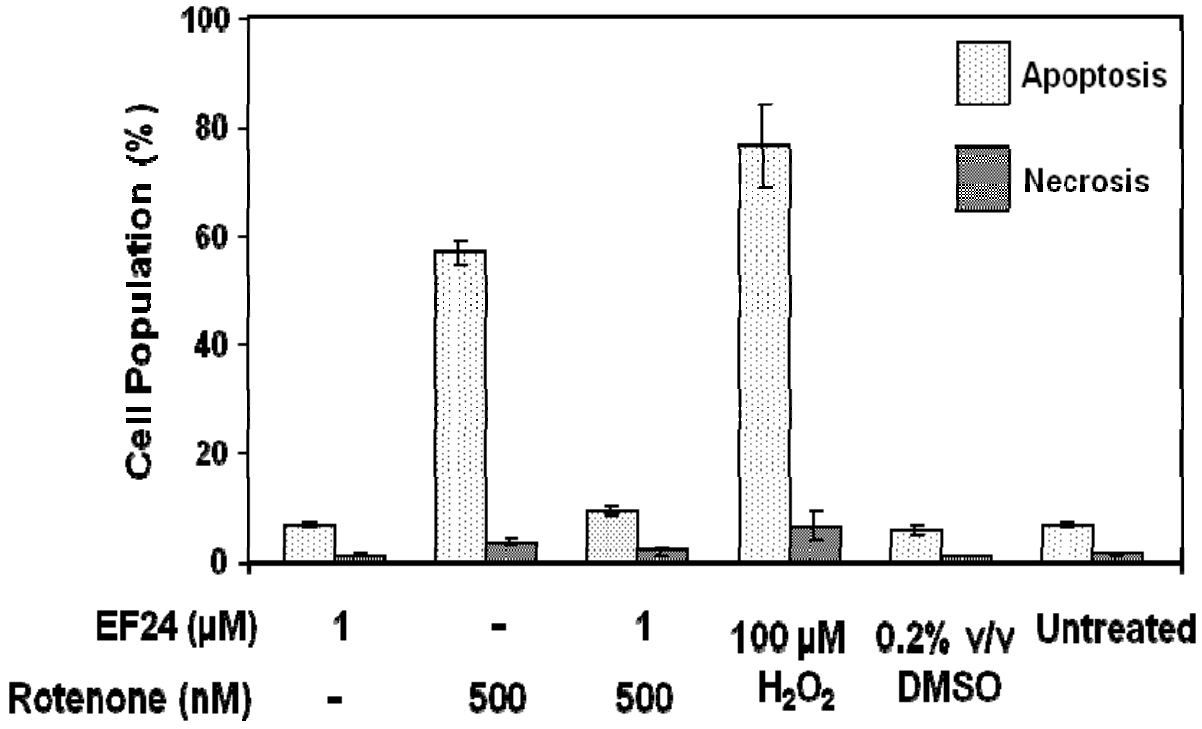

Figure 4.6. The protective effect of EF24 against rotenone induced apoptotic and necrotic cell death in PAE cell line was measured by using double staining with Annexin V-FITC/ propidium

iodide and monitored via flow cytometric assay. Cells were pretreated with 1 μM of EF24 for 6 hrs and exposed to 500 nM of the toxicant rotenone for an extra 42 hrs. Also as controls, cells treated just with 500 nM rotenone, 2.5% v/v DMSO, 1μM EF24 were included. As a control for non-specific effect, untreated cells were also included. Each bar represents average of triplicate values, and error bars their corresponding standard deviation.

PARP assay

PARP serves as a marker of cells undergoing apoptosis. PARP assay has been done to support the fact that rotenone induced nitrosative stress stimuli can lead cells to mostly apoptotic cell death over necrotic cell death. My data show 300 nM rotenone stress on cells for 42 hrs increases cleavage of PARP level over control (4.7). Excess generation of NO* facilitates to separate the PARP carboxy-terminal catalytic domain (89kDa) from amino-terminal DNA binding domain (24kDa), which activates the apoptotic pathway. My data also show cells pretreated with 1μM EF24 can prevent nitrosative stress induced PARP cleavage (4.7). EF24 can scavenge the excess NO* and acts as a prophylactic by mitigating the apoptotic stimuli.

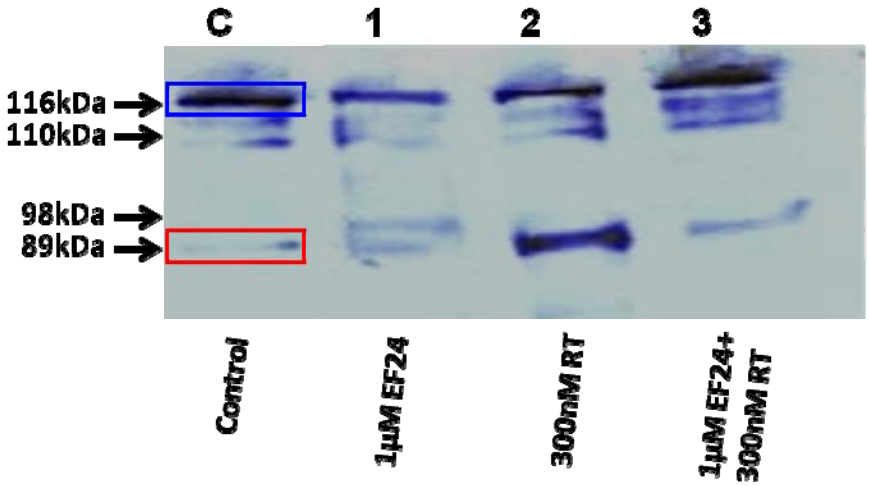

Figure 4.7. Protective effect of EF24 against rotenone induced poly (ADP-ribose) polymerase (PARP) cleavage, marker of apoptosis progression, in PAE cells. PARP cleavage was analyzed via Westernblot analysis (n=1). Whole cell protein extracts were separated using polyacrylamide gel electrophoresis and transferred to a polyvinylidene fluoride (PVDF) membrane, followed by immunoblot analysis utilizing antibodies anti-PARP. Four cell extracts were prepared from: untreated control PAE cells, lane C; cells treated with 1μM of EF24 for 48 h, lane 1; cells treated with 300 nM of rotenone for 42 h, lane 2; and cells pretreated with 1 μM EF24 for 6 hrs followed by addition of 300 nm rotenone and secondary incubated for 42 h, lane 3. The band corresponding to intact PARP protein (116-kDa) is delineated with blue rectangle in Lane C (top). Also in Lane C, the cleavage product of PARP (89-kDa) is delineated with a red rectangle (bottom). Position of protein markers in kDa are annotated to the left of the blot.

S-nitrosylation of PDI mediates synphilin-1 aggregation in model cells of PD

Fig. 4.8 (panels A through E) is a set of confocal microscopy images of GFP-tagged synphilin-1 expressed in transiently transfected PAE cells as a function of different conditions. The results clearly indicate the aggregation of synphilin-1 when exposed to 300 nM rotenone (panel A). As compared to this, pre-treatment of cells with 1 mM EF24 prior to 300 nM rotenone exposure resulted in a markedly diminished level of synphilin-1 aggregation (as evidenced through GFP fluorescence; panel B). Other experiments revealed a relatively homogeneous cytosolic distribution of GFP in cells transfected with pEGFP C2 plasmid alone (panel C). In contrast, cells transfected with EGFP- synphilin-1 constructs show a punctuated (or speckled) cytosolic distribution of green fluorescent signal (panel E). This observation indicates that over expression of synphilin-1 fused to EGFP protein, provided subcellular accumulation of the recombinant fusion protein, called aggregosomes. Cells, treated with the vehicle alone (DMSO; Fig. 4.8D) did not differ in the expression of EGFP-synphilin-1 as compare to untreated cells (Fig. 4.8E).

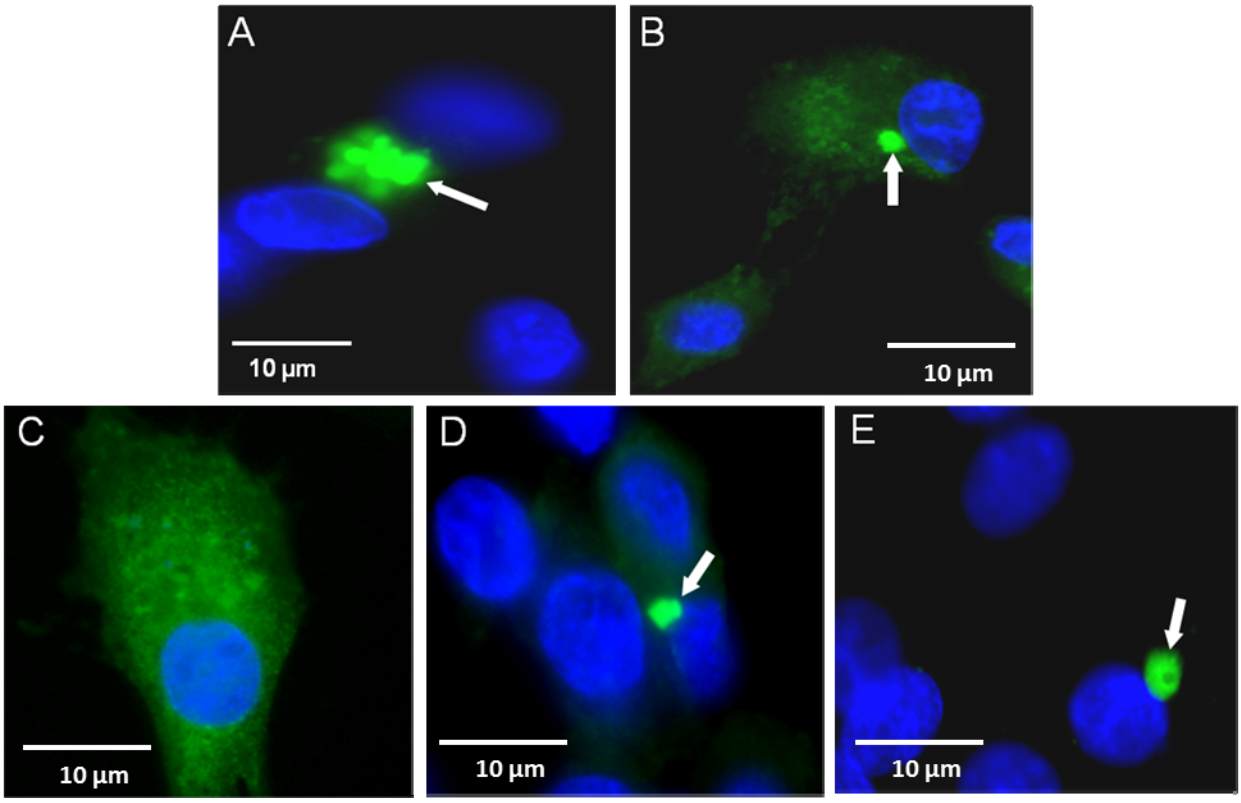

Figure 4.8. Effect of EF24 and rotenone on synphilin-1 distribution in PAE cell. Confocal microscopy images of PAE cells reveal the presence of intracellular aggregates in cells transfected with EGFP-tagged synphilin-1. Transfected PAE cells were DMSO treated or stressed with rotenone and stained by immunofluorescence as detailed in the Materials and methods section. (A) Cells exposed to 300 nM rotenone for 12 h alone, (B) or pretreated with 1 µM EF24 following treatment with 300 nM rotenone. Controls were (C) cells transfected with vector pEGFP-C2, (D) Cells transfected with pEGFP-tagged synphilin-1 construct and treated with DMSO 2.5 v/v and (E) untreated. Nucleus was stained with DAPI, (blue color). White arrows indicate the presence of aggregates corresponding to the recombinant fusion protein.

In summary, these results showed that cells treated with rotenone induced nitrosative stress apparently increased the green fluorescence protein fused to synphilin-1 (or EGFP-synphilin-1) by forming cytosolic inclusion bodies, whereas pre-treatment with 1 μM EF24 mitigated the aggregation of the fused EGFP-synphilin-1 to a significant levels. Figure 4.9 represents similar results in SH-SY5Y cell. I have performed this experiment in human neuronal SH-SY5Y cell line with similar conditions to the experiment in PAE cell line. My data reveal pre-treatment of SH-SY5Y cells with 1 mM EF24 prior to 300 nM rotenone exposure resulted in a markedly diminished level of synphilin-1 aggregation.

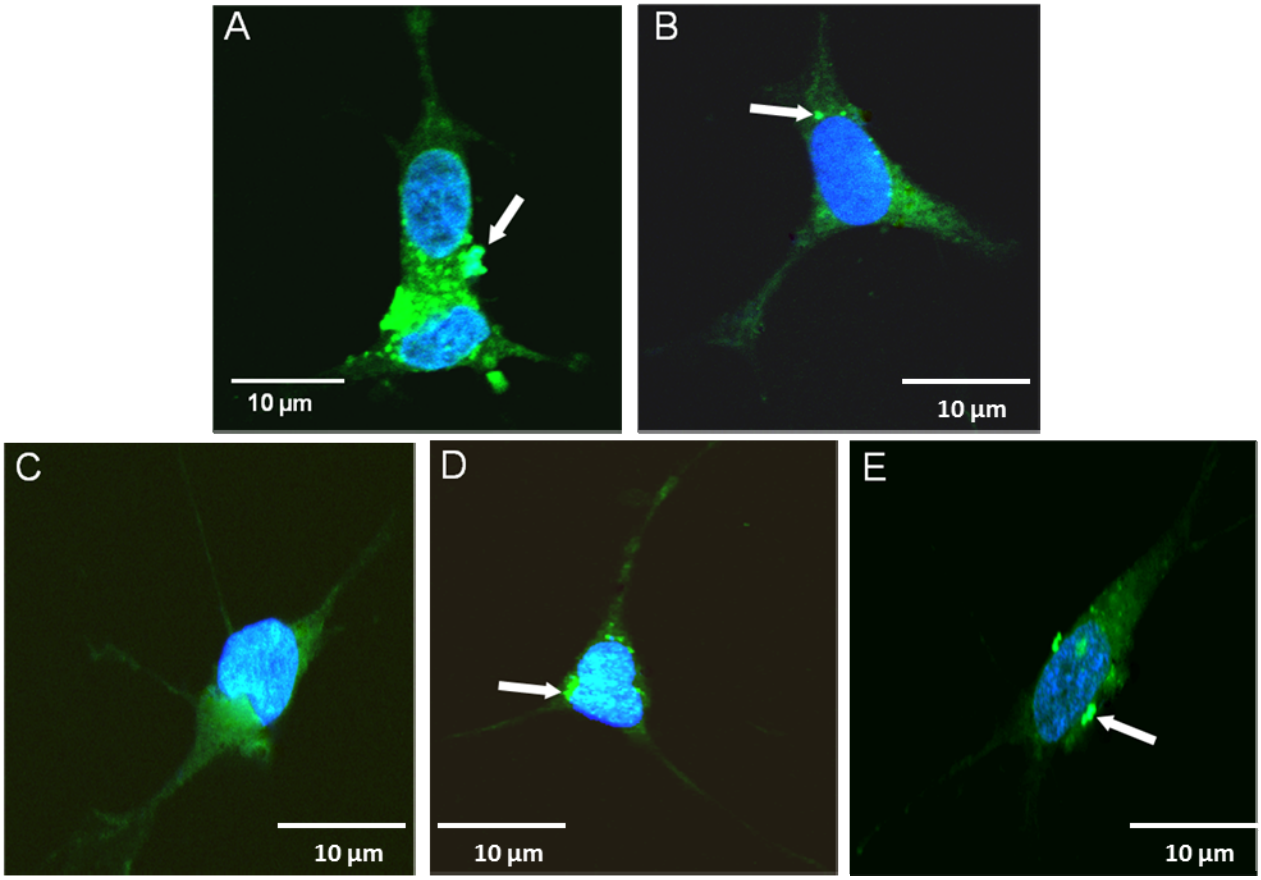

Figure 4.9. Effect of EF24 and rotenone on synphilin-1 distribution in SHSY5Y cell. Confocal microscopy images of SHSY5Y cells reveal the presence of intracellular aggregates in cells transfected with EGFP-tagged synphilin-1. Transfected PAE cells were DMSO treated or stressed with rotenone and stained by immunofluorescence as detailed in the Materials and methods section. (A) Cells exposed to 300 nM rotenone for 12 h alone, (B) or pretreated with 1 μM EF24 following treatment with 300 nM rotenone. Controls were (C) cells transfected with vector pEGFP-C2., (D) Cells transfected with pEGFP-tagged synphilin-1 construct and treated with DMSO 2.5 v/v and (E) untreated. Nucleus was stained with DAPI, (blue color). White arrows indicate the presence of aggregates corresponding to the recombinant fusion protein.

Figure 4.10A is a SDS-gel confirming expression of human-PDI in *E. coli* and Figure 4.10B is a confocal microscopy image confirming that PDI is expressed at a high level within the PAE cells and localized mostly in the endoplasmic reticulum and to a much lower level in the cytosol in PAE cells.

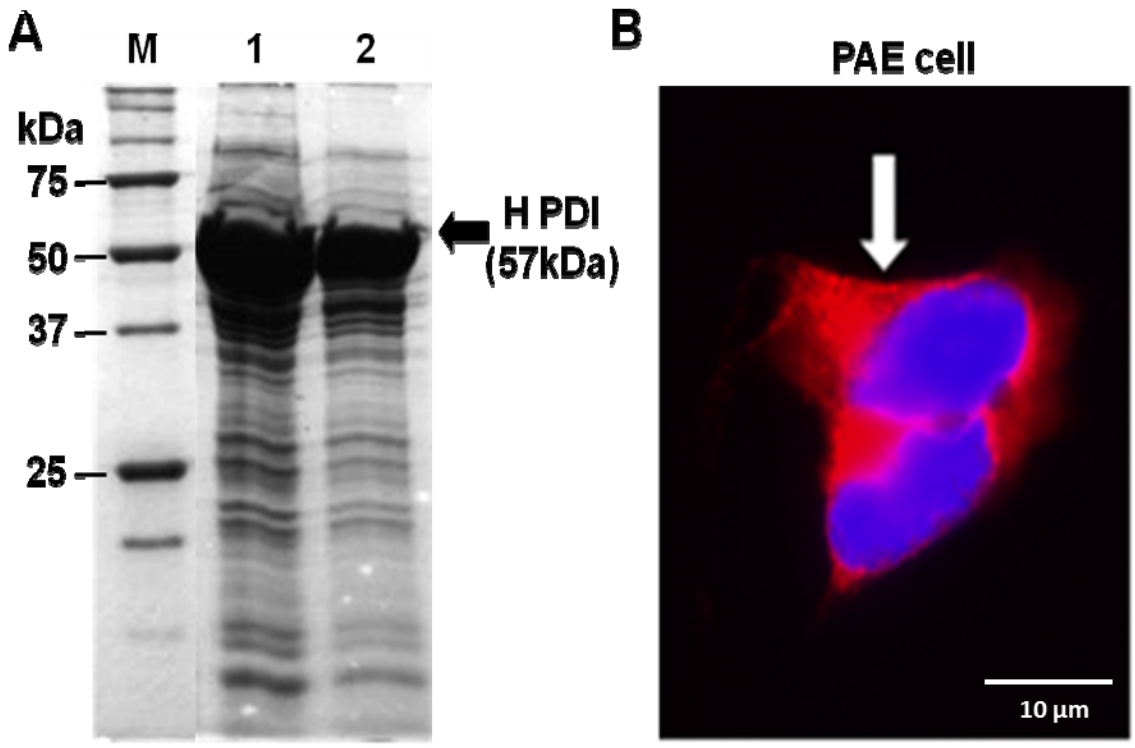

Figure 4.10. Expression of human PDI (57kDa) in bacterial (A) and mammalian (B) cells. Partially Ni-NTA-purified column protein extracts from selected colony of transformed E. coli competent cells expressing human PDI were separated using polyacrylamide gel electrophoresis and stained with Coomassie brilliant blue (A): lane M, protein markers; lane 1, elution 1 with 200 mM imidazol and lane 2, elution 2 with 300 mM imidazole. Representative confocal image of transfected PAE cell expressing human PDI (57kD) (B); white arrow indicate the presence of PDI mainly in the cytosol, confirmed by immunocytochemistry using PDI antibody (red fluorescence signal); cell nuclei was counterstained with 4',6-diamidino-2-phenylindole (DAPI), shown in blue color.

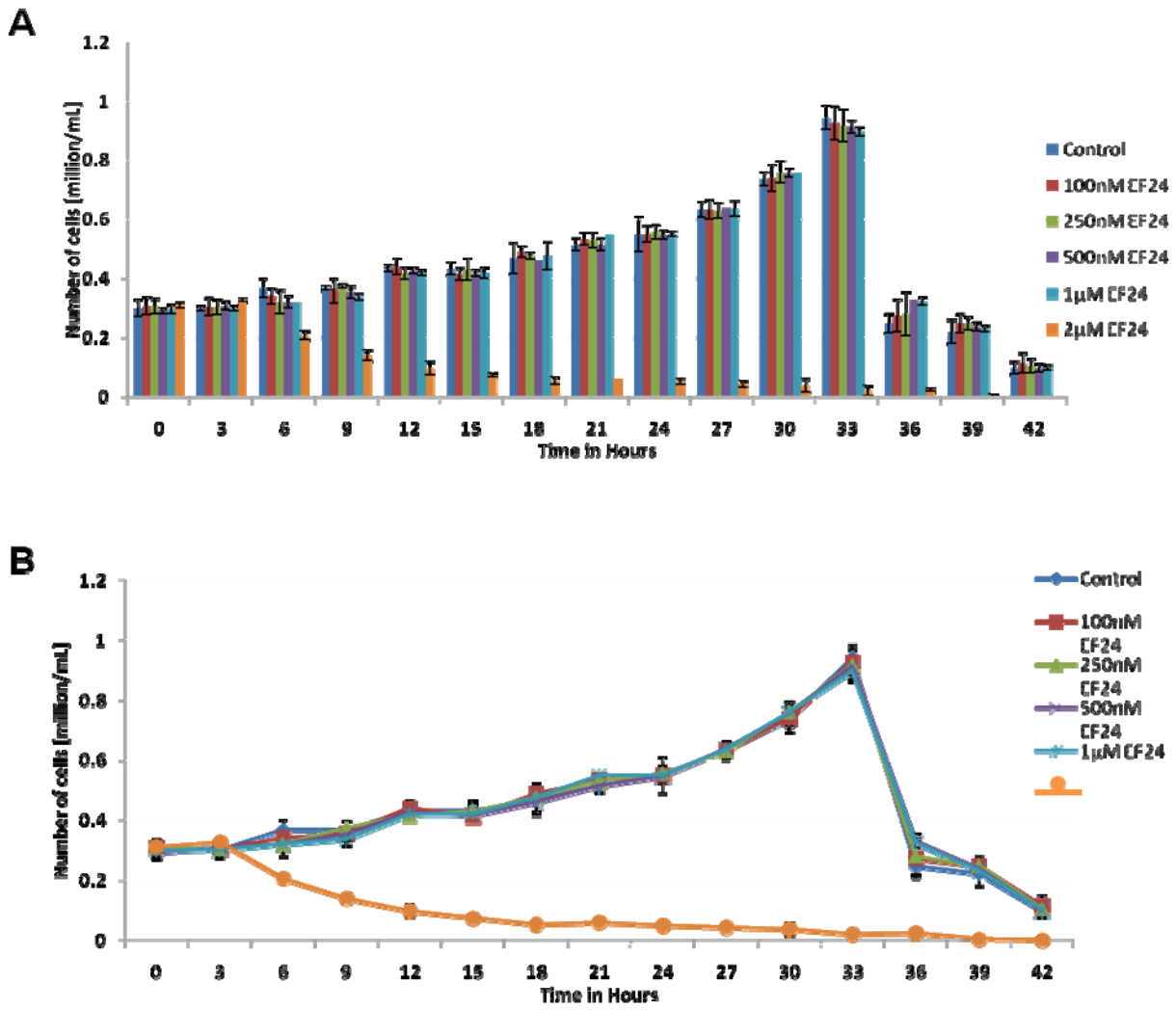

Figure 4.11. The effect of EF24 on PAE cell line, (A) the bar diagram shows effect of EF24 with different concentrations from 100 nM to 2µM (B) the line diagram shows effect of EF24 with different concentrations from 100 nM to 2µM. Control is the untreated cells.

Dose response assay of EF24

Figure 4.11A and 4.11B show the dose response assay of EF24 in PAE cell line. My data reveals EF24 shows no cytotoxicity at 1μM, but it is cytotoxic at 2 μM concentration. Therefore, I have selected 1μM of EF24 to perform my assays in cell.

4.4 Discussion

The mitochondrial respiratory chain (complexes I-V) is the major site of ATP production in eukaryotes (31). Rotenone, inhibitor of the mitochondrial respiratory chain, has been widely used to study the role of the mitochondrial respiratory chain in apoptosis. Recent evidence has demostrated that rotenone leads to apoptotic cell death (mechanism is discussed in introduction section, pg 64).

Here, I hypothesized that the bioavailable EF24 can diminish the chances of apoptotic cell death through mitigating nitrosative stress by scavenging excess NO*. To test my hypothesis, I first exposed EF24 to a model NO* donor under *in vitro* conditions. My data indicated the formation of a nitrated product suggesting that EF24 was capable of scavenging NO* as a free radical scavenger. Next, I determined whether EF24 was capable of rescuing human PDI from nitrosative attack with *in vitro* study. In agreement with previous studies, my data reveal that nitrosative stress results in the loss of PDI catalytic function (32). i.e., PDI-facilitated regeneration rate of the well-known PDI substrate protein RNase A in the presence of a model NO* donor reverts to values obtained in the absence of PDI, suggesting the loss of catalyst activity due to modification of PDI active site by NO*. However, the observed rate of regeneration of RNase A in the presence of PDI, NO* and EF24 equals levels observed with

unmodified PDI (i.e., rate observed in the absence of NO*). This indicates EF24 is able to scavenge elevated levels of NO* and form stable adducts. Although the mechanism of action and location NO* on the polyphenol is not investigated here, my study demonstrates that PDI function can remain unaffected under conditions of nitrosative stress as long as scavenging EF24 is present.

Here, I determined whether EF24 was capable of mitigating nitrosative stress by scavenging excess generation of NO* in cell lines. By using PAE cell line, I investigated the cytotoxicity of rotenone and prophylactic effect of EF24 against rotenone through differential nuclear staining cytotoxicity assay. Although I was unable to detect the mechanism of cell death (Apoptotic or necrotic) by this assay, my study shows that rotenone induced cytotoxicity reduced to a significant level in the presence of EF24.

My next study was to determine whether rotenone induced nitrosative stress leads cell death through apoptotic or necrotic pathways. I used flowcytometric assay to determine the pathway of rotenone induced cytotoxicity in PAE cell line and prophylactic affect of EF24 against rotenone induced nitrosative stress related apoptotic or necrotic cell death. My data demonstrated that rotenone causes cytotoxicity in PAE cell line mostly through the apoptotic pathway and EF24 administration reduces the apoptotic cell death significantly by mitigating nitrosative stress.

I have also done PARP analysis to confirm rotenone induced nitrosative stress leads cell death essentially through apoptotic pathway. Excessive generation of NO* by mitochondrial complex-I inhibitor rotenone leads PARP cleavage *via* caspase activity which in turn activates apoptotic stimuli in eukaryotic cell. I determined that rotenone induced PARP cleavage is reduced significantly in the presence of EF24. This suggests that EF24 can prevent ROS-dependent apoptotic cell death.

Taken together I conclude that rotenone activates activates the programmed cell-death stimuli and results in apoptotic cell death *via* caspase-9 and caspase-3 activation→PARP cleavage→DNA fragmentation; EF24 acts as a prophylactic against rotenone induced nitrosative stress related apoptotic cell-death.

Scheme 4.1 is the representative model, which shows the effect of PDI in Ubiquitin Protease System (UPS) of a cell. Recent studies showed that brains manifesting sporadic Parkinson's or Alzheimer's disease, that PDI is S-nitrosylated, a reaction transferring a nitric oxide (NO) group to a critical cysteine thiol to affect protein function (22). Nitrosative stress induced S-nitrosylation of PDI inhibits its enzymatic activity, leads to the accumulation of polyubiquitinated proteins, and activates the unfolded protein response. S-Nitrosylation also abrogates PDI-mediated attenuation of neuronal cell death triggered by ER stress, misfolded proteins or proteasome inhibition. Thus, PDI prevents neurotoxicity associated with ER stress and protein misfolding, but NO* blocks this protective effect in neurodegenerative disorders through the S-nitrosylation of PDI, which opens up the pathway of apoptotic cell death.

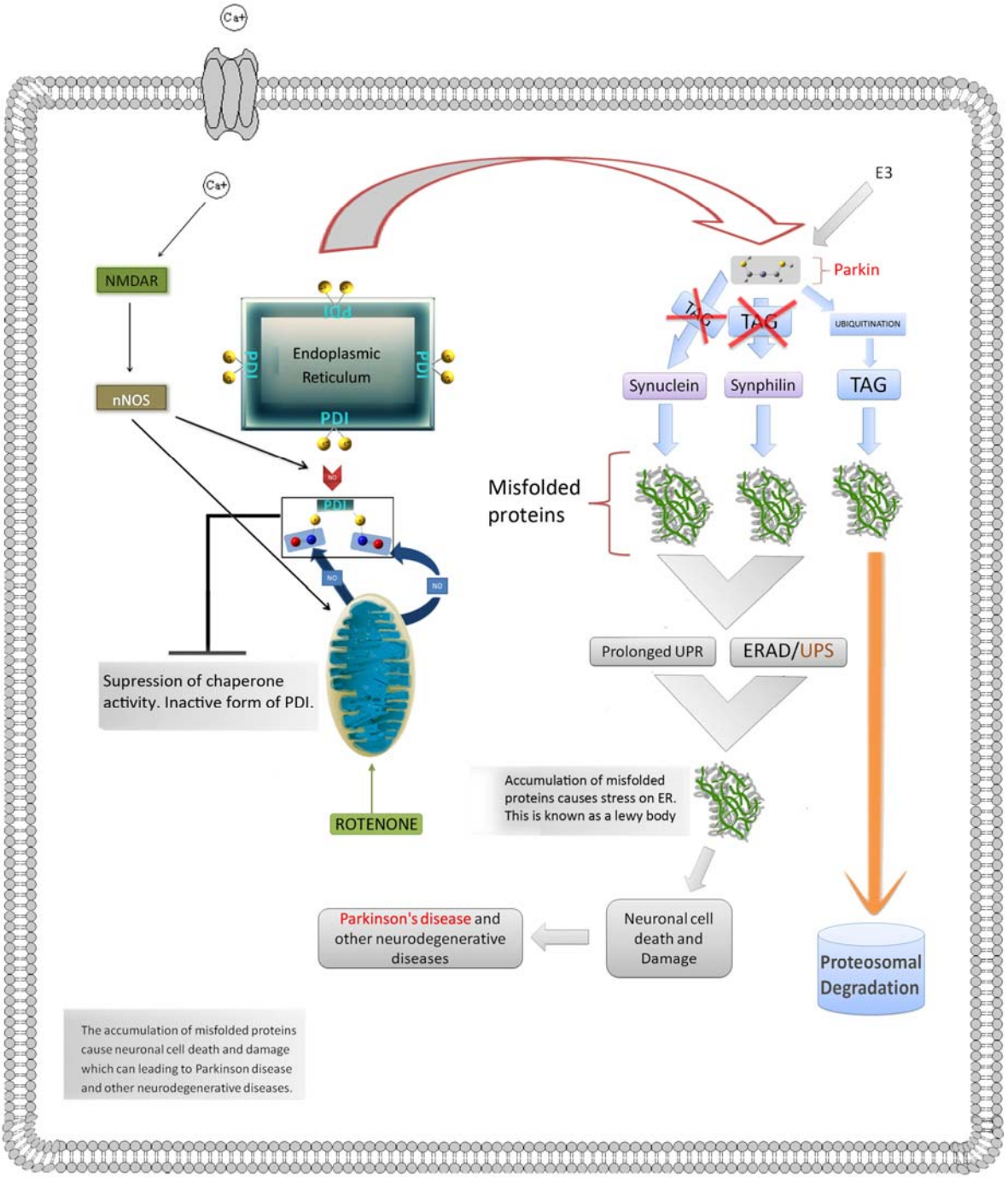

Scheme 4.1. A representative model shows how PDI plays a vital role in Ubiquination protease system and nitrosative stress induced S-nitrosylation leads to apoptotic cell death.

Finally, I examined the impact of cytosolic aggregation of synphilin-1 in the SHSY5Y and PAE cell line under rotenone-induced nitrosative stress as previously demonstrated (22). GFP-labeled synphilin aggregation was monitored using confocal microscopy. In comparison to control experiments, incubation of the cell line with rotenone clearly demonstrated cytosolic aggregation of synphilin-1 consistent with previous results suggesting that healthy PDI inhibits aggregation of synphilin-1 (22). As one of the controls, I tested whether unstressed cells expressing PDI could prevent synphilin-1 constituted Lewy-body-like inclusions that can be formed in the cytosol after synphilin-1 overexpression (22). My data revealed very limited diffused synphilin-1 localization in cytosol (Fig. 4.8E and 4.9E). In contrast, rotenone treated cells showed discrete inclusions of synphilin-1 in the cytosol. These results suggest that rotenone-dependent elevation of nitric oxide attenuated the protective effect of PDI on synphilin-1 inclusions (Fig. 4.8A and 4.9A).

Next, cells were preincubated with EF24 prior to rotenone exposure to determine whether EF24's NO* scavenging ability demonstrated *in vitro* could be translated inside the cell. Confocal microscopy data monitoring GFP-tagged synphilin-1 clearly indicate that unlike rotenone-induced nitrosative stressed cells (Fig. 4.8A and 4.9A), cells pre-treated with EF24 followed by rotenone treatment showed a drastic decrease in discrete Lewy-like inclusions in cytosol (Fig. 4.8B and 4.9B). These results suggest that EF24 can intracellularly rescue S-nitroso modification of PDI as seen under elevated levels of nitrosative stress and prevent Lewy-neurite formation in my experimental model system and thus, EF24 acts as a potent prophylactic against rotenone induced apoptotic cell death.

Chapter 5:

The Impact of Nitrosative-Stress-Linked PDI Damage on Estrogenic Status of Cells

5.1 Introduction

The role of PDI on protein folding is been well-studied in the previous chapters. Recent studies have demonstrated PDI plays a very crucial role in breast cancel study by maintaining the homeostasis of estrogen receptors (15, 17). In this chapter I have dicussed the impact of rotenone-induced chemical modification of PDI on estrogenic status; prevention against the alteration of estrogenic status by small molecule intervention. Breast cancer is the second leading cause of cancer-related deaths in women worldwide and approximately almost 1.5 million women are diagnosed with breast cancer annually (1). It is well-known that estrogen plays important physiological roles not only in women but also in men and that the biological effects of estrogen are mediated by estrogen receptors. Estrogen receptor super-family consists of two homologous nuclear receptors, estrogen receptor alpha (Erα) and estrogen receptor beta (Erβ) (2). Erα and Erβ exhibit different transcriptional activities and functions in breast cancer. Erα is expressed in approximately 70% of human breast cancer patients (3).The ratio between Erα and Erβ is important to maintain cellular homeotsasis. Evidence has demonstrated overexpression of Erα relative to Erβ in breast cancer cells compared to normal tissues suggesting that disruption of Erβ/Erα expression may lead to breast carcinogenesis (4). The abundance of Erβ in the male urogenital tract has also refocused attention on the role of estrogen in males (5). Similar to Er, G-protein coupled ER1 (GPER; previously known as GPR30) can be activated by a wide variety of Er agonists like 17β-estradiol as well by partial antagonists such as tamoxifen. The role of GPER in breast cancer is still not clear (6). Among the plethora of biological effects, angiogenesis, cell

proliferation and invasiveness are most common features exerted during breast cancer, which are related to direct interaction of estrogen with an intracellular receptor that activates the expression of genes encoding proteins (7). The hormonal actions of estrogen are as important to maintain the normal female physiology including the development of target organs as it contributes to tumor formation in certain target organs. In addition, estrogen receptors have also been reported to play crucial role in bone maintenance as well as in mediating E2-induced rapid signal transduction (2-5).

PDI (Fig.3.1A), a chief ER resident oxidoreductase molecular chaperone, plays a central role in oxidative protein folding catalysis (8-11). In addition, it was suggested that PDI can interact directly with ERα (12-14) with its Er-interacting property very similar to Hsp90 and Hsp70, two well-known chaperone proteins that can alter Er functions (15, 16). PDI, with its possible impact on Erα, acts as a modulator of estrogen's hormonal activity in different target cells. The intracellular PDI-bound estrogens can be released from PDI to initiate the Er-mediated transcriptional activity as well as mitogenic actions (17). Studies suggest that PDI plays a critical role in estrogen responsiveness by functioning as a molecular chaperone and PDI alone is capable of interacting with Erα and influencing its activity (18). I observed that, PDI can alter Erβ to Erα ratio significantly by altering the levels of two proteins in opposite directions, down-regulation of Erα and up-regulation of Erβ. The human estrogen receptors are expressed in breast cancer MCF-7 cells and play a major role in tumorigenic processes (19).

In this study, I chose to evaluate PDI's ability to maintain Erα and Erβ levels in MCF-7 cell under control and nitrosative stress conditions. Initially, I gathered the evidence to show that PDI is S-nitrosylated (SNO-P), and NO-induced chemical modification of PDI abolishes its ability to maintain Erβ/Erα ratio by altering the levels of Erβ and Erα. Using a battery of biochemical and

molecular techniques, I have demonstrated PDI colocalization with Erα in MCF-7 nuclei under normal and nitrosative stress condition, using a variety of molecular and biochemical approaches. The selected polyphenol, EF24 (Fig. 3.1B) was then introduced to determine whether they can rescue PDI-dependant Erα and Erβ function and furthermore, prevent the change in receptor proteins levels. My results indicate that EF24 promotes the homeostasis of estrogen in target cell. The implications for prevention of nitrosative stress effect induced endogenous estrogens related different disorders are discussed.

5.2 Materials and Methods

Reagents and cell line.

Reagents were purchased as follows: Mouse monoclonal PDI (Abcam, Cambridge, MA, USA), rabbit polyclonal Erα (Santa cruz, Santa cruz, CA, USA), Erβ (Invitrogen, Carlsbad, CA, USA) and GAPDH (Glyceraldehyde 3-phosphate dehydrogenase, Cell Signalling, Danvers, MA, USA), horseradish peroxidase (HRP)-conjugated goat anti-mouse and/or goat anti-rabbit IgG (KPL Biomedical) and MCF-7 (Obtained from ATCC, Manassas, VA).

Cell Culture.

Human breast adenocarcinoma cells (MCF-7) were cultured in RPMI-1640 media (Roswell Park Memorial Institute-1640, pH 7.2, Hyclone Laboratory) supplemented with 10% fetal bovine serum (Atlanta Biologicals) and 100 U/ml penicillin-streptomycin (Sigma). Cells were incubated in 5% CO_2 and 78% relative humidity at 37 °C. MCF-7 cells (1×106 cells/well) were seeded onto 6-well plates in RPMI-1640 at 37 °C in 5% CO_2 incubator. After 12 hrs, cells were treated with different concentrations of EF24 and various concentrations of rotenone.

Rotenone and EF24 treatment.

Cells were treated with 1μM EF24 for 3 hrs and followed by treatment with 400 nM of rotenone for 2 hrs. Total cellular protein extracts Ire prepared by washing the cells with cold Tris-buffered saline, collected by centrifugation (3003g, 5 min at 48ºC), and extracted by sonicating in buffer containing 10 mM Tris–HCl (pH 7.4), 10 mM EDTA, 2% (w/v) SDS and protease inhibitors (Sigma). Total protein concentrations were measured using a bicinchonic acid kit (Pierce) and subjected to immunoblot analyses.

Immunoblot analyses.

Blots were incubated in blocking buffer (5%, w/v, dried skimmed milk in Tris-buffered saline, pH 7.4, and 0.1% TIen 20) then developed using anti-PDI monoclonal antibody (1:500 abcam) or anti-Erα antibody(1:100 dilution) or anti-Er-β antibody (1:100 dilution) or anti-GAPDH (Glyceraldehyde 3-phosphate dehydrogenase, 1:1000 dilution) diluted in blocking buffer and applied for 1 h at RT and incubated with horse radish peroxidase (HRP)-conjugated goat anti-mouse or anti-rabbit (KPL Biomedical) in 1% BSA in TBST for 30 min. Chemiluminescence (ECL-plus or SuperSignal Ist Pico Chemiluminescent Substrate) was used according to the manufacturer's (Amersham or Pierce Biotechnology Inc.) instructions for detection of protein. Antibody binding was revealed using peroxidase-conjugated secondary antibodies and enhanced Chemiluminescence (ECL-plus or SuperSignal west Pico Chemiluminescent Substrate) according to facturer's (Amersham or Pierce Biotechnology Inc.) protocols.

Confocal microscopy and immunocytochemistry.

For confocal microscopy, cells were pre-treated with 1μM EF24 for 3 hrs, followed by 400 nm rotenone for 2 hrs as described above. For controls, cells were treated with DMSO, EF24, and rotenone, as mentioned in the experimental samples. Next, cells were fixed with methanol (100%) and incubated at –20 °C for 5 min before blocking with 5% normal goat serum (NGS). Then, cells were incubated overnight at 4ºC with respective primary antibodies i.e., anti-PDI (monoclonal, 1:500), anti- Er-α or anti-Er-β (1:100) in 1% NGS. The slides were washed and reacted with Fluorescein isothiocyanate (FITC) conjugated goat anti-rabbit IgG (for Erα and or Erβ), and Rhodamine conjugated goat anti-mouse IgG (for PDI) in 1:100 dilution. The cells were counter-stained with 10 mg/mL 4′-6-Diamidino-2-phenylindole (DAPI), mounted with DAKO medium (DAKO Corporation, CA) and visualized by confocal microscopy (Zeiss LSM 700 confocal).

5.3 Results

Impact of reactive oxygen species on PDI and attenuation by polyphenol EF24.

Immunoblot assay was done with PDI antibody to show the effect of rotenone and EF24 on expression level of PDI in MCF-7 cell. Result shows that the levels of expression of PDI as a function of increasing concentrations of rotenone (Fig. 5.1A). A dose-dependent decrease in oxidoreductase expression is observed as rotenone levels increase as evidenced by immunoblot analysis Lane 3 and 4). This attenuation in PDI expression may couple with the modification of the oxidoreductase active site and loss of oxidoreductase activity. Remarkably, pretreatment of the cells with EF24 prior to rotenone infusion shows that the polyphenol is able to rescue PDI

expression (Lane 5 and 6) and mitigate loss of oxidoreductase functionality. Densitometric analysis (Fig. 5.1B) of this immunoblot assay using Glyceraldehyde 3-phosphate dehydrogenase (GAPDH) as the intrinsic control confirmed that intervention by EF24 restores PDI levels to those observed in the absence of rotenone-dependent ROS infusion.

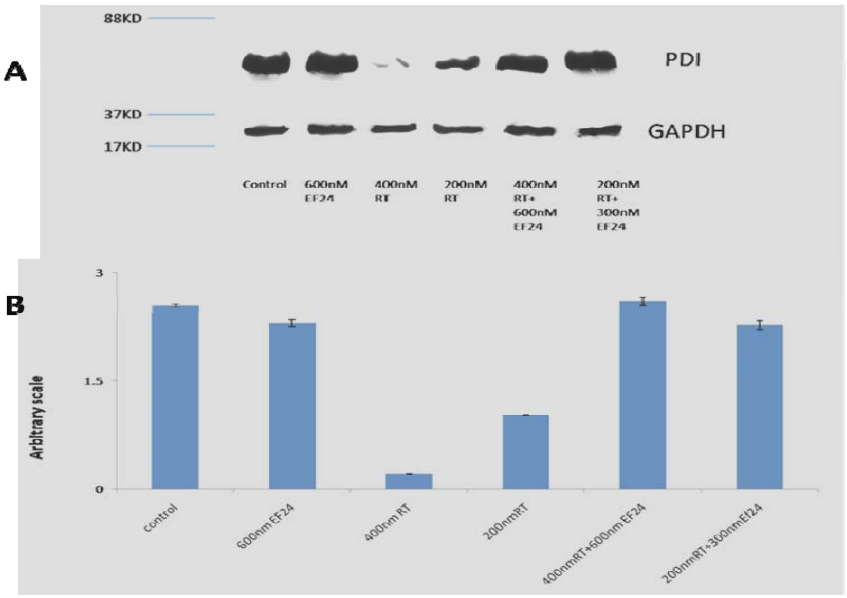

Figure 5.1. Effect of EF24 and rotenone on PDI expression in MCF-7 cells (A) MCF-7 cells were treated with rotenone and EF24 at different concentrations (range) and cell lysates were analyzed by immunoblot using PDI antibody (monoclonal). Lane 1, untreated cell lysates. Lane 2, cells were treated with 600 nm EF24 alone for 5 hrs. Lane 3 and 4, cells were treated with 400 nm and 200 nm rotenone for 2 hrs. Lane 5 and 6, cells were stressed with 400 nm and 200 nm rotenone for 2 hrs after pre-incubation with 600 nm and 300 nm EF24 for 3 hrs. GAPDH was used as a loading control. Results are representatives of triplicates (B) Densitometric analysis of PDI protein level in MCF-7 cells

S-nitrosylation of PDI in MCF-7 cells is associated with down-regulation of Erα but up-regulation of Erβ.

Fig 5.2 and 5.3 are results from immunoblot assays performed with Erα and Erβ antibodies to show the effect of rotenone and EF24 on expression level of Erα and Erβ in MCF-7 cells; immunoblotting and densitometric analysis of these immunoblot assays using GAPDH as the control confirmed that PDI-dependent Erα levels were significantly decreased as a function of rotenone concentration (lane 1 vs. 3 and 4 in fig. 5.2). In contrast, and in agreement with previous studies, Erβ levels rose as a function of rotenone concentration and PDI compromise (Lane 1 vs. 3 and 4 in Fig. 5.3).

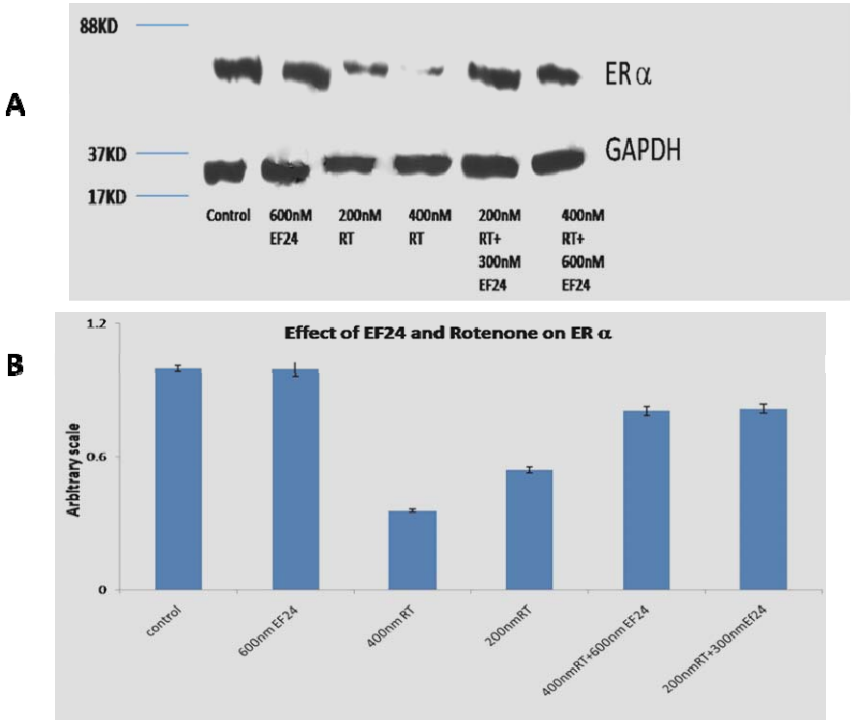

Figure 5.2. Effect of EF24 and rotenone on ERα expression in MCF-7 cells (A) MCF-7 cells were treated with Rotenone and EF 24 at different concentrations and cell lysates were analyzed by Western blot with Erα antibody. Lane 1, untreated cell lysates. Lane 2, cells were treated with 600 nm EF24 alone for 5 hrs. Lane 3 and 4, cells were treated with 200 nm and 400 nm rotenone for 2 hrs. Lane 5 and 6, cells were stressed with 200 nm and 400 nm rotenone for 2 hrs after pre-incubation with 300 nm and 600nm EF24 for 3 hrs. GAPDH was used as a loading control. Results are representatives of triplicates (B) Densitometric analysis of Erα protein level in MCF-7 cells.

The PDI-dependent Erβ/Erα ratio increased to a significant level in the presence of rotenone. My data demostrate the impact of EF24 incubation on the cell line prior to rotenone addition (Fig. 5.2 and 5.3). In the presence of EF24 and rotenone, both Erα and Erβ levels were returned to those in the absence of rotenone. The observed Erβ/Erα ratio was also found to be in agreement with the results obtained in the absence of rotenone. Those observed during homeostasis (lane 1 and 2 in Fig. 5.2 and 5.3) measurement of Er receptor proteins. This observation reveals that in MCF-7 cells upon S-nitrosylation of PDI, the Erβ to Erα ratio would have significantly increased.

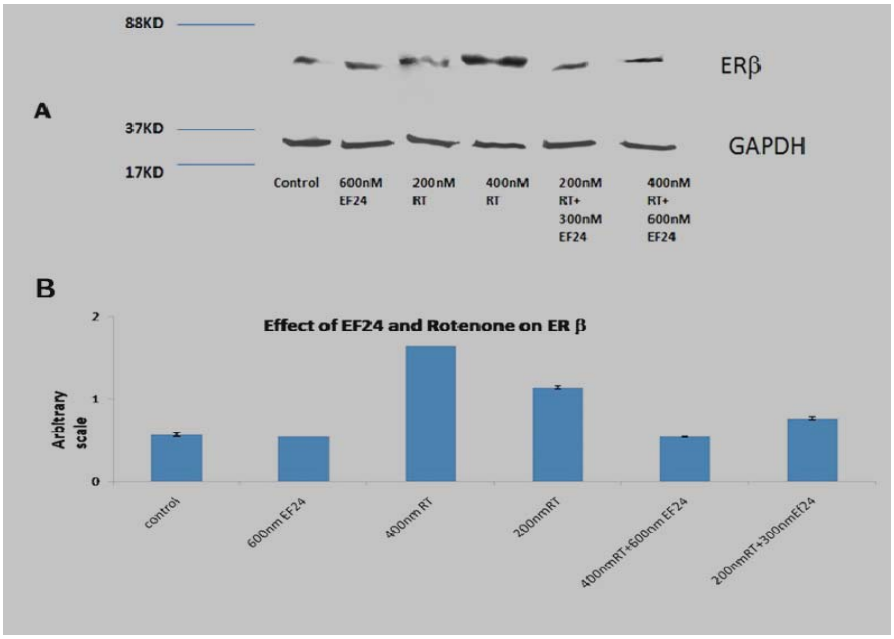

Figure 5.3. Effect of EF24 and rotenone on Erβ expression in MCF-7 cells (A) MCF-7 cells were treated with Rotenone and EF24 at different concentrations and cell lysates were analyzed by Western blot with Erβ antibody. Lane 1, untreated cell lysates. Lane 2, cells were treated with 600 nm EF24 alone for 5 hrs. Lane 3 and 4, cells were treated with 200 nm and 400 nm rotenone for 2 hrs. Lane 5 and 6, cells were stressed with 200 nm and 400 nm rotenone for 2 hrs after pre-incubation with 300 nm and 600 nm EF24 for 3 hrs. GAPDH was used as a loading control. Results are representatives of triplicates (B) Densitometric analysis of Erβ protein level in MCF-7 cells.

EF24 helps to maintain Erβ/Erα ratio in MCF-7 cells.

MCF-7 cells pretreated with EF24 for 3 hrs prior to the addition of rotenone and subsequent 2 hrs incubation showed no significant changes of Erα and Erβ protein levels in MCF-7 cells. EF24 can scavenge the nitrosative stress of rotenone on PDI and maintain ERα protein level by preventing the down-regulation of Erα (lane 1 vs. 5 and 6 in Fig. 5.2A) and simultaneously

maintains Erβ protein level in cells by preventing up-regulation of Erβ (lane 1 vs. 5 and 6 in Fig. 5.3A). Densitometric analysis of these immunoblot assays using GAPDH as the control showed down-regulation of Erα and up-regulation of Erβ upon rotenone treatment but this imapct (of rotenone) is rescued by EF24 (Fig. 5.2B and 5.3B).

Effect of rotenone on Erα expression level in MCF-7 cells and prophylactic intervention of EF24.

Confocal microscopic and immunocytochemistry analysis performed to analyze the effect of rotenone and EF24 on MCF-7 cells (Fig. 5.4) show Erα expression level decreases significantly when cells Ire stressed with 400 nm rotenone for 2 hrs (Fig. 5.4F). In contrast, the ERα expression level in cells (Fig. 5.4G), pretreated with 1μM EF24 for 3 hrs and followed by 400 nm rotenone insult for 2 hrs, closely resembles to Erα expression level in untreated cell. As a control for non-specific effects, untreated (Fig. 5.4D) and 1μM EF24 treated (Fig. 5.4E) cells were included. These results show that EF24 has prophylactic effect against nitrosative stress and plays vital role in maintaining Erα expression level in MCF-7 cells.

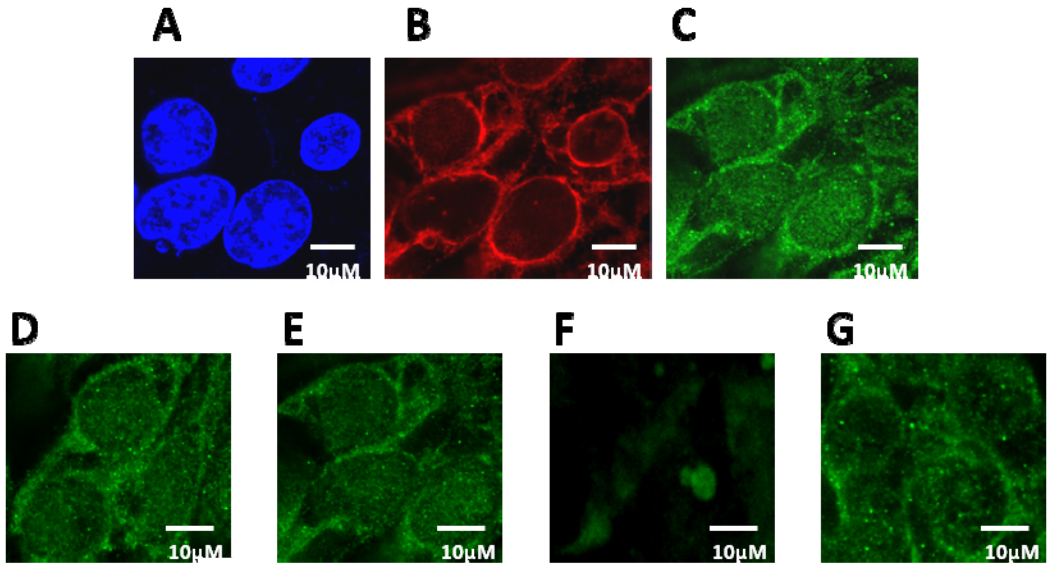

Figure 5.4. Expression and localization of PDI and Erα in MCF-7 cells, and effect of EF24 and rotenone on Erα distribution in MCF-7 cells. Confocal fluorescence images of MCF-7 cells reveal the distribution of PDI and Erα in cells. (A) Cells stained with DAPI showing nucleus in blue color (B) Cells stained with rhodamine showing PDI in red color, (C) Cells stained with FITC showing Erα in green color, (D) Expression of Erα in untreated cells, (E) Erα expression level when cells were treated with 1μM EF24 alone, (F) Erα expression level when cells were exposed to 400 nm rotenone for 2 h, and (G) Cells pretreated with 600 nm EF24 for 3 hrs followed by 400 nm rotenone treatment for 2 hrs. All the cover-glasses were counterstained with DAPI, to delimitate the nucleolus (blue color).

Effect of rotenone on Erα and PDI colocalization in MCF-7 cells and prophylactic intervention of EF24.

As it has been earlier determined that PDI binds with Erα and helps to maintain Erα level in MCF-7 cells, I was interested to investigate whether there is colocalization of PDI and Erα under both homeostasis and stress conditions. Confocal images show Erα and PDI colocalization diminizes significantly when cells were stressed with 400 nm rotenone for 2 hrs (Fig. 5.5C). Again, the colocalization levels in cells (Fig. 5.5D), pretreated with 600 nm EF24 for 3 hrs and followed by 400 nm rotenone insult for 2 hrs, is compared to controls. As a control for non-specific effects, untreated (Fig. 5.5A) and 1μM EF24 treated (Fig. 5.5B) cells were included. These results show that EF24 has prophylactic effect against nitrosative stress and plays vital role in maintaining homeostasis of Erα in MCF-7 cells.

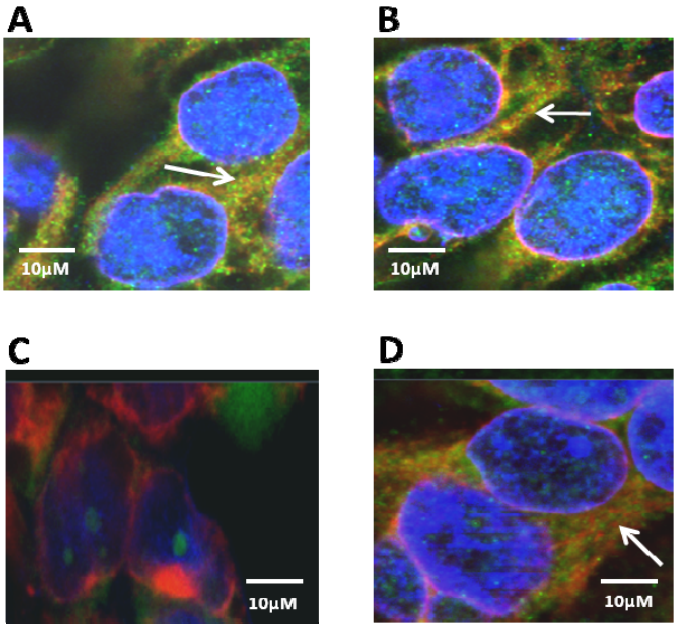

Figure 5.5. Confocal fluorescence images of MCF-7 cells reveal the colocalization (yellow zone indicated by White arrow) of PDI and Erα in cells. MCF-7 cells were untreated or stressed with rotenone and processed for immunofluorescence as detailed in the Materials and methods section. (A) Colocalization in untreated cell, (B) Colocalization after cells were treated with 1 μM EF24 treatment, (C) Colocalization in cells after 400 nm rotenone insult for 2 h, and (D) Colocalization was compared to control when cells were pretreated with 600 nm EF24 for 3 hrs followed by 400 nm rotenone treatment for 2 hrs. All the cover-glasses were counterstained with DAPI, rhodamine, and FITC to delimitate the nucleolus (in blue color), PDI (in red color), and Erα (in green color) respectively.

5.4 Discussion

PDI is a well-known protein folding catalyst that possesses high-capacity intracellular estrogen-binding properties and can modulate the estrogen receptor proteins levels (15). The

estrogen receptor protein-interacting ability of PDI may offer an explanation for the intriguing property of estrogen status maintenance in target tissues (such as breast cancer tissue). Inherent interaction of PDI with estrogen receptor protein is an important modulator of estrogen's hormonal activity. My results provide definitive evidence demonstrating that PDI can significantly alter the ratio of Erβ to Erα by altering the levels of these two proteins in opposite directions under nitrosative stress condition. This unique function of PDI offers new mechanistic insights into the modulation of estrogenic status in target cells. This is important because nitrosative stress represents a threat to estrogen receptor protein levels through PDI and alterations in these levels have been shown to be associated with onset of defective reproductive organs development (16).

My study has established that EF24, is able to protect PDI function under conditions of nitrosative stress by scavenging free radical (NO*) and forming stable adducts which result in homeostasis of Erβ/Erα ratio. This finding offers new mechanistic insights into intervention of estrogenic status in target cells. Importantly, my data demonstrate that EF24 can serve as lead prophylactics in the search for small molecules that can prevent the nitrosative stress-related damage in estrogen status which is pivotal in reproductive organs development. My elucidation of an NO-mediated dysfunction of PDI provides a possible mechanistic link between free radical production, and inactive PDI in breast cancer cell lines via abnormal level of estrogenic status. My results also provide a route for prophylacxis (through EF24). The elucidation of this SNO-PDI-mediated pathway that contributes to neuronal disorder, and the prophylactic mechanism of a polyphenol might permit the development of new therapeutic approaches for cancer and other disorders associated with excessive NOS production related PDI dysfunction.

Chapter 6:

Summary and Concluding Remarks

6.1 Summary and concluding remarks

Protein traffic in the ER comprises incoming nascent chains that need to fold; outgoing bioactive polymers constitute the secretory pathway; and, terminally misfolded debris constitutes the retrotranslocatory pathway (25). Efficient catalytic function of PDI is pivotal to facilitating the majority of incoming traffic along the secretory pathway. Compromised PDI activity can compromise fold maturation, reduce secretory traffic and increase retrotranslocatory flux; in turn, retrotranslocatory debris destined for the proteosome can overwhelm the cytosolic housekeeping machinery and lead to the onset of neuropathies (Scheme 4.1) (25, 26).

Even under conditions of homeostasis, the evolution of PDI as an oxidoreductase can reduce fold maturation yields in the physical folding step of oxidative folding resulting in compromised processing of secretory traffic. Results from this study imply that the self-limited catalytic potential of PDI may detract a portion of the incoming flux from exiting the ER through the secretory pathway (Chapter 2). Such a subset of the incoming flux would then constitute the retrotranslocatory pathway and impose a burden on the cytosolic housekeeping machinery. The retrotranslocatory flux from the ER to the cytosol can thus set-up conditions where aggregation-prone cytosolic proteins such as synphilin-1, synuclein, Aβ escape surveillance by housekeeping leading to the onset of neuropathies such as Alzheimer's and Parkinson's diseases (4, 25, 26).

Nitrosative and oxidative stress, associated with the generation of excessive reactive oxygen or nitrogen species, are thought to contribute to neurodegenerative disorders. Many such diseases are characterized by conformational changes in proteins that result in their misfolding and

aggregation (25). Accumulating evidence implies that at least two pathways affect protein folding: the ubiquitin-proteasome system (UPS) and molecular chaperones (26). Normal protein degradation by the UPS can prevent accumulation of aberrantly folded proteins. Molecular chaperones, PDI, glucose-regulated protein 78, and heat shock proteins, can provide neuroprotection from aberrant proteins by facilitating proper folding and thus preventing their aggregation. My recent studies have linked oxidative and nitrosative stress to protein misfolding and neuronal cell death.

It was suggested that PDI can interact directly with estrogen receptor (Erα) [18-20] with its estrogen-interacting property very similar to Hsp90 and Hsp70, two well-known chaperone proteins that can alter ER functions [21-22]. PDI, with its possible Erα chaperoning activity, acts as a modulator of estrogen's hormonal activity in different target cells (23). The intracellular PDI-bound estrogens can be released from PDI to instigate the Er-mediated transcriptional activity as well as mitogenic actions [23]. My study demonstrated that during nitrosative stress, excess generation of NO* species leads to compromise of PDI's activity; in turn, this causes a diminution of colocalization with estrogen receptor (Erα). Such a scenario can alter the homeostasis of estrogenic status and leads to cancer.

A goal of this dissertation was to determine whether polyphenolic phytochemical can protect PDI from free radical stress. My combined data reveal that though polyphenloic intervention, PDI can be rescued from chemical modification under ROS-stress. As a result, its catalytic activity can be restored. Restored catalytic activity of PDI is important for maintaing levels of secretory traffic under ROS stress; neuroprotection of select cell types through mitigation in the accumulation of neurodegenerative biomarkers; and in the estrogenic status of other cell types.

6.2 Future directions and discussion

After intensive studies with the prophylactic properties of EF24 against free-radical stress, I was interested to further my research to investigate other chemical compounds which can serve as lead compounds against neuropathy. Therefore, future direction of this dissertation was designed to investigate the prophylactic effect of those compounds against free-radical stress induced pathogenesis. It has been postulated that the pathogenesis of Parkinson's disease (PD) is associated with mitochondrial dysfunction (1). Rotenone, an inhibitor of mitochondrial complex I, provides models of PD both *in vivo* and *in vitro* (2). During the search for lead compounds against free radical stress, I investigated the neuroprotective effect of Na-D-β-hydroxybutyrate (NaβHB), a ketone body, against rotenone toxicity by using SH-SY5Y dopaminergic neuroblastoma cells. Pretreatment of cells with NaβHB provided significant protection to SHSY5Y cells. NaβHB attenuated the rotenone-induced activation of caspase-9 and caspase-3. These data demonstrated that NaβHB had a neuroprotective effect that supported the mitochondrial respiration system by reversing the inhibition of complex I. My preliminary results provide an indication that ketone bodies, the alternative energy source in the mammalian brain, appear to have therapeutic potential in PD and opens up a broad area of future research where therapeutic effect of these ketone bodies against neurodegenerative diseases would be a valuable investigation.

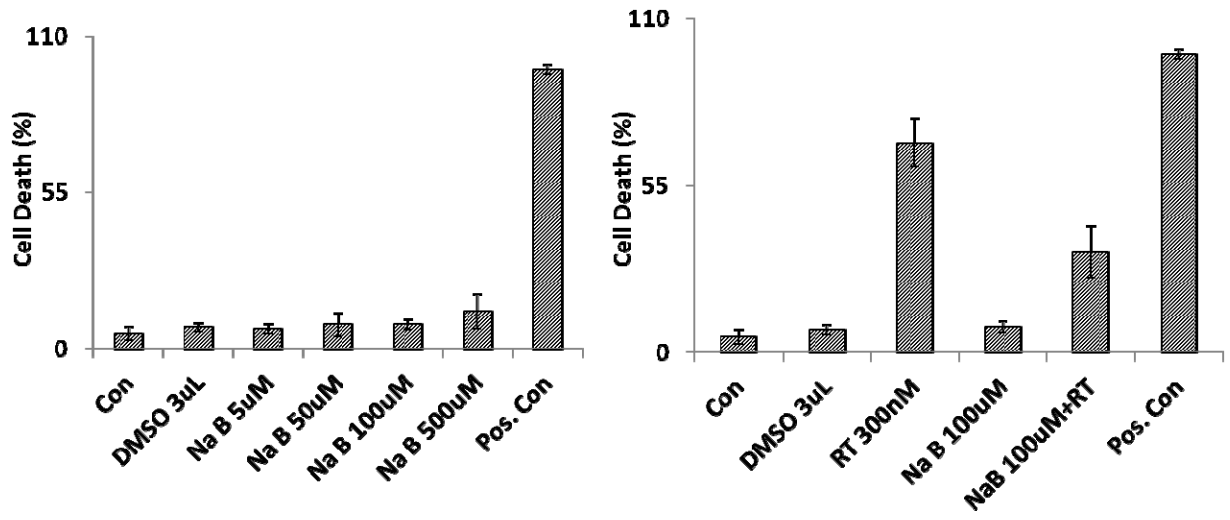

Figure 6.1. Cytotoxicity assay in SH-SY5Y cells. (A) Shows the cytotoxic effect of different concentrations of sodium beta hydroxy butyrate (NaβHB) treatment (24 hrs) on the viability of SH-SY5Y cells. (B) Shows the protective effect of NaβHB (100µM) on rotenone induced cytotoxicity of SH-SY5Y cells. Cells were stained with hoechst (live cells) and propidium iodide (PI; dead cells) and further the viability is detected using differential nuclear staining assay.

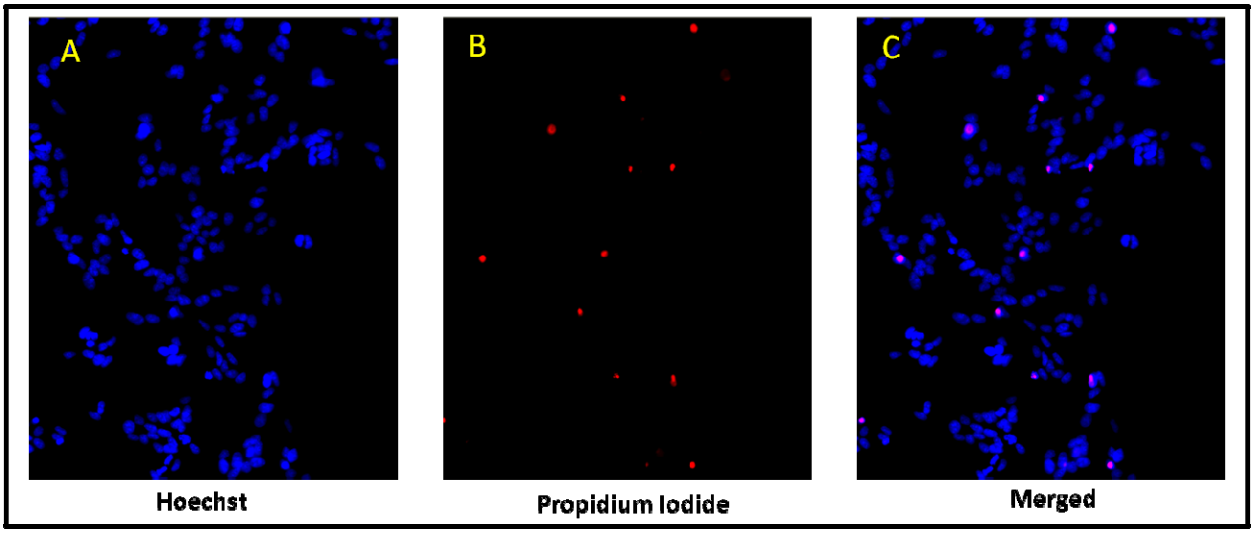

Figure 6.2. Representative images of untreated SH-SY5Y cells by using differential nuclear staining assay. The three images correspond to the same portion of the 3X3 montage, captured with 20X objective utilizing BD Pathway Bioimager system and AttoVison software. (A) Hoechst emission signal from stained cells indicates the total number of nuclei (cells) present in the image, shown in blue. (B) Propidium iodide emission signal from labeled cell nucleus indicates the number of death cell in the image, shown in red. (C) Merged Hoechst and PI image, from signals of the two fluorescence channel; the magenta color is an outcome of co-localization of red and blue colors, indicating the number of dead cells in the image.

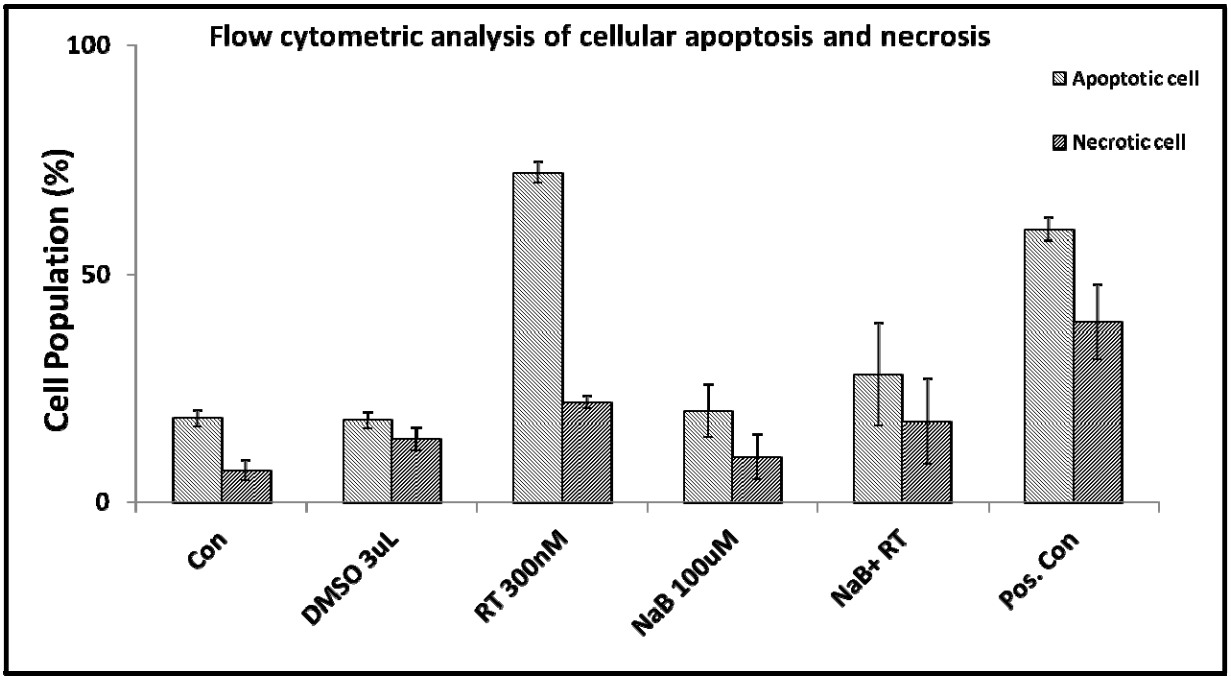

Figure 6.3. Detection of cellular apoptosis/ necrosis in SH-SY5Y cells induced by NaβHB (100 μM) and rotenone (RT) treatment. Cells were treated with NaβHB for 6 hrs and 24 hrs duration and with RT for 18hrs followed by staining with annexin-V FITC (apoptotic marker) and PI

(necrotic marker). Afterwards the percentage of apoptotic and necrotic cell population was quantitated using a flow cytometer.

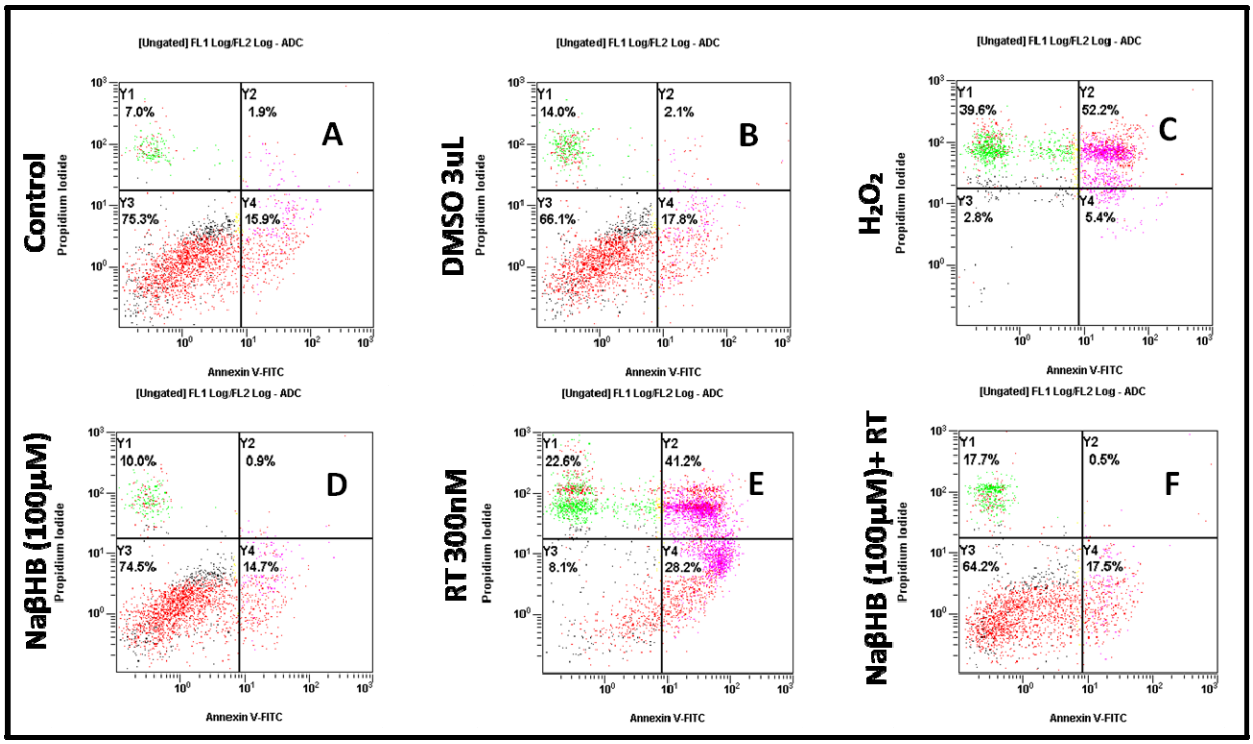

Figure 6.4. Histogram of flow cytometric analyses on SH-SY5Y cells. (A), (B), (C) show the untreated control, vehicle control (Dimethyl sulfoxide; DMSO) and positive control (150 mM H_2O_2) respectively. (D) and (E) show the effect of sodium beta hydroxy butyrate (NaβHB ; 100 μM) and rotenone (300 nM) respectively. (F) shows the protective effect of NaβHB on the rotenone-induced cytotoxicity and apoptotic cell death.

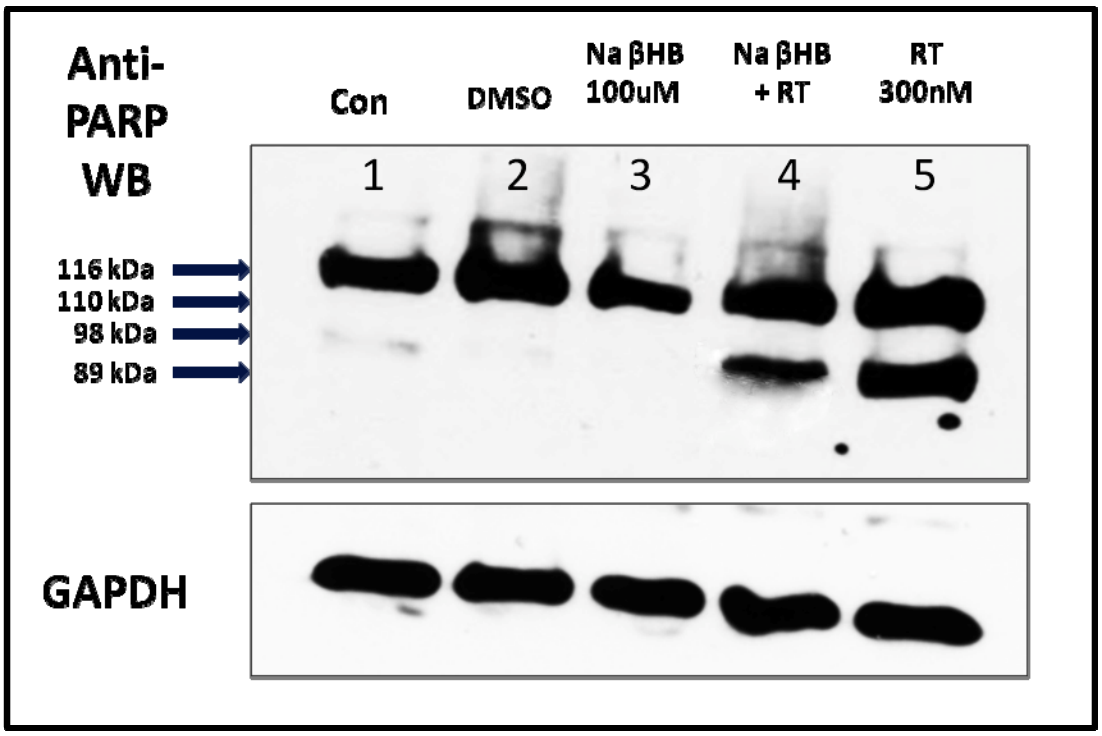

Figure 6.5. Protective effect of NaβHB (100 μM) against rotenone (300 nM) induced poly(ADP-ribose) polymerase (PARP) cleavage (a marker of apoptosis progression) in SH-SY5Y cells. PARP cleavage was analyzed via Isternblot analysis (n=1). Whole cell protein extracts Ire separated using polyacrylamide gel electrophoresis and transferred to a polyvinylidene fluoride (PVDF) membrane, folloId by immunoblot analysis utilizing antibodies anti-PARP.

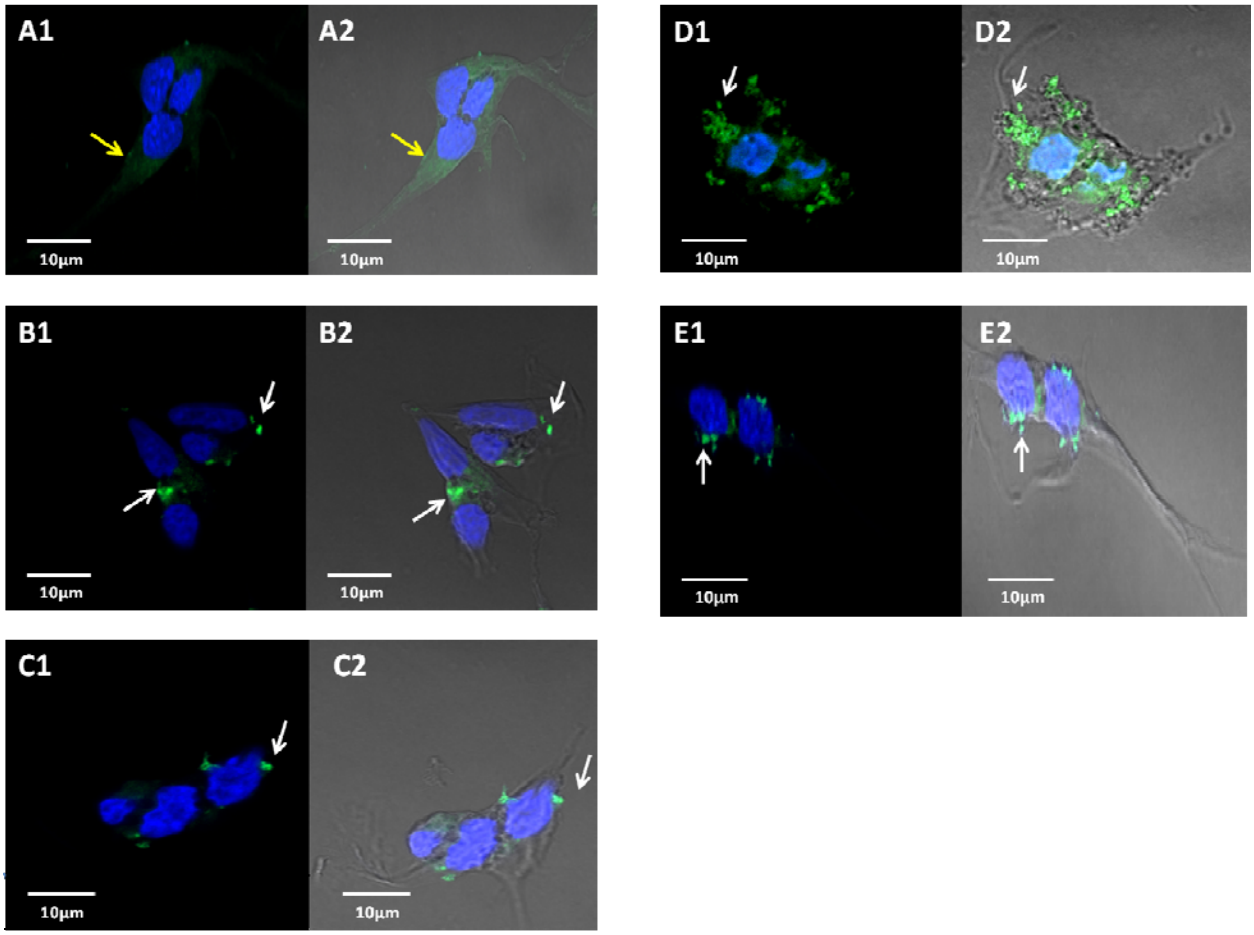

Figure 6.6. Confocal fluorescence images of SHSY5Y cells reveal the presence of intracytoplasmatic aggregates in cells transfected with EGFP or EGFP-tagged synphilin-1 plasmid. Transfected SHSY5Y cells were untreated or stressed with rotenone and processed for immunofluorescence as detailed in the Materials and methods section. (A) cells transfected with pEGFP-C2 without synphilin-1 insert; (B) cells untreated; (C) Cells treated with DMSO 2.5 v/v; (D) Cells exposed to 300 nM rotenone for 12 h alone; (E) cells pretreated with 500 µM NaβHB for 3 h were exposed to 300 nM rotenone for 12 h. All the cells were counterstained with DAPI to delimitate the nucleolus (blue color). White arrows indicate the presence of aggregates

corresponding to the recombinant fusion protein and yellow arrow represents GFP expression. Corresponding part of each figure represents Differential Interference Contrast (DIC) picture.

References

Chapter 1

1. Pearson, H. "Genetics: what is a gene?". Nature (2006) 441 (7092): 398–401

2. Cooper, G.M. The Cell: A Molecular Approach 2nd ed.; M. Geoffrey Cooper, (2000), chapter 2; 18-26

3. Anfinsen; C.B.; Haber, E.; Sela, M.; Jr. White, F.H. The kinetics of formation of native ribonuclease during oxidation of the reduced polypeptide chain. Proc. Natl. Acad. Sci. U. S. A. 47 (1961) 1309-1314.

4. Buck, T.M.; Wright, C.M.; Brodsky, J.L. The activities and function of molecular chaperones in the endoplasmic reticulum. Seminars in Cell and Developmental Biology 18 (2007) 751-761.

5. Appenzeller-Herzog, C.B.; Ellgard, L. The human PDI family: versatility packed into a single fold. Biochim. Biophys. Acta 1783 (2008) 535-548.

6. Sitia, R. and Braakman, I. Quality control in the endoplasmic reticulum protein factory. Nature 426 (2003) 891-894.

7. Ellgard, L.; Ruddock, L.W. The human protein disulfide isomerase family:substrate interactions and functional properties. EMBO Rep. 6 (2005) 25-32.

8. Lipton, S.A.; Gu, Z.; Nakamura, T. Inflammatory mediators leading to protein misfolding and uncompetitive/fast off-rate drug therapy for neurodegenerative disorders. Int. Rev. of Neurobiology 82 (2007).

9. Gruber, C.W.; Cemazar, M.; Heras, B.; Matin, J.L.; Craik, D.J. Protein disulfide isomerase: the structure of oxidative folding. Trends Biochem. Sci. 31 (2006) 455-464.

10. Yoshida, H. ER stress and diseases. FEBS J. 274 (2007) 630-658.

11. Wilkinson, B. and Gilbert, H.F. Protein Disulfide Isomerase. Biochim. Biophys. Acta 1699 (2004) 35-44.

12. Cai, H.; Wang, C.; Tsou, C.; Chaperone-like activity of protein disulfide isomerase in the refolding of a proteins with no disulfide bonds. J. Biol. Chem. 269 (1994) 24550-24552.

13. Edman, J.C.; Ellis, L.; Blacher, R.W.; Roth, R.A.; Rutter, W.J. Sequence of protein disulfide isomerase and implications of its relationship to thioredoxin. Nature 317 (1985) 267-278.

14. Freedman, R.B., Gane, P.J., Hawkins, H.C., Hlodan, R., McLaughlin, S.H., and Parry, J.W. (1998). Experimental and theoretical analyses of the domain architecture of mammalian protein disulphide-isomerase. Biol. Chem. 379, 321–328.

15. Norgaard, P., Westphal, V., Tachibana, C., Alsoe, L., Holst, B., and Winther, J.R. (2001). Functional differences in yeast protein disulfide isomerases. J. Cell Biol. 152, 553–562.

16. Credle, J.J., Finer-Moore, J.S., Papa, F.R., Stroud, R.M., Walter, P., 2005. On the mechanism of sensing unfolded protein in the endoplasmic reticulum. Proc. Natl. Acad. Sci. USA 102, 18773–18784.

17. Kennimark, J.; Darby, N.J.; Dijkstra, K.; Nilges, M.; Creighton, T.E. Structure determination of the N-terminal thioredoxin-like domain of protein disulfide isomerase using multidimensional heteronuclear13C/15N NMR spectroscopy. Biochemistry 35 (1996) 7684-7691.

18. Kennimark, J.; Darby, N.J.; Dijkstra, K.; Nilges, M.; Creighton, T.E. The folding catalyst protein disulfide isomerase is constructed of active and inactive thioredoxin modules. Curr. Biol. 7 (1997) 239-245.

19. Hatahet, F.; Ruddock, F.W. Substrate recognition by the protein disulfide isomerases. FEBS J. 274 (2007) 5223-5234.

20. Nakamura, T.; Lipton, S.A. Molecular mechanisms of nitrosative stress-mediated protein misfolding in neurodegenerative diseases. Cell. Mol. Life Sci. 64 (2007) 1609 – 1620

21. Chivers, P.T.; Laboissiere, M.C.A.; Raines, R.T. Protein disulfide isomerase:Cellular enzymology of the CXXC motif, in: N. A. Guzman (Eds.), Prolyl Hydroxylase, Protein Disulfide Isomerase, and Other Structurally-Related Proteins, Marcel Dekker Inc., New York, 1998, pp. 487-505.

22. Lucana, D.O.O.; Wedderhoff, I.; Groves, M.R. ROS-mediated signalling in bacteria: zinc-containing Cys-X-X-Cys redox centres and iron-based oxidative stress, J. Signal Transduct. (2011) 9 pages.

23. Pal, R.; Cristan, E.A.; Schnittker, K.; Narayan, M. Rescue of ER oxidoreductase function through polyphenolic phytochemical intervention: implications for subcellular traffic and neurodegenerative disorders, Biochem. Biophys. Res. Commun. 392 (2010) 567-571.

24. Uehara, T.; Nakamura, T.; Yao, D.; Shi, Z.Q.; Gu, Z.; Ma, Y.; Masliah, E.; Nomura, Y.; Lipton, S. A. S-nitrosylated protein-disulphide isomerase links protein misfolding to neurodegeneration. (2006) Nature 441, 513–517

25. Tsibris, J.C. et al., Selective inhibition of protein disulfide isomerase by estrogens, J. Biol.Chem. 264 (1989) 13967–13970

26. Schultz-Norton, J.R.; McDonald, W.H.; Yates, J.R.; Nardulli, A.M. Protein disulfide isomerase serves as a molecular chaperone to maintain estrogen receptor alpha structure and function. Mol Endocrinol. 2006; 20(9):1982-95

27. Kratochwil, N.A.; Huber, W.; Muller, F.; Kansy, M.; Gerber, P.R. Chemogenomics in drug discovery: a medicinal chemistry perspective, (2002) Biochem. Pharmacol. 64, 1355–1374

28. Mandeville, J.S.; Froehlich, E.; Tajmir-Riahi, H.A. Study of curcumin and genistein interactions with human serum albumin (2009) J. of Pharmaceutical and Biomed. Anal. 49 468–474

29. Carter, D.C.; Ho, J.X. Structure of serum albumin**,** (1994) Adv. Protein Chem. 45 153–203

Chapter 2

1. Narayan, M., Welker, E., Idemeyer, W. J. and Scheraga, H. A. (2000) Oxidative folding of proteins. Accounts of Chemical Research 33, 737-820.

2. Woycechowsky, K. J. and Raines, R. T. (2000) Native disulfide bond formation in proteins. Curr. Opin. Chem. Biol. 4, 533-539.

3. Arolas, J. L., Aviles, F. X., Chang J. Y. and Ventura, S. (2006) Folding of small disulfide-rich proteins: clarifying the puzzle. Trends Biochem. Sci. 31, 292-301.

4. Tu, B. P. and Weissman, J. S. (2004) Oxidative protein folding in eukaryotes: mechanisms and consequences. J. Cell. Biol. 164, 341-346.

5. Wedemeyer, W. J., Welker, E., Narayan, M. and Scheraga, H. A. (2000) Disulfide bonds and protein folding. Biochemistry 39, 4207-4216.

6. Welker, E., Narayan, M., Wedemeyer, W. J. and Scheraga, H. A. (2001) Structural determinants of oxidative folding in proteins. PNAS USA 98, 2312-2316.

7. Welker, E., Wedemeyer, W. J., Narayan, M. and Scheraga, H. A. (2001) Coupling of conformational folding and disulfide-bond reactions in oxidative folding of proteins. Biochemistry 40, 9059-9064.

8. Rothwarf, D. M. and Scheraga, H. A. (1993) Regeneration of bovine pancreatic ribonuclease A. Steady-state distribution. Biochemistry 32, 2671-2679.

9. Rothwarf, D. M., Li, Y. J. and Scheraga, H. A. (1998) Regeneration of bovine pancreatic ribonuclease A: identification of two nativelike three-disulfide intermediates involved in separate pathways. Biochemistry 37, 3760-3766.

10. Iwaoka, M., Idemeyer, W. J. and Scheraga, H. A. (1999) Conformational unfolding studies of three-disulfide mutants of bovine pancreatic ribonuclease A and the coupling of proline isomerization to disulfide redox reactions. Biochemistry 38, 2805-2815.

11. Fink, M., Nieves, P., Chang, S., and Narayan, M. (2008) Non-redox-active small-molecules can accelerate oxidative protein folding by novel mechanisms. Biophys. Chem. 132, 104-109.

12. Wang, Y. H. and Narayan. M. (2008) pH Dependence of the Isomerase Activity of Protein Disulfide Isomerase: Insights into its Functional Relevance. Protein. J. 27, 181-185.

13. Saito, K., Welker, E. and Scheraga, H. A. (2001) Folding of a disulfide-bonded protein species with free thiol(s): competition betIen conformational folding and disulfide reshuffling in an intermediate of bovine pancreatic ribonuclease A. Biochemistry 40, 15002-15008.

14. Hawkins, H. C. and Freedman, R. B. (1991) The reactivities and ionization properties of the active-site dithiol groups of mammalian protein disulphide-isomerase. Biochem. J. 275, 335-339.

15. Weissman, J. S. and Kim, P. S. (1993) Efficient catalysis of disulphide bond rearrangements by protein disulphide isomerase. Nature 365, 185-188.

16. Wilkinson, B. and Gilbert, H. F. (2004) Protein disulfide isomerase, Biochim. Biophys. Acta 1699, 35-44.

17. Tian, G., Xiang, S., Noiva, R., Lennarz, W. J. and Schindelin, H. (2006) The crystal structure of yeast protein disulfide isomerase suggests cooperativity betIen its active sites. Cell 124, 61-73. Erratum in: (2006) Cell 124, 1085-1088.

18. Shin, H. C. and Scheraga, H. A. (2004) Catalysis of the oxidative folding of bovine pancreatic ribonuclease A by protein disulfide isomerase. J. Mol. Biol. 300, 995-1003.

19. Xiao, R., Wilkinson, B., Solovyov , A., Winther, J. R., Holmgren, A., Lundström-Ljung, J. and Gilbert. H. F. (2004) The contributions of protein disulfide isomerase and its homologues to oxidative protein folding in the yeast endoplasmic reticulum. J. Biol. Chem. 279, 49780-49786.

20. Xu, G., Narayan, M. and Scheraga, H. A. (2005) The oxidative folding rate of bovine pancreatic ribonuclease is enhanced by a covalently attached oligosaccharide. Biochemistry 44, 9817-9823.

21. Narayan, M., Welker, E. and Scheraga, H. A. (2003) Native conformational tendencies in unfolded polypeptides: development of a novel method to assess native conformational tendencies in the reduced forms of multiple disulfide-bonded proteins. J. Am. Chem. Soc. 123, 2909-2910.

22. Veprintsev, D. B., Permyakov, S. E., Permyakov, E. A., Rogov, V. V., Cawthern, K. M., Berliner, L. J. (1997) Cooperative thermal transitions of bovine and human apo-alpha-lactalbumins: evidence for a new intermediate state. FEBS Lett. 412, 625-628.

23. Gilbert, H. F. (1998) Protein disulfide isomerase. Methods Enzymol. 290, 26-50.

24. Fewell, S. W., Travers, K. J., Weissman, J. S. and Brodsky, J. L. (2001) The action of molecular chaperones in the early secretory pathway. Annu. Rev. Genet. 35, 149-91.

25. Romisch, K. (2004) A cure for traffic jams: small molecule chaperones in the endoplasmic reticulum. Traffic 5, 815-820.

26. Romisch, K. (2005) Endoplasmic reticulum-associated degradation. Annu Rev Cell Dev. Biol. 21, 435-456.

Chapter 3

1. Chang, J.Y.; Li, L. Pathway of oxidative folding of R-Lactalbumin: A model for illustrating the diversity of disulfide folding pathways, Biochemistry. 41 (2002) 8405-8413.

2. Chang, J.Y. Evidence for the underlying cause of diversity of the disulfide folding pathway, Biochemistry. 43 (2004) 4522-4529.

3. Wedemeyer, W.J.; Welker, E.; Narayan, M.; Scheraga, H.A. Disulfide bonds and protein folding, Biochemistry. 39 (2000) 4207-4232.

4. Huggins, C.; Tapley, D.F.; Jensen, E.V. Sulphydryl-disulfide relationships in the induction of gels in proteins by urea, Nature. 167 (1951) 592-594.

5. Gilbert, H.F. Molecular and cellular aspects of thiol-disulfide exchange, Adv. Enzymol. Relat. Areas Mol. Biol. 63 (1990) 69-172.

6. Nakamoto, H.; Bardwell, J.C.A. Catalysis of disulfide bond formation and isomerization in the Escherichia coli periplasm, Biochimica et Biophysica Acta. 1694 (2004) 111 –119.

7. Goldberger, R.F.; Epstein, C.J.; Anfinsen, C.B. Acceleration of reactivation of reduced bovine pancreatic ribonuclease by a microsomal system from rat liver, J. Biol. Chem. 238 (1963) 628–635.

8. Gilbert, H.F. The formation of native disulfide bonds, in: Pain, R.H. (Eds.), Mechanisms of Protein Folding, Oxford University Press, Oxford, 1994, pp. 109-111.

9. Pal, R.; Cristan, E.A.; Schnittker, K.; Narayan, M. Rescue of ER oxidoreductase function through polyphenolic phytochemical intervention: implications for subcellular traffic and neurodegenerative disorders, Biochem. Biophys. Res. Commun. 392 (2010) 567-571.

10. Chivers, P.T.; Laboissiere, M.C.A.; Raines, R.T. Protein disulfide isomerase:Cellular enzymology of the CXXC motif, in: N. A. Guzman (Eds.), Prolyl Hydroxylase, Protein Disulfide Isomerase, and Other Structurally-Related Proteins, Marcel Dekker Inc., New York, 1998, pp. 487-505.

11. Lyles, M.M.; Gilbert, H.F. Catalysis of the oxidative folding of ribonuclease A by protein disulfide isomerase: pre-steady-state kinetics and the utilization of the oxidizing equivalents of the isomerase, Biochemistry. 30 (1991) 619–625.

12. Rao, K.R.; Brew, K. Calcium regulates folding and disulfide-bond formation in R-lactalbumin, Biochem. Biophys. Res.Commun. 163 (1989) 1390-1396.

13. Ewbank, J.J.; Creighton, T.E. Structural characterization of the disulfide folding intermediates of bovine R-lactalbumin, Biochemistry. 32 (1993) 3694-3707.

14. Permyakov, E.A.; Berliner, L.J. R-Lactalbumin: Structure and function, FEBS Lett. 473 (2000) 269-274.

15. Chang, J.Y.; Li, L. Pathway of oxidative folding of R-lactalbumin: A model for illustrating the diversity of disulfide folding pathway, Biochemistry. 41 (2002) 8405-8413.

16. Augusto, O.; Boninia, M.G.; Amansoa, A.M.; Linaresa, E.; Santosa, C.C.X.; De Meneze, S.L. Nitrogen dioxide and carbonate radical anion: two emerging radicals in biology, Free Radic. Biol. Med. 32 (2002) 841-859.

17. Kikugawa, K.; Hiramoto, K.; Okamoto, Y.; Hasegawa, Y.K. Enhancement of nitrogen dioxide-induced lipid peroxidation and DNA strand breaking by cysteine and glutathione, Free Radic. 21 (1994) 399–408.

18. Lucana, D.O.O.; Idderhoff, I.; Groves, M.R. ROS-mediated signalling in bacteria: zinc-containing Cys-X-X-Cys redox centres and iron-based oxidative stress, J. Signal Transduct. (2011) 9 pages.

19. Adams, B.K.; Cai, J.; Armstrong, J.; Herold, M.; Lu, Y.J.; Sun, A.; Snyder, J.P.; Liotta, D.C.; Jones, D.P.; Shoji, M. EF24, a novel synthetic curcumin analog, induces apoptosis in cancer cells via a redox-dependent mechanism, Anticancer Drugs. 16 (2005) 263-75.

20. Tajmir-Riahi, H.A. An overview of drug binding to human serum albumin: protein folding and unfolding, Scientia Iranica. 14 (1994) 87-95.

21. Kratochwil, N.A.; Huber, W.; Muller, F.; Kansy, M.; Gerber, P.R. Predicting plasma protein binding of drugs: a new approach, Biochem. Pharmacol. 64 (2002) 1355–1374.

22. Wang, Y.H.; Narayan, M. pH dependence of the isomerase activity of protein disulfide isomerase: insights into its functional relevance, Protein J. 27 (2008) 181-185.

23. Adams, B.K.; Ferstl, E.M.; Davis, M.C.; Herold, M.; Kurtkaya, S.; Camalier, R.F.; Hollingshead, M.G.; Kaur, G.; Sausville, E.A.; Rickles, F.R.; Snyder, J.P.; Liotta, D.C.; Shoji, M. Synthesis and biological evaluation of novel curcumin analogs as anti-cancer and anti-angiogenesis agents, Bioorg. Med. Chem. 12 (2004) 3871– 3883.

24. Shin, H.C.; Scheraga, H.A. Catalysis of the oxidative folding of bovine pancreatic ribonuclease A by protein disulfide isomerase, J. Mol. Biol. 300 (2004) 995-1003.

25. Painter, L.; Harding, M.M.; Beeby, P.J. J. Chem. Soc. Synthesis and Interaction with Human Serum Albumin of the First 3,*18*-Disubstituted Derivative of Bilirubin.ChemInform.18 (1998) 3041–3044.

26. Xu, G.; Narayan, M.; Scheraga, H.A. The oxidative folding rate of bovine pancreatic ribonuclease is enhanced by a covalently attached oligosaccharide, Biochemistry. 44 (2005) 9817–9823.

27. Trott, O.; Olson, A.J. AutoDock Vina: improving the speed and accuracy of docking with a new scoring function, efficient optimization and multithreading, J. Comput. Chem. 30:31(2) (2010) 455-461.

28. Tu, B.P.; Weissman, J.S. Oxidative protein folding in eukaryotes mechanisms and consequences, J.C.B. 164 (2004) 341-346.

29. Mamathambika, B.S.; Bardwell, J.C. Disulfide-linked protein folding pathways, Annu. Rev. Cell Dev. Biol. 24 (2008) 211–35.

30. Pal, R.; Miranda, M.; Narayan, M. Nitrosative stress-induced Parkinsonian lewy-like aggreagates prevented through polyphenolic phytochemical analog intervention, Biochem. Biophys. Res. Commun. 404 (2010) 324-329.

31. Huang, B.; Chen, C. Detection of protein S-Nitrosation using Irreversible Biotinylation Procedures (IBP), Free Radical Biology & Medicine. 49 (2010) 447–45

32. Gonzalez, V.; Pal, R.; Narayan, M. The oxidoreductase behavior of protein disulfide isomerase impedes fold maturation of endoplasmic reticulum-processed proteins in the pivotal structure-coupled step of oxidative folding: implications for subcellular protein trafficking. Biochemistry. 27 (2010) 49(29).

Chapter 4

1. Ranjan P., Shrivastava P., Singh M. S., Sodhi A., Heintz H. N. Baculovirus P35 inhibits NO-induced apoptosis in activated macrophages by inhibiting cytochrome c release, (2004) J. of Cell Sci. 117, 3031-3039

2. Isenberg, J. S., Klaunig, J. E. Role of the Mitochondrial Membrane Permeability Transition (MPT) in Rotenone-Induced Apoptosis in Liver Cells, (2000) Toxicol. Sci. 53, 340–351

3. Chauvin, C., De Oliveira, F., Ronot, X., Mousseau, M., Leverve, X., Fontaine, E. Rotenone Inhibits the Mitochondrial Permeability Transition-induced Cell Death in U937 and KB Cells,(2001) J. Biol. Chem. 276, 41394–41398

4. Higuchi, M., Proske, R. J., Yeh, E. T. Implication of mitochondria-derived reactive oxygen species, cytochrome C and caspase-3 in N-(4-Hydroxyphenyl)retinamide-induced apoptosis in cervical carcinoma cells, (1998) Oncogene 17, 2515–2524

5. Shimizu, S., Eguchi, Y., Kamiike, W., Waguri, S., Uchiyama, Y., Matsuda, H., Tsujimoto, Y. Retardation of chemical hypoxia-induced necrotic cell death by Bcl-2 and ICE inhibitors: possible involvement of common mediators in apoptotic and necrotic signal transductions, (1996) Oncogene 12, 2045–2050

6. Sherer, T. B., Betarbet, R., Stout, A. K., Lund, S., Baptista, M., Panov, A. V., Cookson, M. R., Greenamyre, J. T. An in vitro model of Parkinson's disease: linking mitochondrial impairment to altered α-synuclein metabolismand oxidative damage (2002) J. Neurosci. 22, 7006–7015

7. Heussler, V. T., Fernandez, P. C., Botteron, C., and Dobbelaere, D. A. N-acetylcysteine blocks apoptosis induced by N- a -tosyl-L-phenylalanine chloromethyl ketone in transformed T-cells (1999) Cell Death Differ. 6, 342–350

8. Kelso, G. F., Porteous, C. M., Coulter, C. V., Hughes, G., Porteous, W. K., Ledgerwood, E. C., Smith, R. A., Murphy, M. P. Selective targeting of a redox-active ubiquinone to mitochondria within cells (2001) J. Biol. Chem. 276, 4588–4596

9. Koren, R., Hadari-Naor, I., Zuck, E., Rotem, C., Liberman, U. A., Ravid, A. Vitamin D is prooxidant in breast cancer cells.(2001) Cancer Res. 61, 1439–1444

10. Chrestensen, C. A., Starke, D. W., Mieyal, J. J. Acute Cadmium Exposure Inactivates Thioltransferase (Glutaredoxin), Inhibits Intracellular Reduction of Protein-glutathionyl-mixed Disulfides, and Initiates Apoptosis, (2000) J. Biol. Chem. 275, 26556–26565

11. Kroemer, G., Dallaporta, B., Resche-Rigon, M. The mitochondrial death/life regulator in apoptosis and necrosis, (1998) Annu. Rev. Physiol. 60, 619–642

12. Martinou, J. C. Apoptosis. Key to the mitochondrial gate (1999) Nature 399, 411–412

13. Tan, S., Sagara, Y., Liu, Y., Maher, P., Schubert, D. The Regulation of Reactive Oxygen Species Production during Programmed Cell Death, (1998) J. Cell Biol. 141, 1423–1432

14. Pal, R., Miranda, M., Narayan, M. Nitrosative stress-induced Parkinsonian Lewy-like aggregates prevented through polyphenolic phytochemical analog intervention, (2010) BBRC 404, 324-329

15. Satoh, M. S., Lindahl, T. Role of poly(ADP-ribose) formation in DNA repair, (1992) Nature 356, 356-358

16. Lazebnik, Y. A. et al. Cleavage of poly(ADP-ribose) polymerase by a proteinase with properties like ICE, (1994) Nature 371, 346-347

17. Kratochwil, N. A., Huber, W., Muller, F., Kansy, M., Gerber, P. R. Predicting plasma protein binding of drugs: a new approach, (2002) Biochem. Pharmacol. 64, 1355–1374

18. Mandeville, J. S., Froehlich, E., Tajmir-Riahi, H. A. Study of curcumin and genistein interactions with human serum albumin, (2009) J. of Pharmaceutical and Biomed. Anal. 49 468–474

19. Cohen, G. M. Caspases: the executioners of apoptosis, (1997) Biochem. J. 326, 1-16

20. Nicholson, D. W. et al. Identification and inhibition of the ICE/CED-3 protease necessary for mammalian apoptosis, (1995) Nature 376, 37-43

21. Tewari, M. et al. Yama/CPP32 beta, a mammalian homolog of CED-3, is a CrmA-inhibitable protease that cleaves the death substrate poly (ADP-ribose) polymerase, (1995) Cell 81, 801-809

22. Oliver, F. J. et al. Importance of poly (ADP-ribose) polymerase and its cleavage in apoptosis. Lesson from an uncleavable mutant, (1998) J. Biol. Chem. 273, 33533-33539

23. Uehara, T., Nakamura, T., Yao, D., Shi, Z. Q., Gu, Z., Ma, Y., Masliah, E., Nomura, Y., Lipton, S.A. S-nitrosylated protein-disulphide isomerase links protein misfolding to neurodegeneration, (2006) Nature 441, 513–517

24. Rothwarf, D. M., Scheraga, H.A. Regeneration of bovine pancreatic ribonuclease A. 1. Steady-state distribution, (1993) Biochemistry 32, 2671–2679

25. Wang, Y. H., Narayan, M. pH dependence of the isomerase activity of protein disulfide isomerase: insights into its functional relevance, (2008) Protein J 27, 181–185

26. Shin, H. C., Scheraga, H. A. Catalysis of the oxidative folding of bovine pancreatic ribonuclease A by protein disulfide isomerase, (2004) J. Mol. Biol. 300, 995–1003

27. Rothwarf, D. M., Li, Y. J., Scheraga, H. A. Regeneration of bovine pancreatic ribonuclease A: identification of two nativelike three-disulfide intermediates involved in separate pathways, (1998) Biochemistry 37, 3760–3766

28. Xu, G., Narayan, M., Scheraga, H.A. he oxidative folding rate of bovine pancreatic ribonuclease is enhanced by a covalently attached oligosaccharide, (2005) Biochemistry 44, 9817–9823

29. Lema C., Varela-Ramirez A. and Aguilera RJ. Differential nuclear staining assay for high-throughput screening to identify cytotoxic compounds, (2011) J Curr Cell Biochem 1(1), 1-14

30. Varela-Ramirez, A., Costanzo, M., Carrasco, Y. P., Pannell, K. H., Aguilera, R. Cytotoxic effects of two organotin compounds and their mode of inflicting cell death on fMy mammalian cancer cells, (2011) J. Cell Biol. Toxicol. 27(3), 159-168

31. Li, N., Ragheb, K., Lawler, G., Sturgis, J., Rajwa, B., Melendez, J. A., Robinson, J. P. Mitochondrial complex I inhibitor rotenone induces apoptosis through enhancing mitochondrial reactive oxygen species production, (2003) j. of bio. Chem. 278, 8516–8525

32. Pal, R., Cristan, E. A., Schnittker, K., Narayan, M. Rescue of ER oxidoreductase function through polyphenolic phytochemical intervention: implications for subcellular traffic and neurodegenerative disorders, (2010) BBRC 392, 567-571

33. Fesik, S. W. Insights into programmed cell death through structural biology. (2000) Cell 103, 273-282

Chapter 5

1. Nilsson, Sari Mäkelä, Eckardt Treuter, Michel Tujague, Jane Thomsen, Göran Andersson, Eva Enmark, Katarina Pettersson, Margaret Warner, and Jan-Åke Gustafsson. Mechanisms of Estrogen Action, Vol. 81, No. 4, October 2001, pp. 1535-1565

2. Nilsson, S. et al., Mechanisms of estrogen action, Physiol. Rev. 81 (2001) 1535–1565.

3. Zhu, B.T.; Conney, A.H. Functional role of estrogen metabolism in target cells: review and perspectives, Carcinogenesis 19 (1998) 1–27.

4. Reid, G.; Denger, S.; Kos, M.; Gannon, F. Human estrogen receptor-alpha: regulation by synthesis, modification and degradation, Cell. Mol. Life Sci. 59 (2002) 821–831.

5. Kousteni, S.; et al., Reversal of bone loss in mice by nongenotropic signaling of sex steroids, Science 298 (2002) 843–846.

6. Beckman, J.S.; Beckman, T.W.; Chen, J.; Marshall, P.A.; Freeman, B. A. Apparent hydroxyl radical production by peroxynitrite: implications for endothelial injury from nitric oxide and superoxide, Proc. Natl. Acad. Sci. USA 87 (1990) 1620 –1624.

7. Lipton, S.A.; Choi, Y.B.; Pan, Z.H.; Lei, S.Z.; Chen, H.S. Sucher, N.J.; Loscalzo, J.; Singel, D.J.; Stamler, J.S. A redox-based mechanism for the neuroprotective and neurodestructive effects of nitric oxide and related nitrosocompounds, Nature 364 (1993) 626 – 632.

8. Turano, C.; Coppari, S.; Altieri, F.; Ferraro, A. Proteins of the PDI family:unpredicted non-ER locations and functions, J. Cell. Physiol. 193 (2002) 154–163.

9. Coppari, S. et al., Nuclear localization and DNA interaction of protein disulfide isomerase ERp57 in mammalian cells, J. Cell. Biochem. 85 (2002) 325–333.

10. Edman, J.C.; Ellis, L.; Blacher, R.W.; Roth, R.A.; Rutter, W.J. Sequence of protein disulfide isomerase and implications of its relationship to thioredoxin, Nature 317 (1985) 267 – 270.

11. Vuori, K.; Pihlajaniemi, T.; Myllyl, R.; Kivirikko, K.I. Site-directedmutagenesis of human protein disulfide isomerase: effect on the assembly, activity and endoplasmic reticulum retention of human prolyl 4-hydroxylase in Spodoptera frugiperda insect cells, EMBO J. 11 (1992) 4213 – 4217.

12. Tsibris, J.C. et al., Selective inhibition of protein disulfide isomerase by estrogens, J. Biol. Chem. 264 (1989) 13967–13970.

13. Primm, T.P.; Gilbert, H.F. Hormone binding by protein disulfide isomerase, a high capacity hormone reservoir of the endoplasmic reticulum, J. Biol. Chem. 276 (2001) 281–286.

14. Landel, C.C.; Potthoff, S.J.; Nardulli, A.M.; Kushner, P.J.; Greene, G.L. Estrogen receptor accessory proteins augment receptor–DNA interaction and DNA bending, J. Steroid Biochem. Mol. Biol. 63 (1997) 59–73.

15. Landel, C.C.; Kushner, P.J. Greene, G.L. Estrogen receptor accessory proteins: effects on receptor–DNA interactions, Environ. Health Perspect. 103 (Suppl. 7) (1995) 23–28.

16. Picard, D. et al., Reduced levels of hsp90 compromise steroid receptor action in vivo, Nature 348(1990) 166–168.

17. Xinmiao Fu; Pan Wang; Bao Ting Zhu. The JMynal of Steroid Biochemistry and Molecular Biology. Volume 112, Issues 1-3, November 2008, Pages 127-137.

18. Schultz-Norton, J.R.; McDonald, W.H.; Yates, J.R.; Nardulli, A.M. Protein disulfide isomerase serves as a molecular chaperone to maintain estrogen receptor alpha structure and function. Mol Endocrinol. 2006; 20(9):1982-95

19. Pajl, Ritur; Cristan, E.A; Schnittker, K; Narayan, K. Biochemical and Biophysical Research Communications. Volume 392, Issue 4, 19 February 2010, Pages 567-571

20. Bao Ting Zhu; Allan H.Conney. Functional role of estrogen metabolism in target cells: review and perspectives. Carcinogenesis vol.19 no.1 pp.1–27, 1998

Chapter 6

1. Uehara, T., Nakamura, T., Yao, D., Shi, Z. Q., Gu, Z., Ma, Y., Masliah, E., Nomura, Y., Lipton, S.A. S-nitrosylated protein-disulphide isomerase links protein misfolding to neurodegeneration, (2006) Nature 441, 513–517

2. Imamura, K., Takeshima, T., Kashiwaya, Y., Nakaso, K., Nakashima, K. D-beta-hydroxybutyrate protects dopaminergic SH-SY5Y cells in a rotenone model of Parkinson's disease, (2006) J.Neurosci. Res. 84(6), 1376-84.

Vitae

Rituraj Pal earned his Bachelor of degree in Veterinary Medicine (DVM) from Ist Bengal University of Animal and Fishery Science, India in 2006. He received his Master of Science degree in Chemistry (Biochemistry) in 2009 from the University of Texas at El Paso. In 2009 he joined the doctoral program in Chemistry. Pal has been the recipient of numerous honors and awards such as the Krutilek memorial graduate scholarship from Graduate School of University of Texas at El Paso. He was also a recipient of a merit scholarship of higher education from State of Ist Bengal. While pursuing his degree, Pal worked as a research associate for the department of Chemistry. He interned as Research assistant at Mayan Pigment Inc. under Dr. Garry Williams in 2008. Pal has presented his research at many national and international conferences and workshops such as; at University of NorthTexas, USA, at University of Zurich, Switzerland in 2009. Pal's dissertation entitled, "Nitrosative stress-induced Parkinsonian Lewy-like aggregates prevented through polyphenolic phytochemical analog intervention; implications for sub cellular trafficking and neurodegenerative disorders" was supervised by Dr. Mahesh Narayan. He has done excellent collaborative research with the faculties of Department of Biological Sciences and Department of Physics. Pal's research led 7 research articles published and many are submitted and under-preparation till date.

Awards and felloships

Recipient of Krutilek Scholarship ($7500) ……..2010-2011
Graduate Research Fund ($1000) …….2010
Graduate scientific travel fund ($800) ……..2009

Publications

[1] **Pal R**, Miranda M, Narayan M*. Nitrosative stress-induced Parkinsonian Lewy-like aggregates prevented through polyphenolic phytochemical analog intervention. Biochem Biophys Res Commun. 2011 Jan 7;404(1):324-9 (pub med)

[2] Jessica Gardea, Laura Rios, **Rituraj Pal**, Jorge L. Gardea-Torresdey, and Mahesh Narayan*, From Folklore to Molecular Pharmacophores: Cultivating STEM Students among Young, First-Generation Female Mexican-Americans. J. Chem. Educ., 2011, 88 (1), pp 41–43 (Sci finder)

[3] Gonzalez V↑, **Pal R**↑, Narayan M*. The oxidoreductase behavior of protein disulfide isomerase impedes fold maturation of endoplasmic reticulum-processed proteins in the pivotal structure-coupled step of oxidative folding: implications for subcellular protein trafficking. Biochemistry. 2010 Jul 27;49(29). (↑ Both shares equal authorship. Article was highlighted online). (pub med)

[4] L. A. Pinales, R. R. Chianelli, W. G. Durrer, **R. Pal**, M. Narayan and F. S. Manciu*, Spectroscopic study of inhibition of calcium oxalate calculi growth by Larrea tridentate. JMynal of Raman Spectroscopy, 7 JUL 2010,DOI: 10.1002/jrs.2742 (Willey library)

[5] **Pal R**, Cristan EA, Schnittker K, Narayan M*. Rescue of ER oxidoreductase function through polyphenolic phytochemical intervention: implications for subcellular traffic and neurodegenerative disorders. Biochem Biophys Res Commun. 2010 Feb 19;392(4):567-71. (pub med)

[6] **Rituraj Pal**, Veronica Gonzalez and Mahesh Narayan*, Reshuffling Activity of Protein Disulfide Isomerase Reduces Refolding Yield in the Structure-forming Step of the Oxidative Protein Folding Reaction. Chemistry Letters, Vol. 39 (2010), No. 3 p.263 (Sci finder)

[7] Suman Sirimulla* , **Rituraj Pal**, Rene Duran, Alvin M. Altamirano, William C. Herndon, Mahesh Narayan, Identification of polyphenolic compounds as nitrosative stress inhibitors by virtual screening and experimental evaluation. Molecular Informatics (ahead of print)

[8] **Rituraj Pal**, Debarshi Roy, Karina Schnittker, Siddhartha Das*, and Mahesh Narayan*, Estrogenic homeostasis in cells rescued through mitigation of nitrosative-stress-linked PDI damage. Archives of Biochemistry and Biophysics (Manuscript in preparation)

[9] **Rituraj Pal**, Armando Varela, Parijat Kabiraj, Marisol Romero, Emmanuel Zubia, Juaquin Rodigo-Garcia, Rene Duran, Laura Garcia, Manuel Miranda, Mahesh Narayan*, Prophylactic effect of EF24 against nitrosative stress induced apoptotic cell death and its binding affinity with human serum albumin (Final version)

[10] **Rituraj Pal**, Emmanuel Zubia, Rene duran, Mahesh Narayan*, Polyphenolic phytochemicals prevent polymerization of proteins under oxidative stress; maintain homeostasis during fold maturation pathway. BMC (Manuscript in preparation)

[11] Parijat Kabiraj, **Rituraj Pal**, Mahesh Narayan*, Na-β,D-hydroxybutyrate prevents rotenone induced cytosolic aggregation of misfolded proteins and apoptotic cell death in PD model (Final version)

Abstracts

[1] Rituraj Pal, Victotria Morris, and Rebecca Dickstein. "Sequencing and cloning of nip gene, a plant gene." Department of Molecular Biology, University of North Texas, 2007

[2] Pal, R., Schnittker, K., Narayan, M. "Preventive mechanism of small-molecule in nitrosative stress effects on an ER-resident oxidoreductase enzyme. SACNAS research Expo. 2008

[3] Rituraj Pal and Mahesh Narayan, "Protein misfolding in ER due to S-nitrosylated PDI causes neurodegenerative disease. University of Zurich, Switzerland, 2009

[4] Karina Schnittker, Rituraj Pal and Mahesh Narayan. "Targeting Nitrosative Stress Effects on an ER-Resident Oxidoreductase through Small-Molecule Ethnopharmaceutical Intervention: Implications for Age-and Neurodegeneration-Related Disorders." 65th SouthIst Regional Meeting of American Chemical Society, 2009.

[5] Rituraj Pal, and Mahesh Narayan, "A Jekyll and Hyde oxidoreductase chaperone in the ER: Implications for neurodegenerative disorders". Gordon research conference, New Hampshire, 2009

Permanent address: Midnapur
West Bengal, India – 721101

This dissertation was typed by Rituraj Pal.